Carbon and greenhouse gas budgets of Europe: trends, interannual and spatial variability, and their drivers

Ronny Lauerwald[1], Ana Bastos[2], Matthew J. McGrath[3], Ana Maria Roxana Petrescu[4], François Ritter[3], Robbie M. Andrew[5], Antoine Berchet[3], Grégoire Broquet[3], Dominik Brunner[6], Frédéric Chevallier[3], Alessandro Cescatti[7], Sara Filipek[8], Audrey Fortems-Cheiney[3,27], Giovanni Forzieri[10], Pierre Friedlingstein[11, 12], Richard Fuchs[13], Christoph Gerbig[2], Sander Houweling[4], Piyu Ke[11,16], Bas .J.W. Lerink[8], Wanjing Li[16], Wei Li[16], Xiaojun Li[17], Ingrid Luijkx[28], Guillaume Monteil[9], Saqr Munassar[2], Gert-Jan Nabuurs[8], Prabir K. Patra[18,19], Philippe Peylin[3], Julia Pongratz[14,20], Pierre Regnier[21], Marielle Saunois[3], Mart-Jan Schelhaas[8], Marko Scholze[9], Stephen Sitch[11], Rona L. Thompson[22], Hanqin Tian[23], Aki Tsuruta[24], Chris Wilson[25,26], Jean-Pierre Wigneron[17], Yitong Yao[3], Sönke Zaehle[2], and Philippe Ciais[3]:

[1]Université Paris-Saclay, INRAe/AgroParisTech UMR EcoSys, Palaiseau, France
[2]Max-Planck-Institute for Biogeochemistry, Jena, Germany
[3]Université Paris-Saclay, CEA/CNRS/UVSQ Laboratoire des Sciences du Climat et de l'Environnement, Gif-sur-Yvette, France
[4]Department of Earth Sciences, Vrije Universiteit Amsterdam, Amsterdam, 1081HV, Netherlands
[5]CICERO Center for International Climate Research, Oslo, Norway
[6]Empa, Swiss Federal Laboratories for Materials Science and Technology, Dübendorf, 8600, Switzerland
[7]European Commission, Joint Research Centre (JRC), Ispra, Italy
[8]Wageningen Environmental Research, Wageningen University and Research (WUR), Wageningen, 6708PB, Netherlands
[9]Lund University, Department of Physical Geography and Ecosystem Science, Lund, Sweden
[10]University of Florence, Department of Civil and Environmental Engineering (DICEA) Via di Santa Marta 3, 50139 Firenze, Italy
[11]Faculty of Environment, Science and Economy, University of Exeter, Exeter, UK;
[12]Laboratoire de Meteorologie Dynamique, Departement de Geosciences, Institut Pierre-Simon Laplace, CNRS-ENS-UPMC-X, Ecole Normale Superieure, Paris, France
[13]Land Use Change & Climate Research Group, IMK-IFU, Karlsruhe Institute of Technology (KIT), Garmisch-Partenkirchen, Germany
[14] Department of Geography, Ludwig-Maximilians-Universität München, Munich, Germany
[16]Department of Earth System Science, Ministry of Education Key Laboratory for Earth System Modeling, Institute for Global Change Studies, Tsinghua University, 100084 Beijing, China
[17]INRAE, UMR 1391 ISPA, Université de Bordeaux, F-33140 Villenave d'Ornon, France
[18]Research Institute for Global Change, JAMSTEC, Yokohama, 2360001, Japan

[19]Research Institute for Humanity and Nature, Kyoto, 6038047, Japan
[20]Max Planck Institute for Meteorology, Hamburg, Germany
[21]Department Geoscience, Environment & Society-BGEOSYS, Université Libre de Bruxelles, Bruxelles, Belgium
[22]Norwegian Institute for Air Research (NILU), Kjeller, Norway
[23]Center for Earth System Science and Global Sustainability, Schiller Institute for Integrated Science and Society, Department of Earth and Environmental Sciences, Boston College, Chestnut Hill, MA, USA;
[24]Finnish Meteorological Institute, Helsinki, Finnland
[25]National Centre for Earth Observation, University of Leeds, Leeds, UK
[26] School of Earth & Environment, University of Leeds, Leeds, UK
[27]Science Partners, Quai de Jemmapes, 75010 Paris, France
[28]Meteorology and Air Quality group, Wageningen University, Wageningen, 6708PB, the Netherlands.

Abstract

In the framework of the RECCAP2 initiative, we present the greenhouse gas (GHG) and carbon (C) budget of Europe. For the decade of the 2010s, we present a bottom-up (BU) estimate of GHG net-emissions of 3.9 Pg CO_2-eq. yr^{-1} (using a global warming potential on a 100 year horizon), and are largely dominated by fossil fuel emissions. In this decade, terrestrial ecosystems acted as a net GHG sink of 0.9 Pg CO_2-eq. yr^{-1}, dominated by a CO_2 sink that is partially counterbalanced by net emissions of CH_4 and N_2O. For CH_4 and N_2O, we find good agreement between BU and top-down (TD) estimates from atmospheric inversions. However, our BU land CO_2 sink is significantly higher than TD estimates. We further show that decadal averages of GHG net-emissions have declined by 1.2 Pg CO_2-eq. yr^{-1} since the 1990s, mainly due to a reduction in fossil fuel emissions. In addition, based on both data driven BU and TD estimates, we also find that the land CO_2 sink has weakened over the past two decades. A large part of the European CO_2 and C sink is located in Northern Europe. At the same time, we find a decreasing trend in sink strength in Scandinavia, which can be attributed to an increase in forest management intensity. These are partly offset by increasing CO_2 sinks in parts of Eastern Europe and Northern Spain, attributed in part to land use change. Extensive regions of high CH_4 and N_2O emissions are mainly attributed to agricultural activities and are found in Belgium, the Netherlands and the southern UK. We further analyzed interannual variability in the GHG budgets. The drought year of 2003 shows the highest net-emissions of CO_2 and of all GHGs combined.

1. Introduction

The REgional Carbon Cycle Assessment and Processes Phase 2 (RECCAP2) initiative aims at re-assessing carbon (C) and greenhouse gas (GHG) budgets of the land and oceans over the recent decade 2010-2019, including their component fluxes. This goal is to be achieved based on an ensemble of ten regional budget analyses at (sub-)continental scale which in total cover the entire global land mass. The first phase of this initiative (RECCAP1), launched more than 10 years ago (Canadell et al. 2011), featured budget analyses of nine large land regions and focused on the period 2000-2009. While in RECCAP1 most regional budget analyses were limited to carbon dioxide (CO_2), the second phase of RECCAP (RECCAP2) now explicitly focuses on the three main GHGs: carbon dioxide (CO_2), methane (CH_4) and nitrous oxide (N_2O). The delineation of land regions has been updated as well, distinguishing now 10 land regions (see Ciais et al. 2022). In this study, we present the European GHG and C budget for the decades 1990-1999, 2000-2009, and 2010-2019 in the framework of RECCAP2.

For RECCAP1, the European GHG and C budget had been presented by Luyssaert et al. (2012). Different from other land budgets of RECCAP1, it already considered the budgets of the three main GHGs CO_2, N_2O and CH_4. Their budget analysis focused on the two 5-year-periods 1996-2000 and 2001-2005. The paper presented here is an update on Luyssaert et al., focusing on the more recent period 2010-2019, including more recent and improved datasets, and additionally considering interannual variability (IAV) of GHG budgets. Note also, that the European region for RECCAP2 is defined differently to that of RECCAP1. The RECCAP2 region of Europe includes the countries of Austria, Albania, Andorra, Belarus, Belgium, Bulgaria, Bosnia and Herzegovina, Croatia, Cyprus, Czech Republic, Denmark, Estonia, Faroe Islands, Finland, France, Germany, Greece, Greenland, Hungary, Iceland, Ireland, Italy, Liechtenstein, Lithuania, Latvia, Luxembourg, North-Macedonia, Malta, Moldova, Montenegro, Netherlands, Norway, Poland, Portugal, Romania, San Marino, Serbia, Slovakia, Slovenia, Spain, Sweden, Switzerland, Ukraine, and United Kingdom - all in their boundaries as accepted by the UN, but excluding oversea territories outside of continental Europe. In contrast, the European region used in RECCAP1 excluded the East European countries of Moldova, Ukraine and Belarus.

More recently, the European GHG budgets for CO_2, CH_4, and N_2O have been reassessed in the framework of the project VERIFY, first covering the periods 1990-2017 (Petrescu et al. 2021a, 2021b), and now extended to the periods 1990-2019 for CH_4 and N_2O (Petrescu et al. 2023) and 1990-2020 for CO_2 (McGrath et al., 2023). VERIFY focused on the comparison of national GHG inventories against other, partially independent estimates from global datasets, models and atmospheric inversions, but also investigated temporal trends in emissions and the contribution from different sectors. The spatial domain of VERIFY was more restricted, with most of the analysis focusing on the 27 EU Member States plus the UK. However, VERIFY also featured a

number of analyses additionally including Norway, Switzerland, Moldova, Ukraine and Belarus. This larger region is more comparable to the European region as defined in RECCAP2, but excluding Iceland and the non-EU countries in the Balkans (Serbia, Albania, Bosnia-Herzegovina, North-Macedonia, Montenegro, and Kosovo). For our analysis of the European C and GHG budgets in the framework of RECCAP2, we use many datasets that have already been used by or prepared for VERIFY, with the aim to deepen our understanding of trends, IAV and spatial patterns in GHG and C fluxes. While VERIFY has investigated long-term trends of GHG emissions with a specific focus on anthropogenic emissions, in RECCAP2 we investigate in more detail spatial patterns and IAV of GHG and C budgets within Europe which are mainly driven by climate variability and landscape processes. Both these research foci are novel and will help to deepen our process understanding with regard to large-scale dynamics of C and GHG budgets and their feedbacks with climate variability and change.

In the spirit of RECCAP, and analogous to other studies mentioned above, we assess the European GHG and C budgets using two approaches: 1) a top-down (TD) approach using atmospheric inversion estimates, and 2) a bottom-up (BU) approach using inventory-based estimates, eddy covariance flux measurements and outputs of various mechanistic models, including Dynamic Global Vegetation Models (DGVMs) and more specialized models. We analyze different types of biospheric C stock change and flux estimates (inventories, upscaled eddy-covariance measurements, DGVMs) to evaluate their agreement with regard to spatial distribution of biospheric C gains and losses. We additionally use independent maps of C gains and losses related to harvest, land use change, fire and other disturbances which will shed more light on the spatial drivers of the European land C sink, and bookkeeping models to isolate the effect of land-use change. For the analysis of the interannual variability of European GHG budgets, we extend the work of Bastos et al. (2016) who were able to link IAV of land CO_2 budget to large-scale climate patterns such as the North Atlantic Oscillation (NAO) and the East Atlantic pattern (EA). In our study, we also include CH_4 and N_2O budgets and finally assess the global warming potential (GWP) of these three GHGs and their IAV.

In the following, we look first into the GHGs (section 3) and carbon (section 4) budgets for the entirety of Europe. We start this analysis with a budget of the most recent decade 2010-2019, before we compare the budgets of the last three decades, analyzing temporal trends and identifying sectors and fluxes that are responsible for those trends. Then, we investigate spatio-temporal variability in GHG sources and sinks within Europe and during the last decade based on regional inversions (section 5), focusing on IAV, recent trends and local hotspots of sinks and sources. Then, we have a closer look at the IAV of the different GHG budgets, exploring to what extent they are driven by climate modes (section 6). In the later part of our study, we investigate how much different, spatialized BU estimates of C stock changes agree among each other and with TD approaches on large-scale spatial patterns in the European land C sink, and what we can learn about the main environmental drivers of the temporal trends in the land C sink (section 7).

In a final section, we investigate how far forest disturbances have affected the European C balance over the last decades (section 8).

2 Methods and Materials

2.1 GHG budgets from bottom-up estimates

We aim to establish BU GHG budgets based on a range of flux estimates for different sectors and flux components, and then compare these to the TD budget estimates of atmospheric inversions. We distinguish between direct anthropogenic emissions of GHG (section 2.1.1) and the land fluxes that focus on GHG exchange between the continental biosphere and the atmosphere (section 2.1.2), largely following the guidelines proposed by Ciais et al. (2022). Our primary focus lies on the land budgets and the question how GHG sinks and sources in continental ecosystems are distributed in space and time and how they evolved over the past decades. This includes managed lands and terrestrial ecosystem-atmosphere exchange fluxes affected by human intervention. Anthropogenic emissions that are not related to ecosystem-atmosphere exchange fluxes are treated separately as direct anthropogenic emissions (F_{direct}, eq. 1)

When several estimates exist for a GHG sink or source, we calculate their median. We further calculate a lower and upper bound estimate, which are either based on an uncertainty estimate reported in the original data, on the spread of individual results where ensembles of DGVMs or inversions are used, or on an uncertainty estimate based on expert judgment. For the latter, we largely adopted estimates of relative uncertainties used in RECCAP1 (Luyssaert et al. 2012, Ciais et al. 2021).

2.1.1 Direct anthropogenic emissions

For anthropogenic emissions, we use the main sectors proposed by IPCC (2006): Energy (F_{energy}), industrial processes and product use (F_{IPPU}), Waste (F_{waste}), and Agriculture, Forestry and Other Land Use (F_{AFOLU}). F_{energy} includes all emissions related to exploration, exploitation, transformation, distribution and use of fossil fuels. F_{IPPU} comprises a variety of industrial processes that release GHGs from chemical or physical transformation of materials. F_{waste} comprises all emissions related to disposal and treatment of solid waste and wastewater, including burning of waste. F_{AFOLU} comprises both all anthropogenic GHG emissions and also all sink removals on managed lands, where managed lands are broadly defined as ecosystems where humans intervene and over which countries claim responsibility for AFOLU fluxes (IPCC 2006). Note that national inventories in Europe use land designated as "managed" as a proxy for anthropogenic emissions and removals from all land, in order to avoid attempting to separate out, for example, background growth in young forests from growth due to increased atmospheric CO_2 concentrations. Thus, F_{AFOLU} accounts for all GHG exchanges between terrestrial ecosystems and the atmosphere. F_{AFOLU} can further be split into sub-categories “Agriculture” (F_{agri}) and “Land Use, Land-Use Change, and Forestry” (F_{LULUCF}), which facilitates integration of these

estimates with other BU estimates focusing only on one of these two sub-categories. Soil carbon changes on agricultural land are counted as part of F_{LULUCF}, which further comprises vegetation and soil carbon changes related to land-use changes and forestry, and F_{agri} thus includes only GHG emissions from urea applications and liming (CO_2), enteric fermentation (CH_4), manure management (CH_4, N_2O), and biomass burning (CO_2, CH_4 and N_2O). Note however, that we only consider F_{agri} as part of F_{direct} (eq. 1), while we consider F_{LULUCF} to be an anthropogenic perturbation of exchange fluxes between terrestrial ecosystems and the atmosphere (section 2.1.2). For our definition of F_{agri} as a component of direct anthropogenic emissions, we further excluded N_2O emissions from agricultural soils and CO_2 emissions related to changes in soil C stocks, as those are included in the land budgets as well.

$$F_{direct} = F_{energy} + F_{IPPU} + F_{waste} + F_{agri} \quad \text{(eq 1)}$$

For F_{energy}, F_{IPPU}, F_{waste}, F_{agri} and F_{LULUCF}, we use several inventory-based assessments that follow the definition of the sectors proposed by IPCC (2006): EDGAR v6.0, GAINS, and UNFCCC (Table 1). These data cover at least the period since 1990, and we can thus calculate consistent budgets for the three decades of the 1990s, 2000s, and 2010s. UNFCCC data are a collection of national GHG inventories that use national activity data with different levels of sophistication, ranging from default emission factors (Tier 1), country- and technology-specific parameters (Tier 2), to more complex methods that may include calibrated, process-based models (Tier 3). UNFCCC data include uncertainty estimates that take into account uncertainties in both emission factors and activity data. More information on these data can be found in Petrescu et al. (2021a, 2021b, 2023) and McGrath et al. (2023). The inventory-based estimates of EDGAR v6.0 and GAINS are based on global activity data, but country- and technology-specific emission factors (Tier 2). For EDGAR, uncertainties were assessed by Solazzo et al. (2021). For UNFCCC data, depending on the tiers used for emission estimates in the national reporting, GHG budgets are better constrained for certain countries, but not in a manner consistent across Europe. In addition, we use an ensemble of fossil-fuel CO_2 emission (F_{fossil}) estimates assembled by Andrew (2020). In agreement with that study, we consider F_{fossil} as the sum of F_{energy} and F_{IPPU} of CO_2. For a detailed description of these datasets, see Andrew (2020). Note that we excluded estimates based on EDGAR and UNFCCC from Andrew (2020) to avoid redundancies. Finally, we included Tier 1 estimates from FAOSTAT for F_{AFOLU}, F_{agri}, and F_{LULUCF} (Tubiello et al., 2013), while the latter flux is used for the land budget. Those estimates are based on the global activity data from the FAOSTAT database, which are sourced from national statistical services reporting this information annually to the FAO, and from generalized emission factors proposed by the IPCC (2006).

221 Table 1: List of bottom-up datasets used in this study.

Data set	Parameters, Sectors	Gases	Period	Temp. resol.	Spatial resol.
		Inventories			
UNFCCC	F_{direct} ,F_{LULUCF} ,ΔC_{GL} ,ΔC_{CL}	CO_2, CH_4, N_2O	1990-2019	Annual	Country
GAINS	F_{direct} ,F_{LULUCF}	CH_4, N_2O	1990-2015	Annual	Country
EDGAR v6.0	F_{direct} ,F_{AFOLU}	CO_2, CH_4, N_2O	1970-2018	Annual	Country
FAOSTAT	F_{AFOLU} ,F_{agri} ,F_{LULUCF} ,$F_{soil\ N2O,man}$,ΔC_{GL} ,ΔC_{CL} ,ΔC_{FL}	CO_2, CH_4, N_2O	1961-2019	Annual	Country
Andrew (2020)	F_{fossil}	CO_2	various	Annual	Country
FAOSTAT	$F_{wood\ harvest}$,$F_{crop\ harvest}$,$F_{wood\ trade}$,$F_{crop\ trade}$	Mass of products	1961-2019	Annual	Country
Hirschler & Oldenburg 2022	$F_{peat\ harvest}$,$F_{peat\ trade}$,$F_{peat\ use}$	Mass of products	2013-2017	none	Country
		Land surface models			
TRENDYv10	NPP, GPP, Rh,Ra,NBP	CO_2	1901-2019	Monthly	0.5°
Global N_2O budget ensemble	$F_{soil\ N2O}$	N_2O	1901-2015	Monthly	0.5°
O-CN (Zaehle et al. 2010, ext. for NMIP2)	$F_{soil\ N2O}$	N_2O	1901-2019	Monthly	0.5°
GMB2020, BU models	$F_{peat\ CH4}$	CH_4	2005-2019	Monthly	0.5°
ORCHIDEE-GMv3.2 (Chang et al. 2021)	$F_{grazing}$	C	1861-2012	Monthly	0.5°
		Other process based models			
MeMo	$F_{methanotrophy}$	CH_4	1990-2009	Monthly	1°
VPRM (Gerbig & Koch 2021)	NEE_C	CO_2	2006-2020		7.5'
		Bookkeeping models			
H&N (as in Friedling-stein et al. 2021)	F_{LUC}	CO_2	1990-2020	Annual	RECCAP2
BLUE (Ganzenmüller et al. 2022)	F_{LUC}	CO_2	1960-2019	Annual	0.25°
		Land cover data			
HILDA+	Land cover, land cover change	-	1960-2019	Annual	0.01°

223

Table 1 - continued

Data set	Parameters, Sectors	Gases	Period	Temp. resol.	Spatial resol.
	Data driven estimates				
FLUXCOM (Jung et al. 2020 BG) - RS v006	GPP, Re_{terr}	CO_2	2001-2020	Monthly	5'
FLUXCOM (Jung et al. 2020 BG) - ERA	GPP, Re_{terr}	CO_2	1990-2018	Monthly	5'
GLASS	GPP, NPP	CO_2	2001-2018	8 Day	500 m
Madani & Parazoo 2020	GPP	CO_2	1982-2016	Monthly	8 km
MODIS	NPP	CO_2	2001-2020	8 Day	500 m
BESS	GPP	CO_2	2001-2016	8 Day	1 km
Yao et al., 2020	Rh_{terr}	CO_2	1985-2013	Annual	0.5°
GFEDv4 (extended.)	F_{fire}	C	1997-2019	Monthly	0.25°
GFASv1.2	F_{fire}	C,CO_2, CH_4, N_2O	2003-2020	Daily	0.1°
Mendonca et al. (2017)	ΔC_{burial}	C		none	COSCAT
Lauerwald et al. (2023)	F_{IW}	CO_2, CH_4, N_2O	present day	none	RECCAP2
Rosentreter et al. (2023)	F_{CWa},F_{CWL}	CO_2, CH_4, N_2O	present day	none	RECCAP2
Zscheischler et al. (2017)	$F_{weathering}$,$F_{litho2river}$,$F_{river\ export}$,ΔC_{litho}	C, CO_2	present day	none	1°
Etiope et al. (2019), updated for Petrescu et al. (2023)	F_{geo}	CH_4	present day	none	1°
EMEP	$F_{soil\ N2O,Ndep}$	N	2000-2019	Daily	0.1°
EFISCEN	ΔC_{FL}	Biomass	2000-2020	5 Year	Country
EFISCEN, gridded version	ΔC_{FL}	Biomass	2000-2020	annual	7.5'
L-VOD	ΔC_{FL}	Biomass	2011-2021	Quarterly	25 km
Byrne et al. (2023)	$F_{wood\ harvest}$,$F_{crop\ harvest}$, $F_{wood\ use}$,$F_{crop\ use}$	C	1961-2019	Annual	5'

*Spatial resolution refers to pixel size of gridded product, or to regions, which can be country areas, COSCAT regions (based on coastal segments and their catchments, Meybeck et al., 2006), or the entire study area (RECCAP2).

2.1.2 Land budgets

While we kept uniformity for anthropogenic emission sectors with the definitions used by the IPCC, we adapted the land budgets in a way that was deemed most suitable for each GHG (Fig. 1). In general, we sub-divided the land systems further into terrestrial ecosystems (vegetation-soil

systems), inland waters, and coastal ecosystems (waters and wetlands). Before we describe the land budget of each GHG further below, we first describe here which flux components and data sources are shared between those budgets. In contrast to terrestrial ecosystems, the emissions from inland waters (F_{IW}), coastal waters (F_{CWa}) and coastal wetlands (F_{CWL}) are treated similarly in each land GHG budget, which means that similar processes, subdivisions, and data sources are considered for each GHG. For these fluxes, we use syntheses of estimates that have been developed within the RECCAP2 initiative (Lauerwald et al., 2023 for F_{IW}; Rosentreter et al.; 2023 for F_{CWa} and F_{CWL}). All these estimates are climatologies of average annual fluxes, which we assumed to be constant and representative for the last three decades.

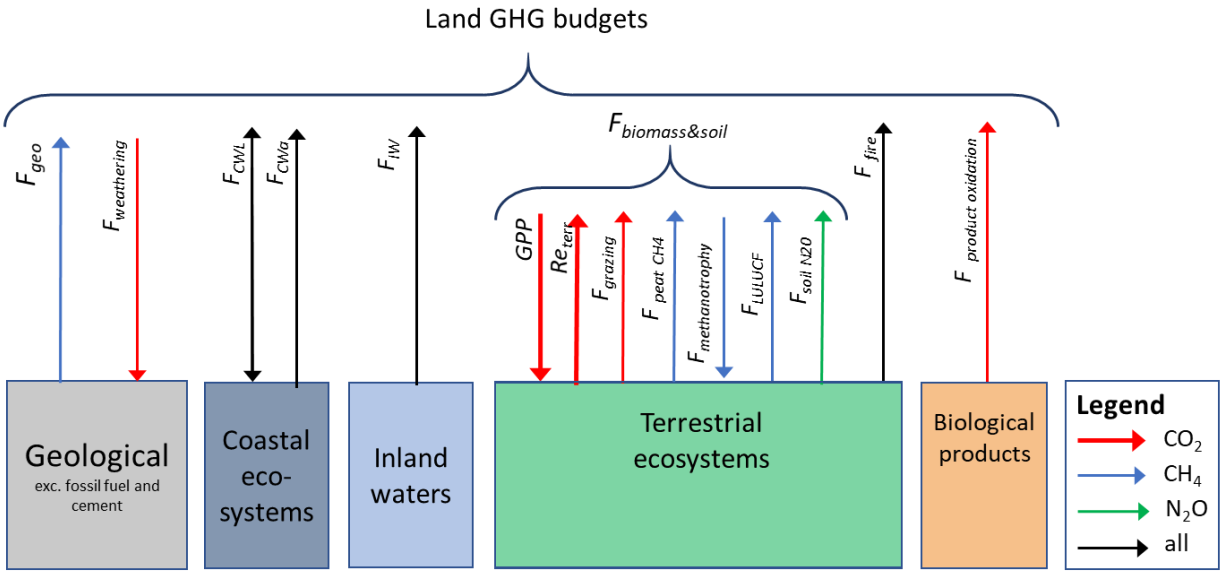

Figure 1: Greenhouse gas fluxes included for the land budget, adapted from Ciais et al. (2022) to include N_2O fluxes and coastal waters. This land GHG budget excludes direct anthropogenic emissions (see text) such as CH_4 emissions from agriculture and waste, industrial processes and fossil emissions.

Another flux, which is included in all three land GHG budgets, is fire emissions (F_{fire}), which relates to in-situ burning of biomass and is thus distinguished from incineration of waste which belongs to F_{Waste}; the burning of crop residues, which is part of F_{agri}; and the burning and decay of crop products ($F_{product\_decay}$), which is a separate flux component in the CO_2 and C budgets (see below). F_{fire} is derived from two data-driven estimates: the CAMS Global Fire Assimilation System (GFAS) (Kaiser et al., 2012) and the global fire emission database (GFED) v4 (van der Werf et al. 2017). GFAS is based on fire radiative power observations from satellite-based sensors. GFAS gives emissions estimates for total C, CO_2, CH_4, CO, and N_2O. GFED is based on remotely sensed data (Moderate Resolution Imaging Spectroradiometer - MODIS and Visible Infrared Imaging Radiometer Suite - VIIRS) of burned area and emission factors. GFED gives only total C emissions, which we treat as CO_2 emissions, but details emissions from fires of

different land use types and thus permits the separation of biomass burning on agricultural land from wildfires. Both GFED and GFAS cover the last two decades. For the GHG budgets of the 1990s, we assumed that fire emissions equaled those of the 2000s. Note that we do not explicitly estimate CO_2 emissions from other forest disturbances such as windthrow, pests or diseases, but these emissions are implicitly included in UNFCCC carbon stock change inventories (and explicitly in the case where the gain-loss method is employed, i.e. approximately half the countries in the European Union and for some disturbances for which even countries with stock-change inventories use a special calculation, like France for extreme windthrow) established by countries, just as fire emissions. A specific estimate of decadal forest carbon stock loss and gain from forest disturbances is given in section 8.

The major fluxes between terrestrial ecosystems and the atmosphere are defined and treated differently for each land GHG budget, as detailed in the following.

Land CO_2 budget

$$F_{land\ CO2} = GPP + Re_{terr} + F_{IW} + F_{product\ oxidation} + F_{grazing} + F_{fire} + F_{CWa} + F_{CWL} + F_{weathering} \quad \text{(eq 2)}$$

$$Re_{terr} = Ra + Rh \quad \text{(eq. 3)}$$

At the center of the land CO_2 budget, we put the balance between gross primary production (GPP) and terrestrial ecosystem respiration Re_{terr}, which is itself the sum of autotrophic (Ra) and heterotrophic (Rh) respiration in the terrestrial biosphere (eq. 3). Note that CO_2 emissions from inland waters (F_{IW}) are largely fed by terrestrial ecosystem respiration (Battin et al., 2023), which is not explicitly included in the flux Re_{terr}. We treat emissions/uptake from coastal water (F_{CWa}) and coastal wetlands (F_{CWL}) separately in this budget, as we assume that they are not included in the estimates of GPP, Ra, Rh or F_{IW}. Note that we did not distinguish F_{LULUCF} in the land CO_2 budget of eq. 2, as we assume this flux to be implicitly included in the other fluxes in that equation. F_{fire} includes emissions from both natural and anthropogenic fires in the landscape. For GPP and net primary production (NPP=GPP-Ra), we used several different estimates for the period 2010-2019 (Table 1). These include estimates from MODIS that are based on remote sensing data on leaf area index (LAI) and the fraction of photosynthetically active radiation (FPAR), from which estimates of GPP and NPP are derived in a semi-empirical way involving a light use efficiency model and gridded information on meteorological drivers as predictors (Zhao et al. 2005). We further used estimates from the Breathing Earth System Simulator (BESS, Jiang & Ryu 2016) and Mandani and Parazoo (2020) that are based on the same remote sensing data, but use different approaches to estimate GPP. Mandani and Parazoo (2020) used a light use efficiency model that was optimized based on flux tower data and inventories (Mandani et al., 2017), while BESS uses a more process-based approach representing the continuous exchange of carbon, water and energy between the biosphere and atmosphere. Finally, we included GLASS data that is based again on the semi-empirical approach of Zhao et al. (2005), but uses improved

LAI and FPAR estimates from combining MODIS and Advanced Very High Resolution Radiometer (AVHRR) remote sensing data.

From FLUXCOM data, we derived estimates of GPP and Re_{terr} that are based on flux-tower observations from the Fluxnet network and upscaled based on machine learning algorithms and meteorological predictor data (Jung et al. 2020). More precisely, we used two versions of this dataset: one that was extrapolated based on remote sensing data only (RS v006), and one that was extrapolated based on both remote sensing data and meteorological forcing data (ERA5). From Yao et al. (2021), we use global estimates of annual soil heterotrophic respiration that are upscaled from 455 observed annual fluxes from the soil respiration database SRDB distributed over 290 sites based on machine learning using meteorological variables, soil moisture and other soil properties, GPP and land cover as predictors. This dataset represents an ensemble of 126 alternative estimates based on different combinations of predictor data sets. We use the mean and range of these estimates as the best estimate and uncertainty range, respectively.

For the land CO_2 budget of the 2010s, we present the median of the GPP estimates mentioned above. A median Re_{terr} was derived from the two FLUXCOM estimates and an alternative data-driven estimate, which we calculated as the sum of *Ra* after GLASS and *Rh* from Yao et al. (2021). For the comparison of land CO_2 budgets of the last three decades, we only used GPP and Re_{terr} from the ERA version of FLUXCOM, since it is the only dataset that covers this entire period (Table 1). Moreover, for the budget of the 2010s decade, this flux estimate was found to be close to the ensemble median of estimates described above (Table S1), which further supports this choice. For comparison, we also derived the median and range of GPP, *Rh*, *Ra* and Re_{terr} for all three decades as simulated by the TRENDY v10 land surface model ensemble that were originally prepared for the Global Carbon Budget 2021 (Friedlingstein et al. 2022). We do not include TRENDY simulations in our budget directly, as DGVM simulations tend to be biased by the poor representation of perturbation, anthropogenic appropriation of biomass, and lateral export fluxes (Ciais et al., 2021). Moreover, we only used simulations from ORCHIDEE v2 (in the following simply referred to as ORCHIDEE), OC-N, LPJwsl, ISBA, ISAM, DLEM, CLM5, and CABLE for which the actual resolution was sufficiently high (0.5°). We excluded ORCHIDEE v3 and SDGVM models from the selection as the spatial patterns of their simulated land-atmosphere net C exchange did not correlate at all with those of the other TRENDY models (see Figure S1).

Harvesting vegetation biomass for wood and crop products, as well as extraction of peat, increases the gap between GPP and Re_{terr}, because this extracted organic matter does not feed directly into Re_{terr} according to our definition of that flux. The same is true for the biomass that is taken out by the grazing of livestock ($F_{grazing}$). While we assume $F_{grazing}$ to represent a flux of C instantaneously and completely returned to the atmosphere, the return of C from the use, decay or burning of wood, crop or peat products ($F_{product\ oxidation}$) is partly delayed and altered by import

and export fluxes across the boundaries of our study area (Table 2). The calculation of $F_{product\ oxidation}$ and $F_{grazing}$ is explained in detail in subsection 2.3.

$F_{grazing}$ is derived from modeled flux rates based on the ORCHIDEE model with prescribed livestock densities and simulated grassland management intensity (Chang et al., 2021). As those simulations cover only the period 1901 to 2012, we scaled the average flux rates from the last 10 years of simulation (2003-2012) to average areas of intensively and extensively managed pastures over the period 2010-2019 derived from HILDA+ (Winkler et al. 2021). For the decades of the 1990s and 2000s, we used the simulation results from Chang et al. (2021) directly. A final flux which is specific to the land CO_2 budget is the atmospheric CO_2 sink related to rock weathering ($F_{weathering}$), which binds CO_2 as dissolved inorganic C which is then exported by rivers to the coast (see C section). For our budget, we used the estimate of average annual $F_{weathering}$ from Zscheischler et al. (2017) after the empirical model developed by Hartmann et al. (2009), assumed to be constant over the last three decades. The individual estimates used for the 2010s' budget are listed in Table S1 in the supplement. Those used for all three decades are listed in Table S2.

Land CH_4 budget

$$F_{land\ CH4} = F_{peat\ CH4} + F_{methanotrophy} + F_{LULUCF} + F_{fire} + F_{IW} + F_{CWa} + F_{CWL} + F_{geo} \quad \text{(eq. 4)}$$

For the land CH_4 budget, we distinguish between peatlands as CH_4 source ($F_{peat\ CH4}$) and terrestrial ecosystems with well-aerated soils, which act as CH_4 sink due to their methanotrophy ($F_{methanotrophy}$) (eq. 4). In addition, we have F_{LULUCF} as net-emission of CH_4, which is related to land use change and land management, and which is neither included in the estimates of $F_{peat\ CH4}$ nor $F_{methanotrophy}$ we use. As data-driven estimates of $F_{peat\ CH4}$ and $F_{methanotrophy}$ are scarce, we resorted to the diagnostic DGVM simulations as synthesized by the Global CH_4 Budget (Saunois et al., 2020) to quantify $F_{peat\ CH4}$ and to the mechanistic methanotrophy model MeMo (Murguia-Flores et al. 2018) to quantify $F_{methanotrophy}$. Note that the MeMo simulations only cover years until 2009, and thus we had to assume the average $F_{methanotrophy}$ over the last ten years of simulation (2000-2009) to be representative for our budget period. For the 2000s and 1990s, we used the published MeMo simulation results directly. Similarly, the DGVM results assembled for the Global CH_4 Budget allowed us to derive ensemble medians and ranges for all three decades. The estimates of F_{LULUCF} were taken from the national inventories collected by UNFCCC. Finally, we include geological emissions of CH_4 (F_{geo}) using data-driven estimates from Etiope et al. (2019), which were recently updated for the VERIFY CH_4 and N_2O budgets (Petrescu et al. 2023). These estimates represent a climatology of average annual fluxes that do not represent interannual variability nor trends at the decadal time scale. We assumed them to be representative for the last three decades. The individual estimates used for the 2010s' budget are listed in Table S3 in the supplement. Those used for all three decades are listed in Table S4.

Land N_2O budget

$$F_{land\ N2O} = F_{soil\ N2O} + F_{fire} + F_{IW} + F_{CWa} + F_{CWL} \quad \text{(eq. 5)}$$

For the land N_2O budget ($F_{land\ N2O}$), direct soil N_2O emissions ($F_{soil\ N2O}$) is the main flux between terrestrial ecosystems and the atmosphere (eq. 5). For a more detailed budget analysis, we split $F_{soil\ N2O}$ into a natural flux component $F_{soil\ N2O,nat}$, and anthropogenic flux components related to management practices such as fertilizer and manure applications and residue management ($F_{soil\ N2O,man}$), as well as indirect emissions related to atmospheric deposition of reactive N ($F_{soil\ N2O,Ndep}$) which were further split into emissions from agricultural ($F_{soil\ N2O,Ndep,agri}$) and other soils ($F_{soil\ N2O,Ndep,other}$). With that last mentioned distinction we account for the fact that the inventory-based assessments of EDGAR and GAINS only report $F_{soil\ N2O,Ndep,agri}$. In general, inventory-based assessments such as EDGAR, UNFCCC, and FAO (see Table 1) cover only emissions from managed lands. Therefore, for $F_{soil\ N2O}$ and $F_{soil\ N2O,nat}$, we resorted to DGVM simulation results as synthesized by the Nitrogen Model Intercomparison Project (NMIP, Tian et al., 2019). For the estimation of N_2O emissions due to atmospheric N deposition on all soils, and on non-agricultural soils in particular, we use simulations results from the DGVM O-CN (Zaehle and Friend, 2010) as they were prepared for the second phase of NMIP, and come up with an alternative data-driven estimate using gridded data of atmospheric N deposition from the European Monitoring and Evaluation Programme (EMEP) and an emission factor of 1% following the guidance of IPCC (2019). From all these specific data sources for the land N_2O budgets, we could derive flux estimates for the last three decades. The individual estimates used for the 2010s' budget are listed in Table S5 in the supplement. Those used for all three decades are listed in Table S6.

2.1.3 Total GHG emissions

Finally, we express the budget of GHG emissions and removals in CO_2 equivalents (CO_2-eq.) using global warming potential at a 100-year time horizon (GWP100), combining flux components from the CO_2, CH_4, and N_2O budgets (sections 2.2.1 and 2.2.2) and using the conversion factors of 27 kgCO_2-eq./kg CH_4 and 273 kg CO_2-eq./kg N_2O proposed by the 6th assessment report (AR6) of the IPCC (IPCC, 2021, Table 7.15). Only for F_{energy} and F_{IPPU}, we used the factor of 29.8 kgCO_2-eq./kg CH_4 proposed by the same source for fossil CH_4 emissions. For the direct anthropogenic emission fluxes F_{energy}, F_{IPPU}, F_{waste} and F_{agri}, we simply summed up the estimated CO_2 equivalents for the individual GHGs. For the land GHG budget ($F_{GHG,land}$), we did the same for F_{fire}, F_{IW}, F_{CWa} and F_{CWL} (eq. 6). Then, we combined the major terrestrial vegetation and soil GHG emissions and sinks ($F_{biomass\&soil}$), which include GPP and Re_{terr} for CO_2, $F_{peat\ CH4}$, $F_{methanotrophy}$ and F_{LULUCF} for CH_4, and $F_{soil\ N2O}$ for N_2O (eq.7). Finally, we obtained $F_{land\ GHG}$ by additionally accounting for F_{geo} for CH_4 as well as $F_{weathering}$ and $F_{product\ oxidation}$ for CO_2 (eq. 6).

$F_{land\ GHG} = F_{fire} + F_{IW} + F_{CWa} + F_{CWL} + F_{biomass\&soil} + F_{geo} + F_{weathering} + F_{product\ oxidation} + F_{grazing}$ (eq. 6)

$F_{biomass\&soil} = \mathrm{GPP} + Re_{terr} + F_{peat\ CH4} + F_{methanotrophy} + F_{LULUCF} + F_{soil\ N2O}$ (eq. 7)

2.2 GHG budgets from top-down estimates

For each of the three GHGs, we use both global, coarsely resolved (≥1°) inversions as well as regional inversions for Europe at a higher spatial resolution (0.5°). Note that the regional inversions do not cover all of our RECCAP2 domain, but are bounded between 15°E to 35°W and 33°N to 73°N, which does not reach the far eastern and western extents of the domain (therefore missing the eastern parts of Ukraine, and most of Greenland and Iceland). However, the excluded area represents less than 4% of the total land area and its contribution to the GHG budgets is likely low compared to the general uncertainties related to atmospheric-inversion estimates (estimates range over a factor of 2 and more). More importantly, regional inversions may be expected to better resolve spatial patterns in GHG sources/sinks at continental scale than global inversions (see Petrescu et al., 2023, Monteil et al. 2020). Therefore, we use these regional inversions for our analysis of spatial patterns in GHG sources and sinks across Europe (section 3).

For our TD CO_2 budget, we use seven global atmospheric inversions based on six inversion models (CAMS, CTE, Jena CarboScope, UoE, NISMON-CO2, CMS-Flux), adjusted for fossil fuel emissions, that were used for the Global Carbon Budget 2021 (Friedlingstein et al., 2022; see this ref. and appendix A4.2 in McGrath et al., 2023 for details). In addition, we use four regional inversions. Three of them (Jena CarboScope Regional, PYVAR-CHIMERE, LUMIA) were used for the VERIFY European budget (McGrath et al., 2023; see this ref. for details on the inversion configurations). The fourth one is a new CIF-CHIMERE inversion, whose configuration is very close to that of the CIF-CHIMERE inversion documented in McGrath et al. (2023), but corrects errors and relies on a prior knowledge of the terrestrial ecosystem fluxes from a ORCHIDEE-MICT (Guimberteau et al., 2018) simulation forced with the ERA5 reanalysis meteorological data. While all of these inversions allow us to derive a TD budget representative for the decade 2010-2019, three of the global inversions further allow us to compare TD budgets for the last three decades. For the CH_4 budget, we use the global inversions that were produced for the global methane budget GMB2020 (Saunois et al. 2020). That ensemble comprises 22 inversions, and covers the period 2000-2017, thus allowing us to derive TD budgets for the last two decades, though the second decade not being fully covered. Further, that ensemble is split into inversions based on ground based mole fraction measurements (XCH_4, 11 SURF inversions) and such based on satellite-based observations of atmospheric XCH_4 (11 GOSAT inversions). In addition, we use three regional inversions (CTE-CH4, FLExKF, FLEXINVERT) that have been prepared and used

for the VERIFY European budget (Petrescu et al. 2023). These estimates cover the full period 2010-2019. For the N_2O budget, we use five global inversions that were produced and used for the global N_2O budget $GN_2OB2020$ (Tian et al. 2020). Those inversions only cover the years 2000-2016, again allowing us to derive TD budgets for the last two decades, though the more recent decade not being fully covered. Finally, we include one regional inversion (FLEXINVERT) that was prepared and used for the VERIFY European budget (Petrescu et al. 2023) in our TD budget for 2010-2019.

2.3 Land C budget

For the assessment of the land C budget, we slightly adapted the accounting scheme proposed by Ciais et al. (2022) (Fig. 2). This scheme defines the net ecosystem exchange of C (NEE_C) as the sum of all C exchange fluxes between land, inland water, and coastal ecosystems or pools of biological products and the atmosphere, all in units of mass of C (eq. 8). These flux components correspond to flux components of the land CO_2 and CH_4 budgets, while we consider exchange fluxes of volatile organic C and C monoxide to be negligible. Note that we did not include F_{LULUCF}, which represents a difference between GPP and RE_{terr} over land affected by land use change and land management. This flux is thus assumed to be implicitly included in our estimates of GPP, Re_{terr} and F_{fire} (in combination with changes by natural drivers), plus the oxidation of agricultural and forestry products and grazing fluxes. Thus, to avoid double counting, we omitted F_{LULUCF} from our budget. Nevertheless, we use estimates of F_{LULUCF}, and more specifically of land use change emissions (F_{LUC}), for comparison and discussion (section 4). The F_{LUC} estimates are derived from two different bookkeeping models: the model by Houghton and Nassikas (2017) (hereafter H&N) and the Bookkeeping of Land Use Emissions model (BLUE, Hansis et al. 2015). We use estimates from H&N as prepared for the Global Carbon Budget 2020 (Friedlingstein et al. 2020), which used land use data from LUH2 (Hurtt et al. 2020). For BLUE, we used data from Ganzenmüller et al (2022) which applied that model to two different land use data sets: LUH2 and HILDA+ (Winkler et al. 2021). Note that bookkeeping model estimates of F_{LUC} only target changes in C stocks due to land use change and harvest, while ignoring forest demography. This may lead to a smaller estimated C sink compared to F_{LULUCF} from inventories, which also account for the latter (Grassi et al., 2023).

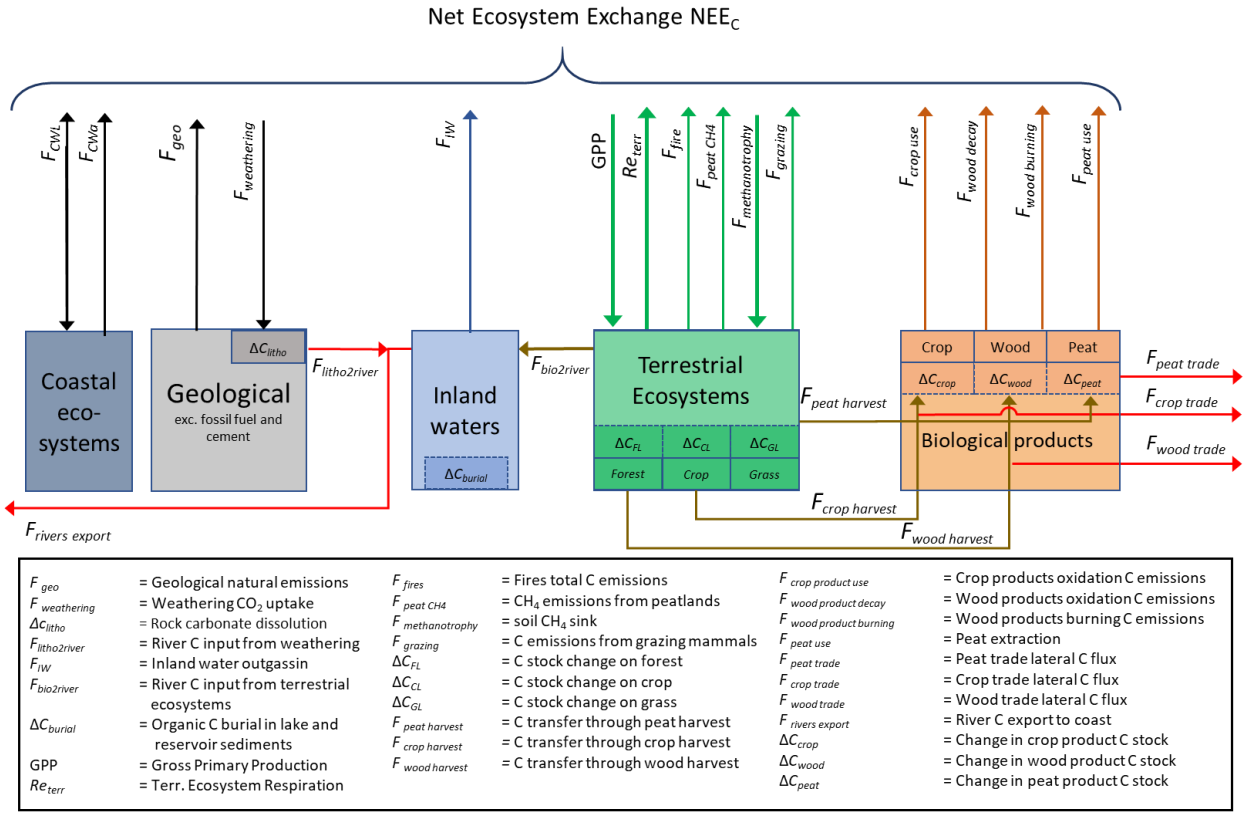

Figure 2: Detailed RECCAP2 accounting framework for the land C budget (adapted from Ciais et al. 2022).

$$NEE_C = F_{geo} + F_{weathering} + F_{IW} + F_{CWa} + F_{CWL} + GPP + Re_{terr} + F_{fires} + F_{peat\ CH4} + F_{methanotrophy} + F_{grazing} + F_{crop\ use} + F_{wood\ decay} + F_{wood\ burning} + F_{peat\ use} \quad \text{(eq. 8)}$$

$$\Delta C_{land} = NEE_C + F_{river\ export} + F_{crop\ trade} + F_{wood\ trade} + F_{peat\ trade} \quad \text{(eq. 9)}$$

For the land C storage budget (ΔC_{land}) of Europe, we further take into account lateral net exports of C from the RECCAP2 region Europe through river transfers ($F_{river\ exports}$) and the net trade of crop, wood, and peat products ($F_{crop\ trade}$, $F_{wood\ trade}$, and $F_{peat\ trade}$, respectively) (eq. 9). $F_{crop\ trade}$ and $F_{wood\ trade}$ are derived from the corresponding FAO databases of product flows per country and year (FAOSTAT, https://www.fao.org/faostat/en/#data, last accessed 2023-06-28) using conversion factors representing dry mass content of harvested products and C content of dry mass. For $F_{wood\ trade}$, we used the conversion factors proposed by IPCC (2019). For $F_{crop\ trade}$, we build on the conversion factors proposed by Ciais et al. (2008) (see Table S7 in the supplement). The FAOSTAT data gives annual amounts of imports and exports to and from each country of our study domain, however without detailing the origin of imports and the destiny of exports.

Aggregating to the European scale, we report thus only net-exports, in which trade fluxes between the countries of our study domain balance each other out. $F_{peat\ trade}$ was derived from Hirschler & Oldenburg (2022) (see Table 1). For $F_{crop\ trade}$ and $F_{wood\ trade}$, we could directly derive estimates for each of the last three decades. For $F_{peat\ trade}$, we had to assume that the inventory-based estimate Hirschler & Oldenburg (2022) for the 2010s is also a good estimate for the two preceding decades. As $F_{peat\ trade}$ is a very small flux compared to $F_{crop\ trade}$ and $F_{wood\ trade}$, we assume a limited impact of this assumption in the overall uncertainties of our C budget.

Then, we estimate the stock changes in the three categories of biological products: ΔC_{wood}, ΔC_{crop}, and ΔC_{peat}. These C stock changes are calculated as the budget of harvest, use, decay and/or burning of the products, and the net-export of the products out of Europe (eqs. 10-12). For crop and wood products, the harvest fluxes ($F_{crop\ harvest}$ and $F_{wood\ harvest}$, respectively) are derived from the FAOSTAT databases and conversion factors just as the corresponding trade fluxes. For crop products, we assume that there is no change in product stocks at annual time-scales (ΔC_{crop} = 0), and the C flux to the atmosphere which is related to consumption of crop products ($F_{crop\ use}$) equals the difference between $F_{crop\ harvest}$ and $F_{crop\ trade}$. For wood products, we use the Tier 2 approach proposed by IPCC (2019), assuming that all fuel wood is burned within one year ($F_{wood\ burn}$) and estimating oxidation of all other wood products ($F_{wood\ decay}$) based on first order decay functions with product-specific half-lives (IPCC, 2019).

$$\Delta C_{wood} = F_{wood\ harvest} + F_{wood\ decay} + F_{wood\ burning} + F_{wood\ trade} \quad \text{(eq. 10)}$$

$$\Delta C_{crop} = F_{crop\ harvest} + F_{crop\ use} + F_{crop\ trade} \quad \text{(eq. 11)}$$

$$\Delta C_{peat} = F_{peat\ harvest} + F_{peat\ use} + F_{peat\ trade} \quad \text{(eq. 12)}$$

In addition, we use alternative estimates of $F_{crop\ harvest}$, $F_{wood\ harvest}$, $F_{wood\ decay}$, $F_{wood\ burn}$, and $F_{crop\ use}$ from an updated version (v4) of the spatialized product presented in Byrne et al. (2023) after the ideas of Ciais et al. (2022) and Deng et al. (2022). These annual maps are also based on trade statistics from the Food and Agriculture Organization of the United Nations (FAO; http://www.fao.org/faostat/en/#data, last access: 15 August 2023) and on energy statistics from the International Energy Agency (IEA; https://wds.iea.org/wds/, last access: 15 August 2023) that have been converted to carbon equivalent and disaggregated with high-resolution proxy data (satellite-derived NPP, population or livestock maps, etc.). For all fluxes included in the C stock budgets of wood and crop products, we derived annual fluxes which we averaged over each of the last three decades. ΔC_{peat} is calculated from the average annual flux of peat harvest ($F_{peat\ harvest}$), consumption ($F_{peat\ use}$) and trade fluxes ($F_{peat\ trade}$) (eq. 12) reported in Hirschler & Osterburg (2022). As mentioned before, we only have fluxes as representative for the 2010s, which we had to use as well as first-order estimates for the preceding two decades.

$F_{river\ export}$ is taken from spatially explicit estimates published by Zscheischler et al. (2017) after the predictive models of Hartmann et al. (2009) and Mayorga et al. (2010). In our accounting

framework, $F_{river\ export}$ is fed by inputs from lithosphere ($F_{litho2river}$) and the biosphere ($F_{bio2river}$) (eq. 13).

$$F_{river\ export} = F_{litho2river} + F_{bio2river} - F_{IW} + \Delta C_{burial} \text{ (eq. 13)}$$

$F_{litho2river}$ represents inputs in the form of carbonate alkalinity which we assume to be non-reactive during transport. This flux incorporates both the weathering CO_2 sink $F_{weathering}$ as well as inputs from dissolving lithogenic carbonates, which we treat as change in lithospheric C stocks (ΔC_{litho}). Both $F_{weathering}$ and ΔC_{litho} are taken from the same spatial dataset by Zscheischler et al. (2017). In contrast, $F_{bio2river}$ represents organic carbon and CO_2 inputs from the biosphere which feed the evasion of CO_2 and CH_4 from inland waters to the atmosphere (F_{IW}) as well as the burial of C in aquatic sediments (ΔC_{burial}) (eq. 13). However, only one part of $F_{bio2river}$ is evading or buried, and the remaining fraction is exported to the coast (as part of $F_{river\ export}$). At decadal time scales, we assume that change of C stock of the inland water compartment is equal to the C burial rates ΔC_{burial}, for which we have estimates of average annual fluxes that were statistically upscaled from observations (Mendonça et al. 2017). Based on the independent estimates of the other flux components, $F_{bio2river}$ is estimated based on mass budget closure (eq. 13). Note further that all flux estimates used in this equation are climatologies of average annual fluxes which we assume to be representative for the last three decades, excluding any trends over this timeframe.

For at least the most recent decade of the 2010s, we provide an alternative estimate of ΔC_{land} based on the stock changes in different C pools (eq. 14). In addition to ΔC_{burial}, ΔC_{litho}, and the C stock changes of the product pools (ΔC_{wood}, ΔC_{crop}, ΔC_{peat}) treated above, this approach required independent estimates of biospheric C stock changes in forest, grass- and cropland (ΔC_{FL}, ΔC_{GL}, ΔC_{CL}).

$$\Delta C_{land} = \Delta C_{litho} + \Delta C_{burial} + \Delta C_{FL} + \Delta C_{GL} + \Delta C_{CL} + \Delta C_{wood} + \Delta C_{crop} + \Delta C_{peat} \text{ (eq. 14)}$$

For ΔC_{FL}, we use the estimates from the European Forest Information SCENario Model (EFISCEN) that cover C stock changes in biomass, deadwood, litter and soil C pools (Nabuurs et al., 2018; Petz et al., 2016; Petrescu et al., 2020). EFISCEN uses national forest inventory data on forest age structure and tree species composition and detailed information on management practices to project forest productivity and C stocks. Note that DGVMs represent forest structure and management practices rather rudimentarily, which is an important shortcoming and the main reason we prefer EFISCEN over TRENDY simulations. For ΔC_{GL} and ΔC_{CL}, we assume that the relevant stock changes at decadal time-scale only concern the soil C stocks. The UNFCCC gives inventory-based estimates of ΔC_{GL} and ΔC_{CL} in general, but also separated into grasslands on mineral vs. organic soils. From the FAO (Tier 1), we have inventory-based ΔC_{GL} and ΔC_{CL} estimates for organic soils only.

559 ## 2.4 Analyses of spatio-temporal patterns in GHG budgets from regional inversions

560 The analysis of spatio-temporal variability in GHG budgets from regional inversions was based
561 on the annual net land flux for each GHG as well as for fossil CO_2 emissions. The long-term
562 trend was estimated on a pixel-by-pixel basis through a linear least squares regression for the
563 period reported. We also analyzed continental and regional scale interannual variability (IAV)
564 based on spatially-aggregated detrended fluxes for each GHG separately, as well as the IAV of
565 the GHG net flux expressed in CO_2 equivalent using GWP20 and GWP100.
566 To better understand IAV in GHG budgets, we followed the approach of Bastos et al. (2016) to
567 assess anomalies in the annual budget of each GHG for specific combinations of phases of the
568 North Atlantic Oscillation and the East Atlantic pattern. For this, we used the NAO and EA
569 teleconnection indices calculated by NOAA CPC and available since 1950 at
570 https://ftp.cpc.ncep.noaa.gov/wd52dg/data/indices/tele_index.nh (last access May 2021). We then
571 calculated the boreal winter (Dec-Feb) mean values for each index, over the period 1950-2020.
572 Given the non-stationarity of the teleconnection indices and short periods covered by our
573 observational data, it is likely for results to be sensitive to the period considered (Li et al., 2022).
574 For comparability of our results with those of Bastos et al. (2016), who analysed only CO_2 and
575 only global inversions, we used the upper (lower) terciles of the reference period in Bastos et al.
576 (2016), i.e. 1982-2013 to then define positive (negative) phases of NAO and EA over the
577 common period of 1990-2020.
578 We then estimate the mean GHG anomalies across all years that correspond to each NAO-EA
579 phase combination (NAO+-EA+, NAO+EA-, NAO-EA+, NAO-EA-) for each GHG individually
580 and also for the combined GWP20 and GWP100. Finally, we analyse the corresponding
581 anomalies in temperature and precipitation. For this, we rely on temperature at 2 m above ground
582 and total precipitation from the ERA5 reanalysis (Hersbach et al., 2020), selected for the period
583 1990-2020. The data were deseasonalized and the mean annual anomalies were calculated for the
584 years corresponding to each NAO and EA phase combination.
585
586 ## 2.5 Analyzing spatial patterns of the European land C sink

587 Trends in C sink strength for seven different products from Sec. 2.2 and 2.3 (global inversions;
588 regional inversions; TRENDYv10; FLUXCOM; VPRM; EFISCEN-Space; L-VOD) were
589 determined by linear regression of the annual fluxes across the years 2010-2019 for each pixel. In
590 order to provide possible explanations for the observed trends in sink strength, we additionally
591 examine trends in both climate variables and land use, both of which are potentially important
592 drivers of large-scale spatial variation. For the meteorological variables, the trends in annual
593 mean air temperature, total precipitation, and mean vapor pressure deficit (VPD) from 2010 to
594 2019 were calculated both using all 12 months in the year and using only the months of the
595 growing season (May, June, July, August). The values were aggregated from the 0.125 degree
596 CRUERA dataset as described in McGrath et al (2023), created from re-aligning ERA5-Land re-

analysis with monthly 0.5-degree CRU observations. The VPD was calculated as described by Sedano and Randerson (2014) from the saturated vapor pressure of water and the relative humidity in the CRUERA dataset. Trends in CO_2 land use emissions were calculated using the BLUE model with the Hilda+ land use/land cover map (Ganzenmüller et al., 2022). For visual comparison and interpretation, all results have been aggregated to a spatial resolution of 1.0 degrees.

2.6 Impact of forest disturbances on biomass carbon stocks

2.6.1 Quantification of losses and gains at decadal scale

We used the disturbance map of Senf & Seidl (2021) based on analysis of changes in Landsat reflectances times series. The detection algorithm flags forested pixels (at 30 m) with a year of disturbance (1986-2020) and a severity index between 0 and 1, with 1 being the most severe type (assumed to be a stand replacing event). The disturbance type is unattributed, and it is not distinguished between anthropogenic and natural disturbances. A 30 m pixel is flagged only once during the entire period based on the most severe disturbance, therefore disturbance severities across Europe are probably underestimated. Using manually interpreted reference plots, the mean absolute error on the timing of the disturbance was estimated at +/-3 years. Here we aggregated this disturbance map to 90 m to match the above-ground biomass (AGB) maps, and defined undisturbed forests at 90 m as forests that have not been disturbed from 1986 to 2020.

The AGB maps developed by CCI-ESA (version 3) for the years 2010, 2017 and 2018 (Santoro & Cartus, 2021) were derived from different satellites, leading to potential local biases that need to be corrected before the analysis. The original projection is EPSG:4326 (global) has a resolution of 100 m at the equator, and the maps have been re-projected in EPSG:3035 (90 m). The potential above-ground biomass (AGB*) is the maximum reachable AGB for a forest long after a stand-replacing disturbance. For each map (2010, 2017 and 2018), AGB* was estimated by calculating the 95% quantile of undisturbed forests (based on the disturbance map) at an 18 km resolution (to capture a sufficient number of undisturbed forests at 30 m), then it has been disaggregated back to 90 m to match the original resolution. Assuming that AGB* is similar between AGB maps, the biases between maps have then been corrected locally using a linear correction function (eq. 15-17), with AGB_i^{raw} being the raw AGB data for each year i, and α_i being the matrix of correction factors. Across the European continent, $\alpha_{2010} = 1.01 \pm 0.06$ (mean ± 1 SD), $\alpha_{2017} = 1.00 \pm 0.07$ and $\alpha_{2018} = 0.99 \pm 0.08$, indicating that there is no systematic bias between maps at European scale.

$$AGB_i = \alpha_i AGB_i^{raw} \quad \text{(eq. 15)}$$

$$\alpha_i = \frac{AGB^*}{AGB_i^*} \quad \text{(eq. 16)}$$

$$AGB^{*} = \frac{AGB^{*}_{2010} + AGB^{*}_{2017} + AGB^{*}_{2018}}{3} \qquad \text{(eq. 17)}$$

For disturbed pixels (at 90 m) in a given local area (at 18 km) and a given decade *T* (1990-2000 for example), the loss of biomass (expressed in MtC/year) during the year of disturbance is approximated by eq. 18, where *x* is a pixel disturbed (90 m) during the period *T*, *A* the total area disturbed, U(x) is the mean AGB of undisturbed neighbors at 18 km and s(x) is the severity of the disturbance (aggregated from 30 m to 90 m). The factor 0.5 corresponds to the conversion from dry biomass to carbon stocks. The undisturbed neighbor AGB is used here because the AGB of the pixels impacted by the disturbance is unknown. The gain of biomass of these disturbed forests from the decade *T* to present time (2017-2018) is calculated according to eq. 19.

$$AGB_{loss} = \frac{A}{2} \sum_{x} (s(x) \times U(x)) \qquad \text{(eq. 18)}$$

$$AGB_{gain} = \frac{A}{2} \sum_{x} AGB_{i}(x) \qquad \text{(eq. 19)}$$

The analysis has been conducted separately for four major European biogeographical regions approximated with the country borders: Mediterranean (Spain, Portugal, Italy, Greece, Croatia, Slovenia), Continental (Romania, Bulgaria, Ukraine, Belarus, Czechia, Poland, Hungary, Slovakia), Atlantic (France, Ireland, United Kingdom, Belgium, Netherlands, Germany, Austria, Switzerland) and Boreal (Norway, Finland, Sweden, Denmark, Estonia, Lithuania, Latvia). Uncertainties for the sources and sinks have been estimated using the absolute difference between the 2017 & 2018 maps.

2.6.2 Disentangling the effect of natural disturbances

Natural disturbances - large pulses of tree mortality that originate from abiotic and biotic factors such as fires, strong winds or insect outbreaks - represent serious peril for maintaining healthy and productive forests (MacDowel et al., 2020; Anderegg et al., 2020). Recent studies have shown an increase in forest vulnerability to such disturbances at European level (Forzieri et al., 2021) consistent with the observed widespread decline in forest resilience (Forzieri et al., 2022; Smith et al., 2022) and the reported intensification of forest damages associated to climate-driven events (Pattaca et al. 2023). Emerging signs of C sink saturation and sink decline in European forest biomass have been associated to such increased disturbance regime (Nabuurs et al., 2013; Korosuo et al., 2023) which is expected to be further exacerbated by climate change (Seidl et al., 2014; Anderegg et al., 2022).

Quantifying the contribution of natural disturbances and associated temporal variations is therefore crucial to evaluate properly their effect on the C budget. To this aim, we complement the analyses described in the previous section with an assessment of the biomass losses due to fires, windthrown events and insect outbreaks documented in the Database on Forest Disturbances in Europe (DFDE). The DFDE reports forest damages in terms of timber volume loss aggregated at country level associated to single disturbance events occurring over the period 1950-2019 (Pattaca et al., 2023; Schelhaas et al., 2003) and retrieved from a literature search.

We provide a synthesis of the natural disturbances documented at European scale in the DFDE in terms of relative importance of each single agent type and in terms of temporal trends over the observational period (Pattaca et al. 2023). We point out that spatial extents and temporal coverage of DFDE slightly differ to those utilized as reference in RECCAP2. However, we believe that aggregated estimates can be considered a reasonably good approximation for the scope of this assessment (section 8.2).

3. Bottom-up greenhouse gas budgets of Europe

This section deals with the BU budget of the three GHGs, first presented individually (sections 3.1, 3.2, and 3.3, respectively), then grouping all GHGs using the global warming potential of CH_4 and N_2O at 100 years horizon (section 3.4). The fluxes of our BU budget are presented in Figure 1. For the most recent decade of the 2010s, we listed our best estimates for these fluxes and our assessment of the level of confidence in these numbers in Table 2. We compare our BU estimates of the GHG budgets against atmospheric inversions, the value ranges of which are listed in Table 3. In addition, we reconstruct the development of GHG budgets over the last three decades, i.e. the 1990s, the 2000s and the 2010s, based on a subset of data sources that cover that time frame as completely and as consistently as possible. For a detailed list of fluxes taken from different sources, we refer the interested reader to Tables S1 to S6.

Table 2: Best estimates for the flux components of the European GHG budget 2010-2019.*

	CO_2 emissions		CH_4 emissions		N_2O emissions		GWP_{100} (as CO_2 equivalents)				
Flux	Tg yr^{-1}	Conf.	Tg yr^{-1}	Conf.	Gg yr^{-1}	Conf.	Tg yr^{-1}	Conf.	CO_2	CH_4	N_2O
	Direct anthropogenic emission										
F_{energy}	3 792	***	6.66	*	108	*	4 020	***	94%	4%	1%
F_{IPPU}	321	***	0.08	*	106	--	353	**	91%	1%	8%
F_{waste}	5	*	6.37	*	52	-	191	*	3%	90%	7%
F_{agri}	11	***	10.72	**	78	*	322	***	3%	90%	7%
Total	4 130	***	23.83	*	343	*	4 867	***	85%	13%	2%
	Land budget										
GPP	-20 085	**									
Re_{terr}	16 740	**									
F_{LULUCF}			0.61	*							
$F_{peat\ CH4}$			2.00	--							
$F_{methanotrophy}$			-0.92	*							
$F_{soil\ N2O}$					906	*					
$F_{soil\&biomass}$	-3 345	*	1.69	--	906	*	-3 052	**	110%	-1%	-8%
$F_{grazing}$	484	*					484	*			
$F_{product\ oxidation}$	1 267	**					1 267	**			
$F_{weathering}$	-42	*					-42	*			
F_{geo}			2.50	**			68	-			
F_{fire}	34	*	0.06	*	3.2	*	36	*	93%	4%	2%
F_{IW}	191	*	4.10	*	17	-	306	*	62%	36%	2%
F_{CWa}	25	*	0.01	-	4.8	*	27	*	94%	1%	5%
F_{CWL}	-15	-	0.01	-	-0.2	--	-15	-	101%	-2%	0%
Total	-1 400	*	8.37	-	930	*	-920	-	152%	-25%	-28%

*The global warming potential at the 100-year horizon (GWP_{100}) is calculated based on IPCC AR6. We assign different level of confidence to our estimates: very high: ±10% (***), high: ±25% (**), moderate: ±50% (*), low: ±100% (-), and very low (--).

688

Table 3: Comparison of our bottom-up land GHG budgets against top-down estimates from atmospheric inversions.

Part of GHG budget assessed	Method of assessment	Estimated flux in Tg CO_2 yr^{-1}, Tg CH_4 yr^{-1}, or Gg N_2O yr^{-1}		
		Best estimate	Lower estimate	Upper estimate
	CO_2 budget			
$F_{land\ CO2}$	Bottom up, eq. 2	-1 426		
	Global inversions	-958	-1478	185
	Regional inversions	-743	-1013	-593
	CH_4 budget			
$F_{total\ CH4}$	Bottom up	32		
	Global inversions, surface observations	32	22	39
	Global inversions, satellite based	28	25	37
	Regional inversions	36	33	44
$F_{land\ CH4}$ - (F_{fire} +F_{geo})	Bottom up	6		
	Regional inversion (CTECH4)	4		
$F_{peat\ CH4}$	Bottom up	2.0	0.6	3.3
	Global inversions, surface observations	2.0	1.7	8.4
	Global inversions, satellite based	2.1	1.7	4.9
	N_2O budget			
$F_{total\ N2O}$	Bottom up	1 274		
	Global inversions	1 472	682	1 594
	Regional inversion (Flexinvert)	1 331		

689

690 **3.1. CO_2**

691 Direct anthropogenic emissions, which do not include F_{LULUCF} nor F_{LUC} in our assessment,
692 dominate the CO_2 budget, and amount to an average flux of 4.1 Pg CO_2 yr^{-1} over the period 2010-
693 2019 (Table 2). The largest contribution (~90%) of direct anthropogenic emissions is attributed to
694 F_{energy}. Another 8% is attributed to F_{IPPU}. Contributions from F_{agri} and F_{waste} are minor. Apart

from the waste sector, we have a high level of confidence in these estimates of direct anthropogenic CO_2 emissions.

For the land CO_2 budget, our BU estimate gives a net sink of an average 1.4 Pg CO_2 yr^{-1} over the period 2010-2019, which counterbalances about one third of the direct anthropogenic emissions (Table 2). We assign a moderate level of confidence (±50%) based on expert judgment to our estimate of this land sink. Our BU estimate is in the range of global atmospheric inversions, but gives a stronger sink than any of the regional inversions considered here (Table 3). The land CO_2 budget is dominated by the imbalance between gross primary production (GPP) and net ecosystem respiration of terrestrial ecosystems (Re_{terr}), which amounts to about 3.3 Pg CO_2 yr^{-1}. While we have a high level of confidence (i.e. ±25%) in *GPP* and Re_{terr} estimates, the balance between both fluxes is more uncertain. Nevertheless, we still assigned a moderate level of confidence (±50%) to the estimated difference GPP-Re_{terr}. This imbalance between both fluxes is largely due to the anthropogenic appropriation of biomass through the harvest and use of wood and crop products, which does not feed into the ecosystem respiration (see Ciais et al., 2021). This appropriated biomass is returned to the atmosphere through the oxidation of the products, which we estimate at ~1.3 Pg CO_2 yr^{-1}. Note that this flux accounts for the imports and export of products, as well as a Tier 2 assessment of stock changes. We assign a high level of confidence to that estimate (±25%). For a more detailed description of this flux, see section 5. Another ~0.5 Pg CO_2 yr^{-1} is returned from biomass to the atmosphere through grazing by livestock. A still sizable source of CO_2 are inland water emissions of roughly 0.2 Pg CO_2 yr^{-1}. Emissions from coastal waters and wildfires are additional, minor land sources of CO_2 to the atmosphere. Rock weathering and coastal wetlands are minor sinks of CO_2.

Overall, our BU CO_2 budget including direct anthropogenic emissions and the land CO_2 budget gives a net source of ~2.7 Pg CO_2 yr^{-1} for the 2010s. Using the smaller selection of data sources of the different flux components that were available for the last three decades, the estimated net source for the 2010s is slightly higher with ~2.9 Pg CO_2 yr^{-1} (Figure 3). This follows differences in GPP. For a consistent analysis over these three decades, GPP and Re_{terr} are taken solely from FLUXCOM ERA5 dataset. Although the FLUXCOM ERA5 values for GPP are close to the median values derived from all together five estimates, and for Re_{terr} even identical to the three estimates for the 2010s (Table S1), the absolute difference is significant in relation to the CO_2 budget where GPP and Re_{terr} are the dominant fluxes that balance each other out to a large degree.

Figure 3 gives the total CO_2 budget for the last three decades as well as changes in certain fluxes that explain the differences between these decadal budgets. Note that not all fluxes used in the budgets are included in this figure, as for some of these fluxes we only have estimates of average annual fluxes that we have to assume to remain constant across the three decades. That concerns F_{IW}, F_{CWa}, F_{CWL}, and $F_{weathering}$. In addition, we had to assume that F_{fire} did not change between

the 1990s and the 2000s. In this analysis, we put the four direct anthropogenic emissions F_{energy}, F_{IPPU}, F_{waste} and F_{agri} together as F_{direct}. Detailed information on decadal changes in each of these fluxes are given in Table S2 in the supplement.

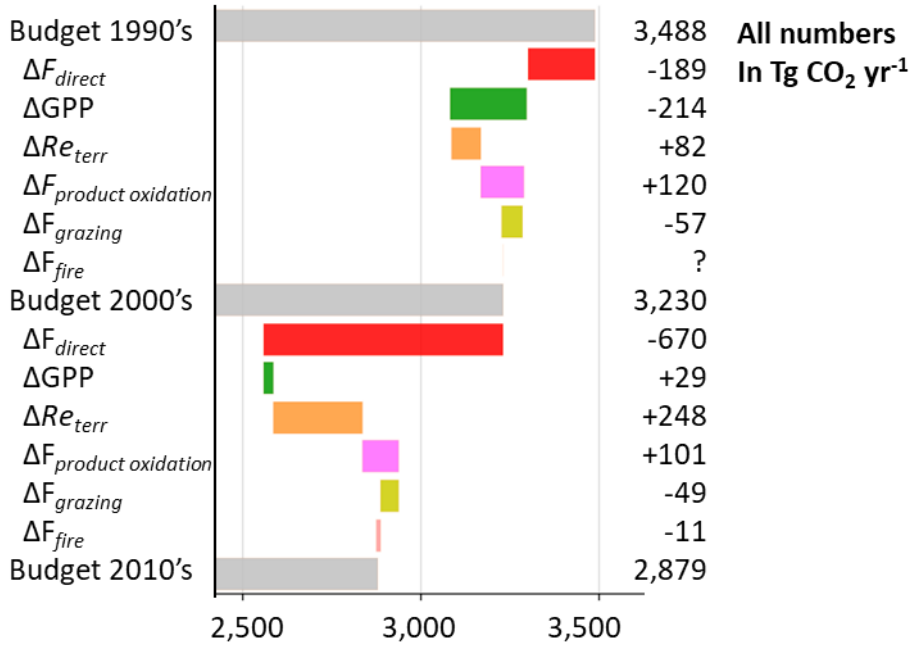

Figure 3: Evolution of European CO_2 budget over the last three decades. Note that there is no estimate for F_{fire} in the 1990s.

We see from Figure 3 that the overall net source has notably decreased from the 1990s to the 2000s and further to the 2010s. For the 2000s, our estimate of 3,230 Tg CO_2 yr^{-1} is quite close to the estimate by Luyssaert et al. (2012) of ~3,270 Tg CO_2 yr^{-1} for RECCAP1. However, as RECCAP1 excluded Ukraine, Belarus, and Rep. of Moldova, a direct comparison is difficult. From the 1990s to the 2000s, the reduction in the net source of 258 Tg CO yr^{-1} is largely due to reductions in F_{direct}. However, 69 Tg CO_2 yr^{-1} are still due to an increase in the land CO_2 sink. Between these two decades, we find an important increase in average GPP which is only partly offset by an increase in Re_{terr}. We further find an increase in $F_{product\ oxidation}$ and a decrease in $F_{grazing}$. The sum of changes in these fluxes give an overall increase in oxidation of anthropogenically appropriated biomass of 64 Tg CO_2 yr^{-1} within Europe, which offsets another fraction of the increase in GPP although it may include imported biomass from other RECCAP2 regions.

From the 2000s to the 2010s, the reduction in F_{direct} is about 3.5 times as strong as between the 1990s and 2000s. A similar trend was found for EU27+UK by the VERIFY synthesis (McGrath et al., 2023; Petrescu et al., 2021a) that shows a significant decrease in net-CO_2 emissions driven by decreased fossil fuel emissions (F_{Energy} + F_{IPPU}) that sets in around 2005 and continues until the end of our RECCAP2 period. However, this reduction in direct anthropogenic emissions was partly offset by a strong reduction in the land CO_2 sink of 318 Tg CO_2 yr^{-1} (Figure 3). From the 2000s to the 2010s, even if average GPP slightly decreased, it was accompanied by a strong increase in Re_{terr} that is three times higher than that between the 1990s and the 2000s. Changes in $F_{grazing}$ and $F_{product\ oxidation}$ are comparable to that between the 1990s and the 2000s, with a similar increase in emissions from anthropogenically appropriated biomass back to the atmosphere of 52 Tg CO_2 yr^{-1}. Being generally a minor flux in the European CO_2 budget (Tables 3, S2), also changes in F_{fire} have only a small influence on decadal trends in the CO_2 budget (Figure 3).

Overall, according to our BU assessment, the strength of the land CO_2 sink has decreased from 1.5 Pg CO_2 yr^{-1} in the 1990s to 1.3 Pg CO_2 yr^{-1} in the 2010s (Table S2). This is comparable to the TD estimates from global inversions that give a decrease from 1.3 (0.3–1.5) Pg CO_2 yr^{-1} to 1.0 (0.0–1.5) Pg CO_2 yr^{-1}, respectively (ensemble median and range, Table S2). For the 2000s, however, our BU estimate diverges substantially from global inversions, with 1.6 Pg CO_2 yr^{-1} vs 0.9 (0.1–1.2) Pg CO_2 yr^{-1}, respectively (Table S2). Thus, while TD assessments show the weakest land CO_2 sink for the 2000s, our BU assessment identifies the 2000s as the decade with the strongest land CO_2 sink.

3.2. CH_4

For the European CH_4 budget 2010-2019, our BU estimates give an average net emission of ~32 Tg CH_4 yr^{-1}. We assign a moderate level of confidence (up to ±50%) to this estimate. This BU estimate lies within the range of TD estimates from the two global inversion ensembles used in GMB2020 by Saunois et al. (2020), of which one is based on surface observations of atmospheric CH_4 concentrations (22 to 39 Tg CH_4 yr^{-1}, median of 32 Tg CH_4 yr^{-1}) and one based on satellite observations (25 to 37 Tg CH_4 yr^{-1}, median of 28 Tg CH_4 yr^{-1}, Table 3). In contrast, our BU estimate lies on the far lower end of TD estimates from regional inversions (33 to 44 Tg CH_4 yr^{-1}, Table 3). About three quarters of European CH_4 emissions, i.e. ~24 Tg CH_4 yr^{-1}, can be attributed to F_{direct}, i.e. the sum of direct anthropogenic emissions F_{energy}, F_{IPPU}, F_{waste}, and F_{agri}. With ~11 Tg CH_4 yr^{-1}, the agricultural sector contributes nearly half of direct emissions. With 6 to 7 Tg CH_4 yr^{-1}, the energy and the waste sector are similarly less strong emitters, while contributions of the industrial production and product use sector are minor.

About one quarter of CH_4 emissions is attributed to natural sources. In contrast to F_{direct}, which is estimated largely from inventory data, we assign a low level of confidence to our BU estimate of the land CH_4 budget. The two largest sources in our land CH_4 budget are inland waters and geological emissions with 4.1 and 2.5 Tg CH_4 yr^{-1}, and a moderate (±50%) and high (±25%) level

of confidence, respectively (Table 2). Peatland emissions are very likely sizable, but very poorly constrained (range of 0.6 to 3.3 Tg CH_4 yr^{-1}, Table S3). Emissions from fires, coastal waters and coastal wetlands do not play a significant role in the land CH_4 budget of Europe. The regional inversion CTE-CH4 gives an estimate for the land CH_4 budget excluding geological and fire emissions. This TD estimate of a net-source of 4.2 Tg CH_4 yr^{-1} is comparable to our corresponding BU estimate of 5.1 Tg CH_4 yr^{-1}.

When comparing the CH_4 budgets for the 1990s, 2000s and 2010s, the BU estimates give a strong decrease in the overall net sources (Figure 4). Note that we have split changes in F_{direct} into changes in F_{agri} as the single largest contributor and the sum of changes in the remaining flux components F_{energy}, F_{IPPU}, and F_{waste}. From the 1990s to the 2010s, the net source decreased by about one quarter, mainly due to reductions in F_{energy}, F_{IPPU}, and F_{waste}. Changes in natural sinks and sources do not appear to be important for the overall CH_4 budget. Note however that for F_{IW} as the largest natural source, no assessment of long-term trends exists.

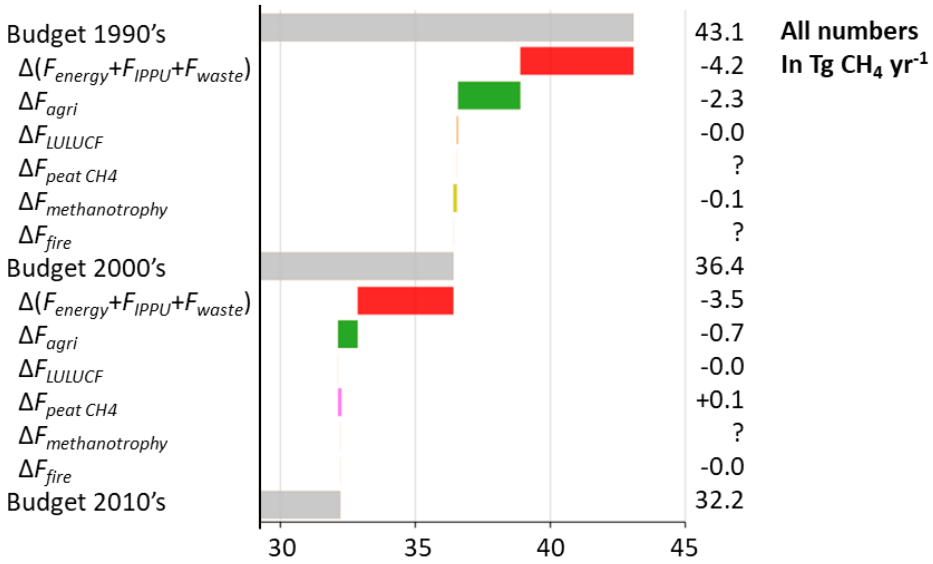

Figure 4: Evolution of European CH_4 budget over the last three decades. Note that there is no estimate for F_{fire} in the 1990s.

Our CH_4 net emission estimate of 36 Tg CH_4 yr^{-1} for the 2000s is higher than the RECCAP1 estimate of 28 Tg CH_4 yr^{-1} by Luyssaert et al. (2012) for the period 2001-2005. The direct comparison is however difficult as the RECCAP1 analysis excluded the Eastern European countries of Rep. of Moldova, Ukraine and Belarus. For EU27+UK, a detailed, inventory based analysis of trends in direct CH_4 emissions from the period 2000-2009 to the RECCAP2 period 2010-2019 was given by Petrescu et al. (2023). They found a decrease in direct emissions by

16.5%, mainly due to reductions in F_{waste} (-10.1%) and F_{energy} (-4.4%). This is comparable to the relative reduction in F_{direct} by 15% from the 2000s to the 2010s identified in our study (see Table S4). However, from the global inversions, we do not see a trend from the 2000s to 2010s, with TD estimates of net source of 32 (23 – 42) Tg CH_4 yr^{-1} vs. 32 (22 – 39) Tg CH_4 yr^{-1}, respectively (median and range, Table S4). Similarly, Petrescu et al. (2023) were not able to confirm the trends from their BU assessment through TD estimates.

3.3. N_2O

For the European N_2O budget 2010-2019, our BU estimates give an average total emission of ~1.3 Tg N_2O yr^{-1}. We assigned a moderate level (±50%) of confidence to this estimate. Our BU estimate is within the range of TD estimates from global inversions used in Tian et al. (2020) (0.7 to 1.6 Tg N_2O yr^{-1}, median of 1.5 Tg N_2O yr^{-1}), and very close to the regional TD estimate from Flexinvert that was used by Petrescu et al. (2023) (1.3 Tg N_2O yr^{-1}, Table 3). In our bottom-up estimate, we attribute only about one quarter of emissions to F_{direct}, to which all four flux components, i.e. F_{energy}, F_{IPPU}, F_{waste}, and F_{agri}, contribute substantially. Note that for F_{agri}, we only include emissions from manure management and biomass burning. Emissions due to fertilizer and manure application as well as residue management are put together as the soil management flux $F_{soil\ N2O,man}$ that is a component of the soil emission flux $F_{soil\ N2O}$, and thus of the land N_2O budget, which we keep separate from F_{direct}.

From the different inventories we use for our budget, we get quite similar estimates for F_{energy} and F_{agri}. However, since the inventories partly use similar activity data and emission factors, we assume only a moderate level of certainty. For the estimate of F_{IPPU}, we are less confident, because the inventory based estimates considered in our study range from 58 Gg N_2O yr^{-1} (UNFCCC) to 210 Gg N_2O yr^{-1} (EDGAR) (see Table S5). Here we assign a very low level of confidence. Similarly, we assign a low level of confidence to F_{waste} for which estimates range from 42 Gg N_2O yr^{-1} (UNFCCC) to 76 Gg N_2O yr^{-1} (GAINS).

The land N_2O budget, which accounts for three quarters of the total emissions, is dominated by soil N_2O emissions ($F_{N2O,soil}$, about 97% of the land N_2O budget). We are confident that the real value for $F_{N2O,soil}$ lies within ±50% ('moderate' level of confidence) of our estimate of ~0.93 Tg N_2O yr^{-1}. Moreover, 0.68 Tg N_2O yr^{-1} of $F_{N2O,soil}$ can be attributed to $F_{soil\ N2O,man}$, while atmospheric deposition of reactive N ($F_{soil\ N2O,Ndep}$) is responsible for another 0.07 Tg N_2O yr^{-1} of soil indirect emissions, and the remaining 0.17 Tg N_2O yr^{-1} can be attributed to natural background emissions $F_{N2O,soil,nat}$ (Table S5). The remaining emissions in the land N_2O budget stem mainly from inland and coastal waters (Table 2). Note further that these fluxes are not fully natural. In Europe, about two thirds of inland water emissions can be attributed to anthropogenic

N inputs from fertilizer, manure and sewage water (Petrescu et al., 2023 based on Yao et al., 2020).

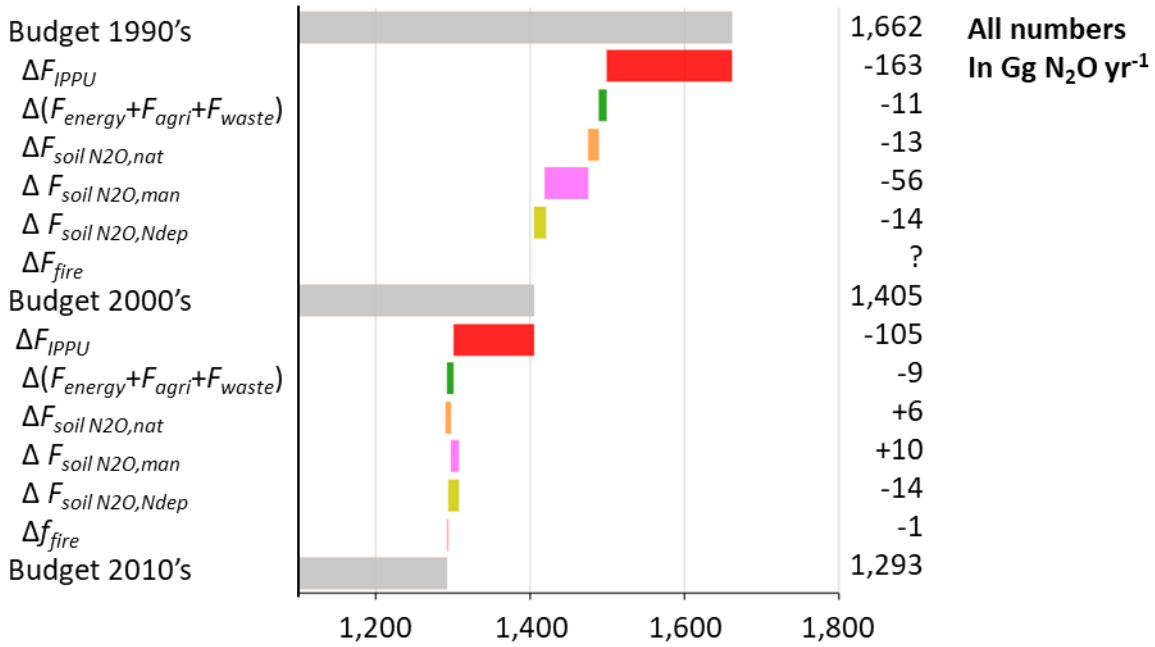

Figure 5: Evolution of European N_2O budget over the last three decades. Note that there is no estimate for F_{fire} in the 1990s.

Figure 5 shows the evolution of decadal N_2O budgets since the 1990s, including the responsible flux changes. From the 1990s to the 2010s, total emissions of N_2O have decreased by about one fifth, mainly due to reductions in F_{IPPU}. From the 2000s to the 2010s, the decrease in our BU emissions is supported by a similar decrease in TD budgets from 1.6 (0.9-1.7) Tg N_2O yr^{-1} to 1.5 (0.6-1.6) Tg N_2O yr^{-1} , respectively, derived from global inversions (median and range; see Table S6). This decrease in net emissions is largely due to a reduction in F_{IPPU}. In contrast, F_{energy}, F_{waste}, and F_{agri} remained relatively constant. As mentioned before, we see a huge spread in different estimates of F_{IPPU}. However, we see a strong decline in F_{IPPU} over the three decades from all three inventories we used for this flux (UNFCCC, EDGAR, GAINS), with a decline that ranges from 141 Gg N_2O yr^{-1} (EDGAR) to 339 Gg N_2O yr^{-1} (GAINS). Interestingly, for the 2000s, the spread between these three inventory-based estimates is quite low, with estimates ranging from 210 to 226 Gg N_2O yr^{-1} only (Table S6). For the 1990s and the 2010s there is a much more pronounced spread between the different data sources that explains the difference in flux changes over the three decades between the different estimates. Despite the large

uncertainties related to F_{IPPU}, we can conclude that reductions in this flux are the most important driver behind reduction in total N_2O emissions.

From the 1990s to the 2000s, there appears to be a notable reduction in $F_{soil\ N2O,man}$, followed by a slight increase to the 2010s. Note that both EDGAR and FAO agree on this trend. For $F_{soil\ N2O,Ndep}$, we derived a continuously-decreasing trend from 99 Gg N_2O yr^{-1} in the 1990s to 71 Gg N_2O yr^{-1} in the 2010s based on EMEP data, the only data source that covers all soils. Comparing EMEP estimates for agricultural soil only ($F_{soil\ N2O,Ndep,agri}$), we see very similar trends and flux sizes from GAINS and EDGAR (see Table S6). In contrast, simulations with O-CN give $F_{soil\ N2O,Ndep}$ that would increase from 106 Gg N_2O yr^{-1} in the 1990s to 135 Gg N_2O yr^{-1} in the 2010s. This may be explained by the fact that with the model OC-N, $F_{soil\ N2O,Ndep}$ is calculated as difference between simulations with and without atmospheric deposition of N, and thus accounts also for indirect effects on N_2O emissions through fertilizing effects and accumulation of N in biomass, litter and soil organic matter. Depending on the residence time in these organic N pools, a historically increased N-deposition may have a certain legacy effect on N_2O emissions. In contrast, the EF-based methods account only for N_2O emissions from direct (de-)nitrification of deposited reactive N itself, and thus only accounts for the instantaneous effect of deposition on N_2O emissions. Overall, for $F_{N2O,soil}$, i.e. the sum of $F_{soil\ N2O,man}$, $F_{soil\ N2O,Ndep}$ and the natural background flux $F_{N2O,soil,nat}$, and largest source of N_2O, our BU assessment gives a slight decrease from the 1990s to 2000s, but there is no notable trend between the 2000s and the 2010s. That agrees with Tian et al. (2020), who did not find a notable trend in soil N_2O emissions for Europe over the last two decades. The decrease from the 1990s to the 2000s may be explained by the EU nitrate directive which has led to a decrease of manure and fertilizer application during the 2000s, which may have led to a subsequent decrease in N_2O emissions (Velthof et al., 2014).

3.4. All GHGs

When we combine the three GHGs for the decade of the 2010s, we obtain a total CO_2-equivalent emission of 4.87 Pg CO_2-eq. yr^{-1} for direct anthropogenic emissions. For the land budget, we obtain a net sink of -0.92 Pg CO_2-eq. yr^{-1}. However, while we have a high level of confidence in the estimated direct emissions, our level of confidence in the land budget is rather low (Table 2). F_{energy} contributes ~80% to direct anthropogenic emissions. CO_2 dominates the CO_2-eq. emissions of both F_{energy} and F_{IPPU} (>90%, Table 2). In contrast, CH_4 dominates the CO_2-eq. emissions of F_{waste} and F_{agri} (~90% in each case).

The land GHG budget is dominated by the strong land CO_2 sink, of which only one third is counterbalanced by net CH_4 and N_2O emissions. Also Luyssaert et al. (2012) had found the European land budget to be a net-sink of GHGs. In contrast, Tian et al. (2016) found the European land budget to be a net-source based on a BU assessment, while a TD assessment showed the budgets to be close to neutral with a huge range of uncertainties. As most important flux components, the net-exchange between plant biomass, vegetation and atmosphere

($F_{soil+biomass}$), as well as the oxidation of harvested products ($F_{product\ oxidation}$) are dominated by CO_2. However, as these fluxes partly balance each other, the overall dominance of CO_2 in the land GHG budget diminished. As a component of the final net land GHG sink of -0.92 Pg CO_2-eq. yr^{-1}, the inland water emissions of 0.31 Pg CO_2-eq. yr^{-1} become an important flux component. While ~62% of F_{IW} are attributed to CO_2, CH_4 has a sizable contribution of 36%, which demonstrates the significant role of this GHG in the land budget. The contribution of N_2O in F_{IW} is nearly negligible. Moreover, the weight of N_2O emissions in the land GHG budget is largely due to soil emissions, of which the major proportion represents anthropogenic perturbations through management and atmospheric deposition of reactive nitrogen (see section 3.3).

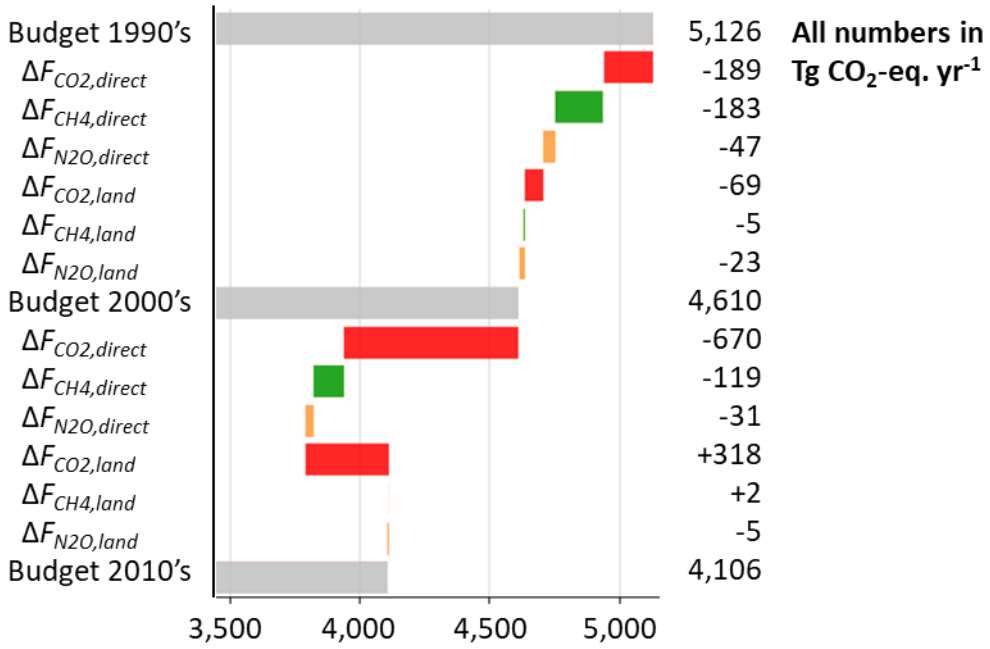

Figure 6: Evolution of European greenhouse gas budget over the last three decades, reported as global warming potential in CO_2 equivalents at 100-year horizon.

Figure 6 shows the evolution of the European GHG budget over the last three decades, summing up direct emissions and land budgets of CO_2, CH_4, and N_2O, and expressing their sum using AR6 global warming potential at the 100-year horizon. The figure further lists how changes in direct emissions vs. changes of the land budgets of the three GHGs contributed to the changes in the GHG budgets between the three decades. Note that for the last decade, the net-emissions here are slightly higher than reported in Table 2, mainly following the lower land CO_2 sink resulting from a narrower selection of datasets covering better the three decades (see section 2.1.2). From the 1990s to the 2010s, net emissions decreased by nearly one fourth. From the 1990' to 2000s, this decrease amounted to ~0.5 Pg CO_2-eq. yr^{-1}, of which about two thirds were due to reductions in direct emissions of CH_4 and CO_2. From the 2000s to the 2010s, net emissions decreased by another ~0.5 Pg CO_2-eq. yr^{-1}, which was mainly due to net decrease in direct CO_2 emissions of

similar size. From the 1990s to the 2000s, the strength in the land CO_2 sink slightly increased, whilst it decreased from the 2000s to the 2010s, largely off-setting the effect of reduced direct emissions of the other two GHGs CH_4 and N_2O. Changes in the land budgets of CH_4 and N_2O are small compared to those in other sectors.

4 Land carbon budget

4.1 Land carbon budget of the period 2010 to 2019

We describe the flux-based C budget of Europe following an adaptation of the scheme proposed by Ciais et al. (2022), which is depicted in Figure 2. The C budget includes CO_2 and CH_4 fluxes from the land GHG budgets in C units (Figure 1), but in addition also changes in C stocks in the biosphere and of biological products, and lateral exchange fluxes between different C stocks and across the boundaries of our study region. Table 4 lists estimates of the different fluxes and stock changes derived from different datasets. Flux names highlighted by an "*" indicate estimates which we finally used in our budget. Other fluxes are listed for comparison.

In our land C budget, we distinguish four compartments that are in exchange with the atmosphere and with each other: the geological compartment, inland waters, terrestrial ecosystems, coastal ecosystems and the biological product pools (Figure 2, Table 4). Terrestrial ecosystems are in the center of the land C budget, with GPP and Re_{terr} being the most important exchange fluxes with the atmosphere. We have calculated the best estimates of GPP and Re_{terr} for our budget as the median values from five and three estimates, respectively, avoiding estimates from land surface models. With the exception of the GLASS estimates of GPP, the individual estimates for each of these two fluxes are very close, and we have a high level of confidence in both GPP and Re_{terr}. In absolute terms, these best estimates are at the lower value range of corresponding flux estimates simulated by the land surface models of the TRENDY v10 ensemble (Table 4). A general overestimation of both fluxes by DGVMs can be explained by the poor representation of perturbation, anthropogenic appropriation of biomass, and lateral export fluxes (Ciais et al., 2021) – the reason for which we avoid using these data.

The difference between GPP and Re_{terr} would result in a net uptake of 0.9 Pg C yr^{-1} by terrestrial ecosystems from the atmosphere. Other exchange fluxes between terrestrial ecosystems and the atmosphere, i.e. F_{fire}, $F_{peat\ CH4}$ and $F_{methanotrophy}$, are of minor importance. The accumulation of C in the biosphere is however diminished to ~0.4 Pg C yr^{-1} by emissions from grazing livestock ($F_{grazing}$), from harvested wood ($F_{wood\ harvest}$), crop ($F_{crop\ harvest}$) and peat ($F_{peat\ harvest}$) products. Another ~0.1 Pg C yr^{-1} are exported from soils to the inland water network ($F_{bio2river}$).

Table 4: Flux estimates (Tg C yr^{-1}) for the European land C budget 2010-2019. (* behind flux name indicates estimates used in budget). We assign different level of confidence to our estimates: very high: ±10% (***), high: ±25% (**), moderate: ±50% (*), low: ±100% (-), and very low (--).

	Estimated flux in Tg C yr^{-1}			
Flux	Best estimate	Range	Conf.	Source
		Terrestrial Ecosystems		
ΔC_{FL}	-130			EFISCEN
ΔC_{FL}	-133			FAO Tier 1
ΔC_{FL} *	-131		*	Median of above
ΔC_{CL} *	22		-	UNFCCC
$\Delta C_{CL,organic\ soils}$	14.7			UNFCCC
$\Delta C_{CL,mineral\ soils}$	7.9			UNFCCC
$\Delta C_{CL,organic\ soils}$	26.3			FAO Tier 1
ΔC_{GL*}	10		-	UNFCCC
$\Delta C_{GL,organic\ soils}$	14			UNFCCC
$\Delta C_{GL,mineral\ soils}$	-2			UNFCCC
$\Delta C_{GL,organic\ soils}$	1.4			FAO Tier 1
		Coastal Ecosystems		
F_{CWa} *	6.9		*	Rosentreter et al., 2023
F_{CWL} *	-4.2		-	Rosentreter et al., 2023
		Biological products		
$F_{crop\ harvest}$ *	-224		**	FAO
$F_{crop\ harvest}$	-256			Byrne et al., 2023
$F_{wood\ harvest}$ *	-142		**	FAO
$F_{wood\ harvest}$	-140			Byrne et al., 2023
$F_{peat\ harvest}$ *	-10		**	Hirschler & Osterburg, 2022
$F_{crop\ use}$ *	207		*	based on FAO, eq. 13
$F_{crop\ use}$	314			Byrne et al., 2023
$F_{wood\ decay}$ *	94		*	FAO
$F_{wood\ burning}$ *	34		*	FAO
$F_{wood\ decay}$	16			Byrne et al., 2023
$F_{wood\ burning}$	63			Byrne et al., 2023
$F_{peat\ use}$ *	9.7		**	Hirschler & Osterburg, 2022
$F_{product\ oxidation}$ *	346		*	sum of 4 fluxes above
$F_{crop\ trade}$ *	17		**	FAO
$F_{wood\ trade}$ *	6		**	FAO
$F_{peat\ trade}$ *	-0.5		*	Hirschler & Osterburg, 2022
$\Delta C_{crop\ products}$ *	0.0		-	Assumption
$\Delta C_{wood\ products}$ *	-8.1		*	eq. 12
$\Delta C_{peat\ products}$ *	-0.8		*	Hirschler & Osterburg, 2022
		Budget summaries		
NEEc*	-362		-	eq. 8
ΔC_{land} *	-309		-	eq. 9
ΔC_{land}	-72		-	eq.10
ΔC_{land}	-103	-314; 8		TRENDY
F_{LULUCF}	-112			UNFCCC

Table 4: - *continued* –

Flux	Estimated flux in Tg C yr^{-1} Best estimate	Range	Conf.	Source
		Terrestrial Ecosystems		
ΔC_{FL}	-130			EFISCEN
ΔC_{FL}	-133			FAO Tier 1
ΔC_{FL} *	-131		*	Median of above
ΔC_{CL} *	22		-	UNFCCC
$\Delta C_{CL,organic\ soils}$	14.7			UNFCCC
$\Delta C_{CL,mineral\ soils}$	7.9			UNFCCC
$\Delta C_{CL,organic\ soils}$	26.3			FAO Tier 1
ΔC_{GL*}	10		-	UNFCCC
$\Delta C_{GL,organic\ soils}$	14			UNFCCC
$\Delta C_{GL,mineral\ soils}$	-2			UNFCCC
$\Delta C_{GL,organic\ soils}$	1.4			FAO Tier 1
		Coastal Ecosystems		
F_{CWa} *	6.9		*	Rosentreter et al., 2023
F_{CWL} *	-4.2		-	Rosentreter et al., 2023
		Biological products		
$F_{crop\ harvest}$ *	-224		**	FAO
$F_{crop\ harvest}$	-256			Byrne et al., 2023
$F_{wood\ harvest}$ *	-142		**	FAO
$F_{wood\ harvest}$	-140			Byrne et al., 2023
$F_{peat\ harvest}$ *	-10		**	Hirschler & Osterburg, 2022
$F_{crop\ use}$ *	207		*	based on FAO, eq. 11
$F_{crop\ use}$	314			Byrne et al., 2023
$F_{wood\ decay}$ *	94		*	FAO
$F_{wood\ burning}$ *	34		*	FAO
$F_{wood\ decay}$	16			Byrne et al., 2023
$F_{wood\ burning}$	63			Byrne et al., 2023
$F_{peat\ use}$ *	9.7		**	Hirschler & Osterburg, 2022
$F_{product\ oxidation}$ *	346		*	sum of our best estimates*
$F_{crop\ trade}$ *	17		**	FAO
$F_{wood\ trade}$ *	6		**	FAO
$F_{peat\ trade}$ *	-0.5		*	Hirschler & Osterburg, 2022
$\Delta C_{crop\ products}$ *	0.0		-	assumption
$\Delta C_{wood\ products}$ *	-8.1		*	eq. 10
$\Delta C_{peat\ products}$ *	-0.8		*	Hirschler & Osterburg, 2022
		Budget summaries		
NEEc*	-362		-	eq. 8
ΔC_{land} *	-309		-	eq. 9
ΔC_{land}	-72		-	eq.14
$\Delta C_{FL} + \Delta C_{FL} + \Delta C_{GL}$	-99		-	our best estimates*
$\Delta C_{FL} + \Delta C_{FL} + \Delta C_{GL}$	-103	-314; 8		TRENDY
F_{LULUCF}	-112			UNFCCC

Note that we assume that our estimates of GPP and Re_{terr} implicitly include the land use change flux F_{LUC}, which we thus did not add explicitly to our C budget. Nevertheless, we list various estimates of F_{LUC} for comparison and discussion. We find strong differences between the two bookkeeping models HN and BLUE, but also between the two estimates based on BLUE using different land cover data as input (Table 4). Between the lowest and highest estimate, there is a factor of 3.5 difference. Therefore, for our best estimate of F_{LUC}, which is the median of the three estimates, we assigned only a low level of confidence.

For $F_{grazing}$, we only have the estimates obtained by Chang et al. (2021) using the land surface model ORCHIDEE. However, as the grazing flux in the simulations is scaled to inventory data on livestock density, we assigned a moderate level of confidence to this flux estimate. While we have a high level of confidence in the estimates of $F_{crop\ harvest}$, $F_{wood\ harvest}$, $F_{peat\ harvest}$, which are all based on inventory data, we have a low level of confidence in $F_{bio2river,}$ because it is only based on a mass budget of fluxes from or to the inland water compartment (eq. 11). For $F_{crop\ harvest}$ and $F_{wood\ harvest}$, our estimates agree well with those from Byrne et al. (2023), which can however easily be explained by the fact that both are based on the same FAOSTAT data.

The three harvest fluxes - $F_{crop\ harvest}$, $F_{wood\ harvest}$, and $F_{peat\ harvest}$ – feed into corresponding product pools, which themselves are a sizable source of C to the atmosphere of ~0.3 Pg C yr^{-1} through use, burning and decomposition of these products ($F_{product\ oxidation}$, as the sum of $F_{crop\ use}$, $F_{wood\ decay}$, $F_{wood\ burning}$ and $F_{peat\ use}$). Emissions from wood and crop products are dominant, with only minor contributions related to peat products. Europe is a net exporter of crop and wood products, but a net importer of peat. However, these net trade fluxes are rather small, representing ≤10% of the corresponding harvest fluxes, and amount to a net-export of only 22 Tg C yr^{-1}. In contrast, in RECCAP1, Luysaaert et al. (2012) identified Europe as a net-importer of 19 Tg C yr^{-1}. That discrepancy may partly be explained by the fact that for RECCAP2, we additionally include Moldova, Ukraine and Belarus, which, according to our calculations based on the FAOSTAT data, are a net-exporter of 16 Tg C yr^{-1} linked to the trade of crop products. While changes in the crop product stock (ΔC_{crop}) are set to 0 Tg C yr^{-1} per definition, we estimate an average increase in the European wood product C stock (ΔC_{wood}) of ~8 Tg C yr^{-1}. Note that for RECCAP1, Luyssaert et al (2012) estimated an increase in wood product C stocks of even 19 Tg C yr^{-1} based on a different inventory data set (Eggers 2002), and for the year 2000 only. For the peat product pool (ΔC_{peat}), we estimate an increase of 0.9 Tg C yr^{-1} based on the inventory data from Hirschler & Osterburg (2022).

The net exchange of C between the geological compartment and the atmosphere is of minor importance in the land C budget. In addition, the dissolution of carbonate minerals (ΔC_{litho}) is of minor importance compared to other C stock changes in the land C budget. The exports of C from the geological compartment to the inland water compartment of 19 Tg C yr^{-1} add to $F_{bio2river}$ of 91 Tg C yr^{-1}. Of the total C input to inland waters ($F_{litho2river}$+ $F_{bio2river}$) of 110 Tg C yr^{-1}, only

about one third is actually exported to the sea. The C burial in sediments (ΔC_{burial}) is a minor contribution to the land C stock change (ΔC_{land}). The emissions of inland waters to the atmosphere of 55 Tg C yr^{-1} may appear small compared to the exchange fluxes between terrestrial ecosystems and the atmosphere, but are still important for the NEE_C, i.e. the balance of all vertical exchange fluxes in the land C budget. Coastal ecosystems in Europe add a small net source of C to the atmosphere, as emissions from estuaries (F_{CWa}) of 6.9 Tg C yr^{-1} are only partly counterbalanced by a net-uptake in coastal wetlands (F_{CWL}) of 4.2 Tg C yr^{-1}.

Based on budget closure, we estimate NEE_C at -0.4 Pg C yr^{-1} during 2010-2019, and we assign a low level of confidence to this estimate. Nevertheless, NEE_C is dominated by the land CO_2 budget, for which we found good agreement between our BU estimate and different TD estimates (section 3.1), which is thus in support of our assessment of NEE_C. When we finally assess the net C stock change in the land C budget by including lateral net exports through trade and river transport (eq. 9), we obtain a flux-derived increase in ΔC_{land} of 0.3 Pg C yr^{-1}. As an alternative result from the calculation of ΔC_{land} as the sum of all C stock changes in the land C budget (eq. 14), we obtain a much lower increase in ΔC_{land} of only 0.1 Pg C yr^{-1}.

For this alternative result, we used independent estimates of terrestrial ecosystem C stock changes that give a net C sink for forests (ΔC_{FL}) of about 130 Tg C yr^{-1}, and net sources from grass- (ΔC_{GL}) and croplands (ΔC_{CL}) of 22 and 10 Tg C yr^{-1}, respectively. While we have a moderate level of confidence in ΔC_{FL}, in particular as the two independent estimates by EFISCEN and FAO agree well (see Table 4), our confidence in ΔC_{GL} and ΔC_{CL} is low. For both ΔC_{GL} and ΔC_{CL}, we used the estimates from the national inventories (UNFCCC). Based on the LUCAS database of repeated measurements of topsoil organic C stocks, De Rosa et al. (2024) have recently estimated a net-loss of topsoil organic C of only 7 Tg C yr^{-1} on agricultural land (i.e. $\Delta C_{GL} + \Delta C_{CL}$) for the EU27+UK over the period 2009-2018. Although EU27+UK represents only a bit more than 80% of our RECCAP2 region, this latest study advocates for a more conservative estimate of soil C losses. Note finally that the national inventories split ΔC_{GL} and ΔC_{CL} further into estimates for mineral soils and organic soils (Table 4). Although organic soils represent only a very minor fraction of croplands and grasslands in Europe (~3% each), they make up the larger part of these emissions. From the FAO, we have Tier 1 estimates for emissions from organic soils, which is twice as high for croplands but only one tenth of what is estimated for grasslands based on the national inventories (Table 4). The estimates of total C losses from organic soils are very similar between UNFCCC and FAO, 29 Tg C yr^{-1} and 28 Tg C yr^{-1}, respectively. However, while the NGHGIs from UNFCCC give a similar magnitude in losses from croplands vs. grasslands, croplands are the dominant emitter in the FAO accounting for 26 Tg C yr^{-1}. This number is in turn still slightly lower than the C loss from organic cropland soils of 33 Tg C yr^{-1} estimated by Carlson et al. (2017) for Europe. These large discrepancies in different estimates show how poorly constrained these storage changes are, and are thus the main justification for the low level of confidence we have in this second estimate of ΔC_{land}.

Note that for RECCAP1, Luyssaert et al. (2012) also calculated a lower land C sink based on inventory-based estimates of stock changes than based on flux estimates, with 0.1 ± 0.1 and 0.2 ± 0.2 Pg C yr^{-1}, respectively. These values are rather comparable to our corresponding estimates of 0.1 and 0.3 Pg C yr^{-1}, respectively. The potential bias due to different definitions of the spatial domain between RECCAP1 and RECCAP2 is significant. Given the huge uncertainties in estimated ΔC_{land}, however, this comparison is rather encouraging.

The TRENDYv10 estimates of ΔC_{land} give an ensemble median of 0.1 Pg C yr^{-1}, which is quite close to our inventory based assessment. However, individual simulations of ΔC_{land} in TRENDYv10 range from ~0 to 0.3 Pg C yr^{-1}, which reveals the high uncertainty of DGVM simulations.

4.2 Evolution of the carbon budget over the last three decades

Figure 7 shows the evolution of the European C budget (ΔC_{land}) over the last three decades, as well as the changes in different fluxes that are responsible for this evolution. Note that a series of C fluxes, although important for the land C budget as such, are not included in this figure as we assume them not to have changed over the last three decades. This concerns F_{IW}, $F_{river\ export}$, F_{geo}, $F_{weathering}$, F_{CWa}, and F_{CWL}. A detailed list of all fluxes averaged for the three decades can be found in Table S8.

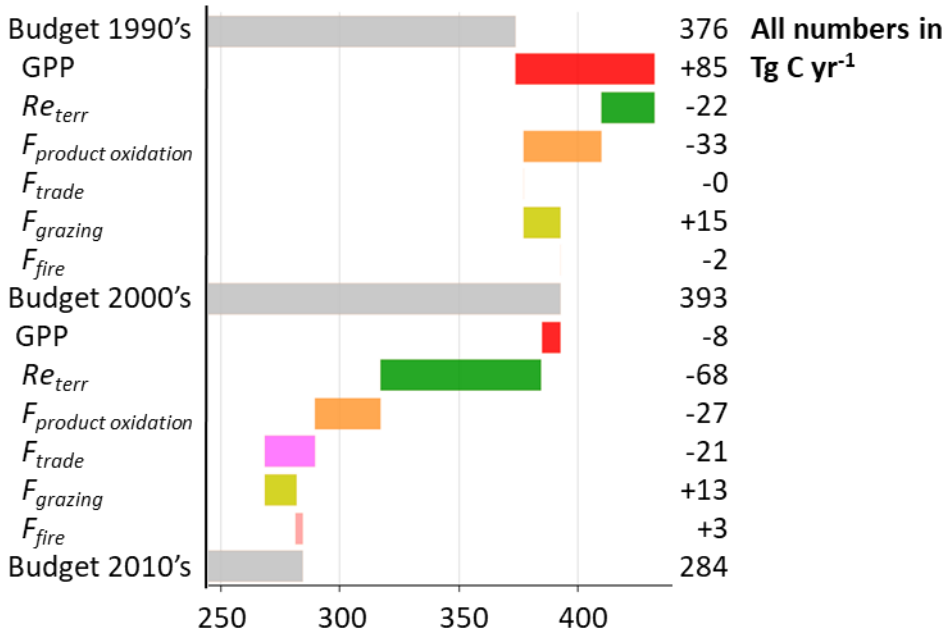

Figure 7: Evolution of European carbon budget over the last three decades based on flux estimates (eq. 9). Note that there is no estimate for F_{fire} in the 1990s.

ΔC_{land} increases slightly from the 1990s to the 2000s, before it decreases substantially to the 2010s. From the 1990s to the 2000s, an increase in GPP is more or less counterbalanced by increases in Re_{terr} and $F_{product\ oxidation}$, while a decrease in $F_{grazing}$ still permits for the slight increase in ΔC_{land}. Changes in F_{trade} are negligible between these two decades. From the 2000s to the 2010s, Re_{terr} increased substantially while GPP even slightly decreased, which appears to be the main reason for the comparatively large drop in ΔC_{land}. In contrast, changes in $F_{product\ oxidation}$ and $F_{grazing}$ seem to continue in about the same magnitude as between the 1990s and 2000s, and changes in F_{trade} and F_{fire} have only a minor effect on ΔC_{land}.

Interestingly, F_{LULUCF} from UNFCCC inventories shows a similar trend, but the implied increase in biosphere C stocks is less pronounced and generally at a lower magnitude. According to these inventories, F_{LULUC} increased from -119 Tg C yr^{-1} in the 1990s to -125 Tg C yr^{-1} in the 2000s, before it falls to its lowest value of -112 Tg C yr^{-1} (Table S7, negative values indicate a sink). Note that trends in these inventories are largely driven by land use data. We can thus assume changes in land use to be an important driver behind the low F_{LULUCF} in the 2010s. The three BK model estimates of F_{LULUCF} considered in this study, consistently represent this flux as net C sink during the 1990s, 2000s, and 2010s of 81 (43 - 150) Tg C yr^{-1}, 82 (72 – 160) Tg C yr^{-1}, and 65 (44 - 156) Tg C yr^{-1}, respectively (median and range of the three estimates, Table S8). Most importantly, all three estimates of F_{LULUCF} indicate the lowest sink for the 2010s, which is consistent with our BU assessment.

From the ensemble medians (range) of TRENDYv10, we find an increase in ΔC_{land} from 78 (-183 to +228) Tg C yr^{-1} in the 1990s to 106 (-240 to +294) Tg C yr^{-1} in the 2000s, but no further increase in the 2010s where ΔC_{land} is simulated at 103 (8 – 314) Tg C yr^{-1}. However, the range in the model results, from net-sources to net-sinks of C, reflects the high level of uncertainties associated with this trend, which can thus be used neither to support nor to refute the trend in our BU assessment.

5 Spatio-temporal patterns in GHG budgets from regional inversions

In this section, we analyze spatiotemporal patterns of fossil CO_2 emissions and land CO_2, CH_4, N_2O fluxes over the period 2010-2019, including local hotspots and areas with large temporal trends, based on the mean of regional inversions re-gridded to 1°.

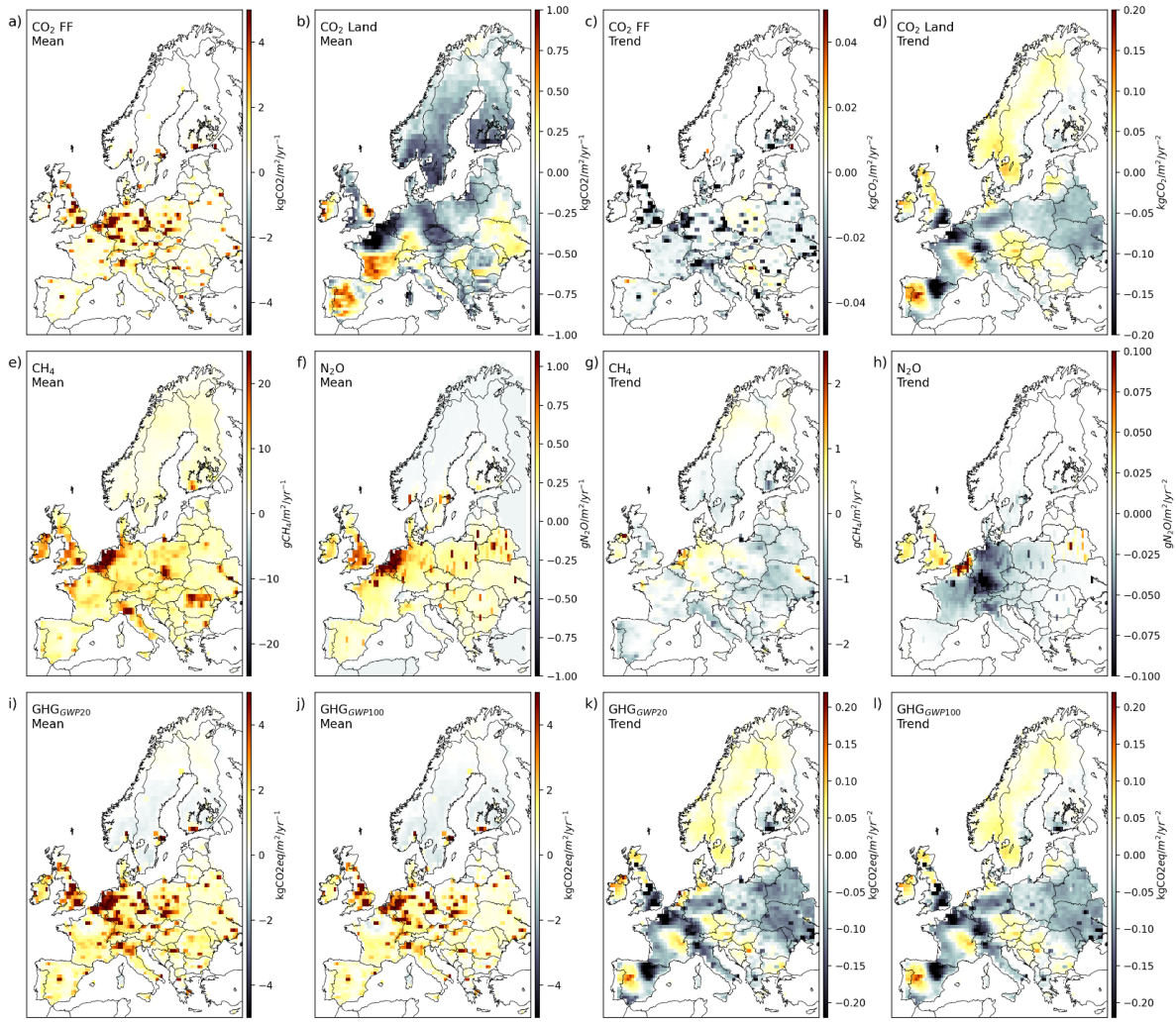

Figure 8. Spatial patterns in GHG budgets from regional inversions for the period 2010-2019: prescribed fossil CO_2 emissions (a, c), land CO_2 fluxes (b, d), CH_4 emissions (e, g), N_2O emissions (f, h), and net GHG balance combining the three GHGs at a 20 year (i, k) and 100 year (j, l) horizon. Left two columns are the means, right two columns are the trends.

5.1 Fossil CO_2 emissions

The spatial distribution and trend of fossil CO_2 emissions prescribed to regional inversions (i.e. not optimized) are shown in Fig. 8a,c. These priors were derived from EDGAR v4.3, BP statistics, and satellite measurements of atmospheric concentration of NO_2 as important co-emittent of CO_2 in fossil fuel combustion, while the spatial disaggregation is entirely based on EDGAR v4.3 and is representative for the year 2010 (see McGrath et al., 2023 for details). Emissions are concentrated over densely populated areas in the UK, Benelux, Italy's Po Valley with emission rates higher than 6 $kgCO_2\ m^{-2}\ yr^{-1}$ over 1º grid cells, and in megacities and point

sources such as power plants and industrial sites. In total, 80% of emissions are located over 23% of the land area when spatial resolution is smoothed to 1° degree like in Fig 8a,c.

Following the numbers assembled by the Global Carbon Atlas (https://globalcarbonatlas.org/, accessed on 2024-01-02) based on Friedlingstein et al. (2022), fossil CO_2 emissions have been going down in Europe since 1990, with an average rate of decrease of -1.5 % yr^{-1}. Emission reductions rates differ between countries with the largest reduction rates being in the UK (-2.8% yr^{-1}), Italy (-2.2% yr^{-1}), intermediate values in France (-1.6% yr^{-1}) and Germany (-1.5% yr^{-1}), Spain (-1.1% yr^{-1}) and in former eastern bloc countries excluding Poland (-1.2% yr^{-1}). In Poland, emissions decreased only by -0.2 % yr^{-1}. Note however that the map of emission trends in Fig. 8c has grid cells with increasing emissions, highlighting that some sectors have continued to increase emissions.

Since 1990, fossil CO_2 emissions have been going down, with an average rate of decrease of -1.1 % yr^{-1} in the EU28 (UK27+UK) and -1.5 % yr^{-1} in Europe (excluding Russia). Coal emissions showed the fastest decrease by -3.2 % yr^{-1} in the EU28 and -2.6 % yr^{-1} in Europe. Emissions from oil burning experienced a smaller decrease (-0.8 % yr^{-1} in EU28) while those from natural gas decreased to a minimum in 2015 and then increased again, resulting in an average trend of -0.9 % yr^{-1} during 2010-2019. Emission reductions rates differ between countries, the largest reduction rates are found in the UK (-2.8% yr^{-1}), Italy (-2.2% yr^{-1}), intermediate values in France (-1.6% yr^{-1}) and Germany (-1.5 % yr^{-1}), Spain (-1.1 % yr^{-1}) and in former Eastern bloc countries excluding Poland (-1.2 % yr^{-1}). In Poland, emissions decreased only by -0.2 % yr^{-1}. In total, 90% of the EU28 emission's reduction originated from the five largest economies (Germany, France, UK, Italy, Spain, Poland), which altogether represent 80% of the mean EU28 emission. Note however that the map of emission trends in Figure 8c has grid cells with increasing emissions, as some sectors have continued to increase emissions.

Note that the spatial activity data for the year ~2015 used for the GRIDFed emission map underlying the trend patterns in Figure 8c are not updated each year, so that the annual national fossil CO_2 emissions reduction are spatially distributed in proportion to emissions per each grid cell. Therefore, the grid cells containing coal plants that closed during the period do not show up with a huge local reduction of emission in Figure 8c. Typically, a large plant (~1000 MW) emits 5 Mt CO_2 yr^{-1}, equivalent to the emissions from a 300,000 people city in Europe (Moran et al., 2022). In 2016, only the UK, Belgium and Sweden announced a phase out of coal in power generation for 2030, whereas in 2022, more than twelve countries committed to it and ten others phased out coal. It is therefore important for the fossil emission map prescribed to inversions to be up to date for the location of disappearing (or appearing) point sources, as shown in Figure 9. Because emissions of power plants which do not exist anymore were wrongly prescribed to atmospheric transport models, all regional inversions likely compensated by adding an increasing land CO_2 sink around decommissioned plants, which biases the patterns of their land CO_2 sink and its trends, making a comparison to bottom-up estimates challenging. This artificial trend of

wrongly assigned increasing land sink can be seen clearly in Figure 8, where the three regions of strongest increase in land sink are located just downwind of power plants which closed (North-Eastern Spain for plants that closed upwind in Asturias, Western Germany for plants hat closed in East of France, and in Belgium and South Western UK for plants that closed in Southern UK, Belgium and Germany close to the Belgian border, as shown in Figure 9).

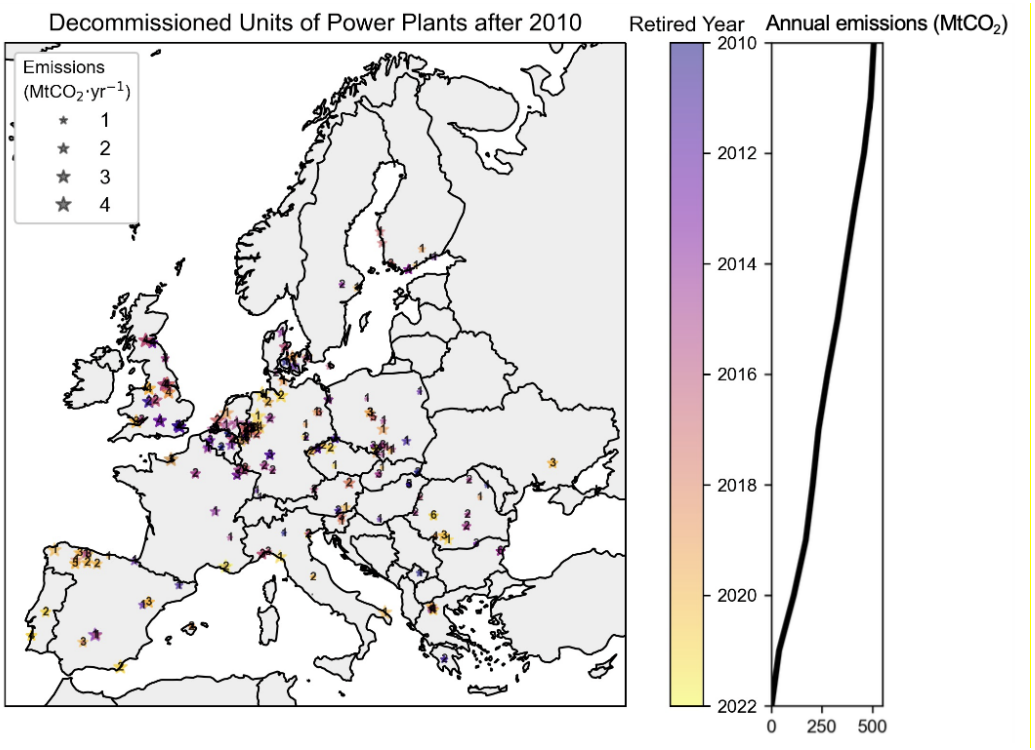

Figure 9. Location of the coal power plants that closed in Europe between 2010 and 2022. The magnitude of the emission prior closure is indicated by the size of each star symbol and the year of closure by the color palette. The right hand plot shows the reduction of corresponding CO_2 emissions since 2010, with a total reduction of 500 $MtCO_2$ by 2022.

5.2 Land CO_2 budget

Figure 8b shows the mean annual net CO_2 land flux excluding fossil CO_2 emissions, as estimated by the mean of regional inversions. The range of the corresponding sinks and sources (negative and positive values) at 1° spatial resolution is three times smaller than the one of fossil CO_2 emissions. According to the mean of regional inversions, most European countries are net CO_2 sinks except Spain, southern UK, southern France and Ukraine. The trend of the land CO_2 sink shows different patterns than the mean value. We verified that the trend of inversions is not given by the trend of their prior land flux. The trend of the prior shows a decreasing CO_2 sink (Fig. S2) where the trend of inversions shows regions with strong increases (North of France, North of

Spain). There are however also large areas where both priors and inversions show strong decreases of the land CO_2 sink (in UK, from Southern Germany to Czech Republic, and in Scandinavia). Interestingly, regions that are weak sinks in the mean flux of inversions (Northern Spain in Fig. 8) show the largest sink increase over time. There is no evidence for 'favorable' trends in climate driving increased plant growth, nor for shifts in land use (such as decreased harvest) in these two regions. The trend of weakening CO_2 sinks in Scandinavia is possibly linked to changes in forest management and the cutting of old forests (Ahlström et al., 2022). On the other hand, Poland and Eastern European countries show a strong CO_2 sink that intensified over time, which may be explained by a substantial increase in forest biomass (Winkler et al., 2023).

5.3 CH_4 emissions

The CH_4 emissions from the mean of regional inversions shown in Fig 8 include anthropogenic and natural emissions. Fossil fuel extraction in Europe is limited mainly to gas extraction in the Netherlands, the North Sea (offshore), and Romania, as well as coal mining in Poland. CH_4 emissions are more diffuse but present high values in agricultural and populated areas (landfills) and in coal mining basins (e.g. the Silesia region of Poland). There are few hotspot regions of CH_4 emissions with emission rates exceeding 0.01 kg CH_4 m^{-2} yr^{-1}, namely in the UK, Benelux and Western Germany, Southern Poland and Italy's Po Valley. These high emissions rates are mainly associated with CH_4 emissions from agricultural activities (e.g., cattle farming (enteric fermentation) and rice cultivation). According to UNFCCC 2022 official inventories submissions, these regions/countries are in the top ten of the CH_4 agricultural emitters, responsible for 70 % of the total CH_4 emissions in the EU27+UK. Following the same sources, emission rates in Belarus and Ukraine are lower on average than in EU27+UK. Note that the regional inversions are constrained by atmospheric observations over Western Europe, but not over Eastern Europe where their solution is close to the prior inventory (Petrescu et al., 2023). This may further explain why with regard to average emissions, global inversions tend to be better in agreement with bottom-up estimates than the regional inversions (see Table 4).

Deng et al. (2022) used global CH_4 inversions from Saunois et al. (2020) updated until 2017, which have a coarser spatial resolution than the three regional inversions used in this study. They found a consistent decreasing trend in inventories and inversions for the EU27 over the period 2000-2017, including both GOSAT-based and surface station-based inversions. Here, from regional inversions limited to a shorter period in 2010-2019, the spatial distribution of the CH_4 emissions trend suggests large decreases in Belarus and Ukraine, no strong increase in Poland (unlike in the prior, see Figure S2) and an increase in Benelux countries, Germany, Ireland, Western France and Scandinavia. The trend of CH_4 emissions from regional inversions is therefore different from the trend of the prior (EDGARv4.2), which shows a small decrease across all European countries and large increases in Ireland and Poland (Fig S2e).

5.4 N_2O emissions

Anthropogenic and natural N_2O emissions from inversions include industrial emissions (point sources) from the production of chemicals and other emissions (diffuse) mainly from agriculture. The map of N_2O emissions optimized by regional inversions shown in Figure 8f shows diffuse emissions with a rate of less than 0.002 kg N_2O m^{-2} yr^{-1}, representing direct and indirect emissions from fertilized croplands and pastures. There are also hotspots of emissions corresponding to industrial emitters and high emission rates from intensive agriculture over Benelux (0.005 kg N_2O m^{-2} yr^{-1}, see de Vries et al. 2021). The trend of N_2O emissions optimized by inversions (Fig. 8h) is slightly negative for all diffuse emissions in Germany and France, consistent with reduced nitrogen fertilizers applications (following the Nitrate Directive of the EEC, 1991), whereas prior emissions used by inversions had no trend (Fig. S2d). On the other hand, point sources show positive or negative trends. Much of the IPPU emissions from nitric acid plants were cut in a similar manner around 2010, with the introduction of the European Emission Trading System that made it economically interesting for companies to apply emission abatement technologies (catalytic reduction of N_2O in the flue gas) to reduce their emissions (Petrescu et al., 2023). Belgium and the Netherlands indicate a strong increase in N_2O emissions (Fig. 8h).

6. Interannual variability of European GHG budgets

Quantifying interannual variability (IAV) and identifying its drivers is important to gain understanding of the processes controlling variations in sources and sinks of GHGs, but also to appropriately separate long-term trends (human-driven) from short-lived variations due to natural climate variability. Variability in the European CO_2 sink has been previously analyzed, including the main drivers of long-term IAV in sources and sinks of CO_2 (Ciais et al. 2010; Luyssaert et al., 2010; Bastos et al., 2016), seasonal compensation effects (Buermann et al., 2018) and the impacts of extreme events on annual carbon budgets (Ciais et al., 2005; Bastos et al. 2014; Bastos et al., 2020). For CH_4 and N_2O, less is known about the magnitude and spatio-temporal distribution of IAV in the European region. It is also unclear how IAV in each of the three GHGs relates to variability in the overall global warming potential (GWP). Depending on the main drivers of variability in each GHG, anomalies may reinforce each other in a particular year (if climatic conditions lead to anomalies of the same sign in all three GHGs) or counterbalance each other partly (if the same climatic conditions lead to anomalies of opposite signs among the GHGs). In this section we compare the magnitude and spatial distribution of IAV in net CO_2, CH_4 and N_2O emissions and their combined GWP at the 20-yr and 100-yr time horizons (GWP_{20} and GWP_{100}, respectively). We then analyze how two important modes of climate variability influencing European climate affect anomalies in the three GHGs separately, as well as their combined GWP.

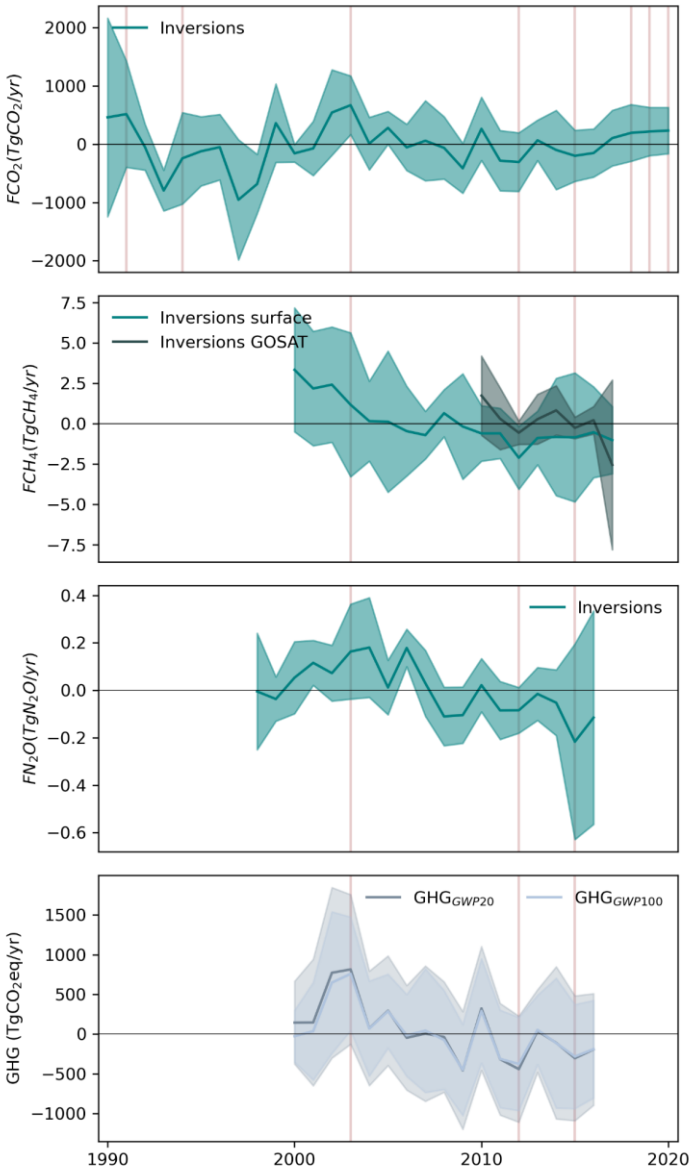

Figure 10 Time-series of annual anomalies of the three GHGs - CO_2, CH_4 and N_2O from top to the third panel, and the respective aggregated GWP_{20} and GWP_{100} anomalies. The vertical red lines indicate years associated with hot and/or drought events.

Figure 10 shows the regionally-integrated annual anomalies of CO_2, CH_4 and N_2O and the respective aggregated GWP_{20} and GWP_{100} anomalies from the global atmospheric inversions. For CH_4, we show separately the in-situ and satellite based inversions, due to their different temporal coverage. Both CH_4 and N_2O show a decreasing trend, while CO_2 shows multi-annual variations with a predominant sink in the 1990s and predominant source fluxes in the 2000s. Hot and dry

years are generally associated with source anomalies, except 2012 and 2015, when drought conditions were more localized and mostly located over southern Europe. The 2003 drought and the 2018-2020 extreme summers were associated with strong CO_2 sources. 2003 is also associated with large CH_4 and N_2O sources, so that 2003 is the year with the highest associated GWP, and 2010 shows a peak in emissions following a downward trend (bottom panel). It should be noted that the spread of the inversions is generally larger than the anomalies themselves for all three GHGs, which indicates a reduced ability to constrain annual anomalies at continental scale.

In Figure 11, we evaluate how anomalies in the three GHGs vary with two important modes of large-scale atmospheric circulation influencing European climate: the North Atlantic Oscillation (NAO) and the East-Atlantic (EA) Pattern. We analyze how far anomalies in each GHG and GWP of all three GHGs combined are related to possible NAO/EA combinations - at European scale, and for four major climate regions within Europe: Atlantic, Continental, Boreal, and Mediterranean. At European scale, we find that both combinations of NAO/EA in-phase (NAO+EA+ and NAO-EA-) are associated with below-average GWP (GHG_{GWP20}). In the case of NAO+EA+, this is because of a combination of below-average values of CO_2 and N_2O, but this is likely driven by outlier values, as the median anomalies for both gasses are close to zero. For NAO-EA-, CO_2 anomalies are predominantly negative, consistent with the results in Bastos et al. (2016), along with generally negative CH_4 anomalies, which are however associated with a large spread among inversions. Because the impacts of NAO and EA are regionally different, we need to analyze the regional dependence of GHG anomalies on climate drivers for each NAO/EA phase. During NAO+EA+, GHG sink anomalies are found for all regions except the Atlantic sector, but this is due to different combinations of anomalies in the three GHGs and of climate conditions: below-average GHG emissions in Continental and Boreal regions are mainly associated with below-average CO_2 anomalies driven by warmer than average conditions and close to normal - but slightly negative - precipitation anomalies (Figure S3). In the Atlantic section, warmer and drier conditions during NAO+EA+ are associated with a positive CO_2 anomaly, which is partly offset by a negative N_2O anomaly, consistent with below average precipitation. For NAO-EA-, the European GHG sink is dominated by negative GHG_{GWP20} anomalies in Continental and Mediterranean regions, mostly associated with below-average CO_2 emissions in both regions and additionally with negative CH_4 anomalies in the Mediterranean. In the Boreal section, negative CO_2 anomalies are linked to below average temperature and precipitation, consistent with results in Bastos et al. (2016) who showed that increased snow cover in winter due to cold winters and later soil-moisture availability led to increased summer GPP, while predominantly cooler temperatures keeping Re_{terr} anomalies low. The above-average N_2O emissions in this region might be associated with the higher soil moisture during summer in this region (see Bastos et al. (2016) for seasonal climate anomalies). The negative anomalies in GHG_{GWP20} in the Mediterranean are also likely explained by differences in the seasonal climate anomalies, with the increased CO_2 sink associated with higher soil-moisture availability during winter and early spring, when vegetation activity is at its peak in this region.

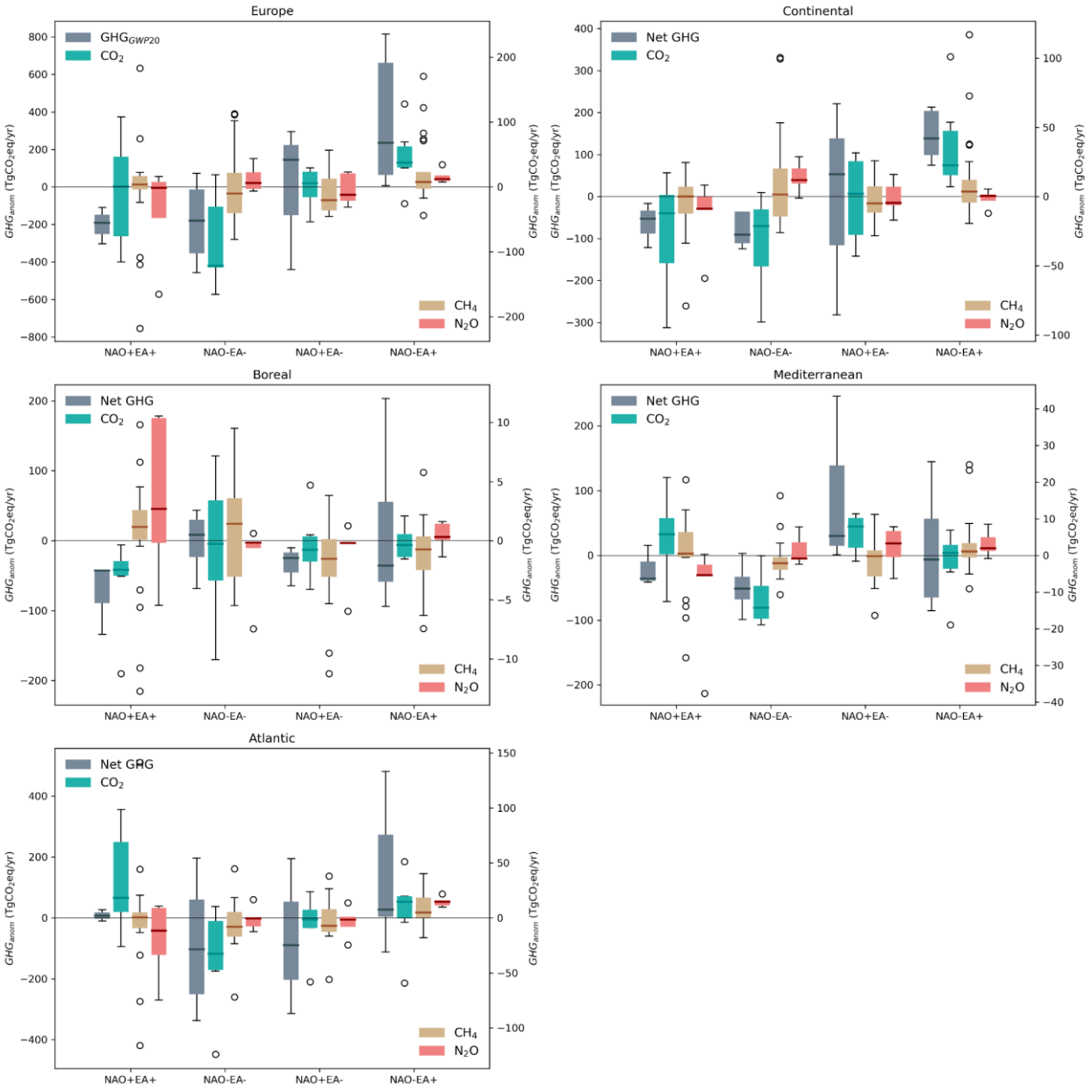

Figure 11: Anomalies in annual CO_2, CH_4 and N_2O fluxes and combined GWP_{20} during the four combined phases of two main atmospheric circulation patterns influencing European climate: the North Atlantic Oscillation (NAO) and the East Atlantic Pattern (EA). The boxplots show the spread across the inversions for the mean of each phase combination. For each individual GHG, the anomalies are calculated for the available time-series length for each GHG, while for the GWP, the data are limited to the period 2000-2016, so that only two years are considered for the two in-phase composites (NAO+EA+ and NAO-EA-).

For the anti-phase combinations, GHG_{GWP20} shows a clear source anomaly for NAO-EA+ and close to neutral but predominantly source anomaly for NAO+EA-, with both phase combinations showing a very large spread (Figure 11). The clear GHG_{GWP20} source anomaly in NAO-EA+ results from positive anomalies in the three GHGs at European scale, while NAO+EA- shows close to neutral anomalies for all three GHGs, although slightly positive for CO_2 and slightly negative for CH_4 and N_2O. The continental scale neutral balance for NAO+EA- is explained by offsetting effects between the Boreal and Mediterranean sectors, the first showing a sink anomaly associated with below-average CO_2 and CH_4 along with close to normal but tendentially warmer and slightly wetter than average conditions (Figure S3). Bastos et al. (2016) showed that the warm conditions for this phase occurred predominantly in winter and spring, so that the CO_2 sink might be associated with earlier onset of the growing season. The positive GHG_{GWP20} anomalies during NAO+EA- in the Mediterranean are associated with CO_2 source anomaly due to lower than average temperatures (especially in winter, the peak of the growing season, see Bastos et al. (2016)) and a N_2O source anomaly likely explained by wetter than average conditions during this phase. Finally, the source anomaly at European scale during NAO-EA+ is mostly explained by positive anomalies in CO_2 and CH_4 in the Continental region, associated with cooler than average and much wetter conditions, and by positive anomalies in all three GHGs in the Atlantic region, associated with warmer and wetter conditions during this phase.

7. Processes and drivers of long-term trends in the European carbon budget

Figure 12 gives a consensus view of the trends of net carbon fluxes and stocks in Europe over the past decade. Negative values indicate an increasing sink or a decreasing source. The various products (TD global inversions, BU data driven models, BU process-based models) show good agreement on trends in northern Spain (region A) and Romania (region C), with a strengthening sink in both places. On the other hand, the Czech Republic (region B) leans more towards a weakening sink. These observations are confirmed by the frequency distributions of the number of products indicating a positive trend in the region when compared against the frequency distribution for all of Europe (right panel, Figure 12). Noticeable lack of agreement between the products is seen in the United Kingdom, the Balkans, Finland and Eastern Europe. The remaining areas show a mix of strengthening and weakening of the sink with agreement between at least five out of the seven products. The distribution across Europe is roughly Gaussian centered at three datasets showing a positive trend (four datasets showing a negative trend), while the distributions of each region are clearly skewed, even if region A is perhaps only offset by one dataset. Due to vastly different magnitudes in the trends between different products (two orders of magnitude in extreme cases), we limit our discussion to the sign of the trend.

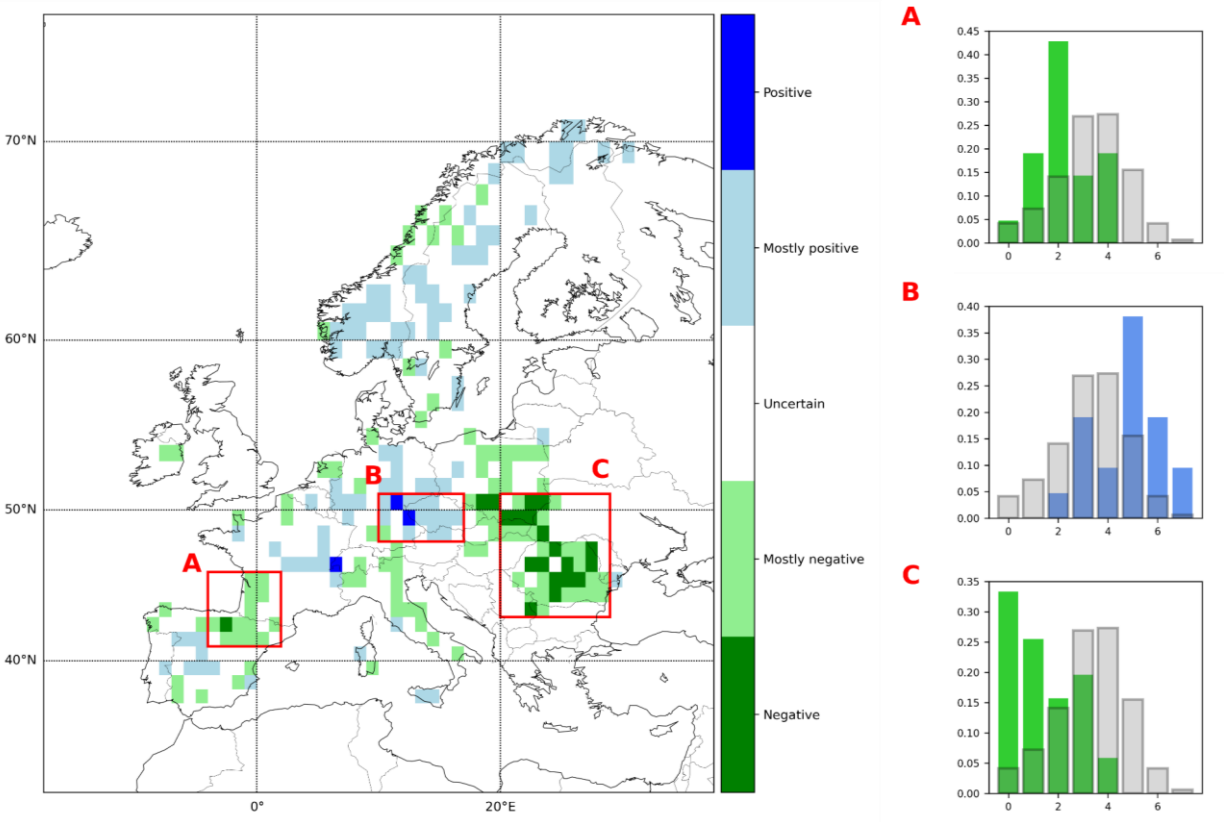

Figure 12: Significant trends in carbon stocks and net fluxes for the period 2010-2019 as indicated by agreement among seven different products: EFISCEN, L-VOD, FLUXCOM, global inversions, regional inversions, TRENDY, and VPRM. "Positive" and "Negative" indicate unanimous agreement, while "Mostly" indicates that five out of seven products have this sign. The sign convention is such that negative values of the annual values indicate a sink into the land surface, while a positive value indicates a source to the atmosphere; negative trends thus indicate strengthening sinks. The three highlighted regions are A: [40N, 45N, 5W, 3E], B: [48N, 51N, 10E, 17E], and C: [43N, 51N, 20E, 30E] moving from west to east, roughly corresponding to northern Spain, the Czech Republic, and Romania, respectively. The right panels show the frequency distribution of pixels with the number of datasets showing a positive trend (increasing emissions or weakening sink), with gray bars showing the distribution for all pixels across Europe and green/blue showing just the pixels in that region.

Figure 13 shows trends for regions A, B, and C for potential environmental drivers of the trends in sink strength observed in Figure 12 (reproduced in the left column in Figure 13). "ELUC" indicates total land use change emissions (F_{LUC}) from 2010-2019 (sum of sink and source terms), while "sink" refers to abandonment of agricultural land and "source" refers to conversion from forest to pasture and cropland, and wood harvest. The different regions show agreement with

different drivers, and indeed, depending on the region, F_{LUC} is driven by different processes: the sink dominates in Romania, while the source term dominates in northern Spain. Broadly increasing temperatures and vapor pressure deficit (VPD) may drive weakening sinks in the Czech Republic and strengthening sinks in Romania, although the spatial patterns appear to resemble more strongly those from land use change.

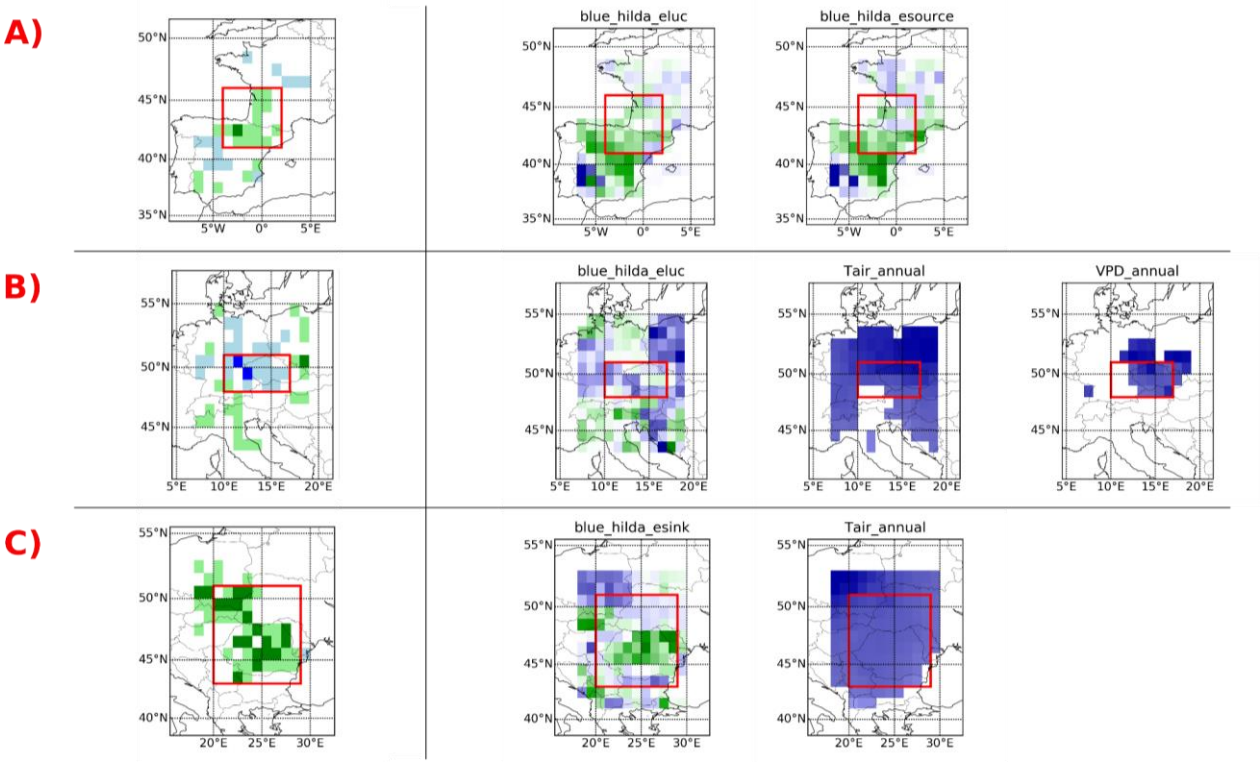

Figure 13: Comparison of dataset agreement from Figure 12 with 2010-2019 trends in various meteorological and land use drivers for three distinct regions. Results have been aggregated to 1.0 degree spatial resolution for easier analysis. Meteorological variables (T and VPD) show pixels for which trends are statistically significant ($P < 0.05$). The drivers shown on the right for each region are those for which the spatial patterns are closest to the observed agreement on the left. Blue indicates positive trends, i.e. increasing emissions/weakening sink, increasing temperature, and increasing VPD.

Land use trends are also shown in Figure 14 using a related approach by looking directly at the land-use and land-cover maps from Hilda+. Hilda+ consists of annual gross changes between urban, cropland, pasture/rangeland, forest, unmanaged grass/shrubland, and sparse/no vegetation areas (Winkler et al. 2021). The increasing sink strength in Romania corresponds to increasing sink due to cropland abandonment in the BLUE-Hilda+ results (region C, bottom right, Figure 13), while the fraction of cropland abandoned is much weaker than in surrounding regions in the pure Hilda+ maps (Figure 14). On the other hand, the increasing change in harvested forest area in the original Hilda+ dataset over the Czech Republic corresponds nicely to the increasing

emissions from BLUE-Hilda+ for the same region, suggesting that harvest may be driving observed trends in that region.

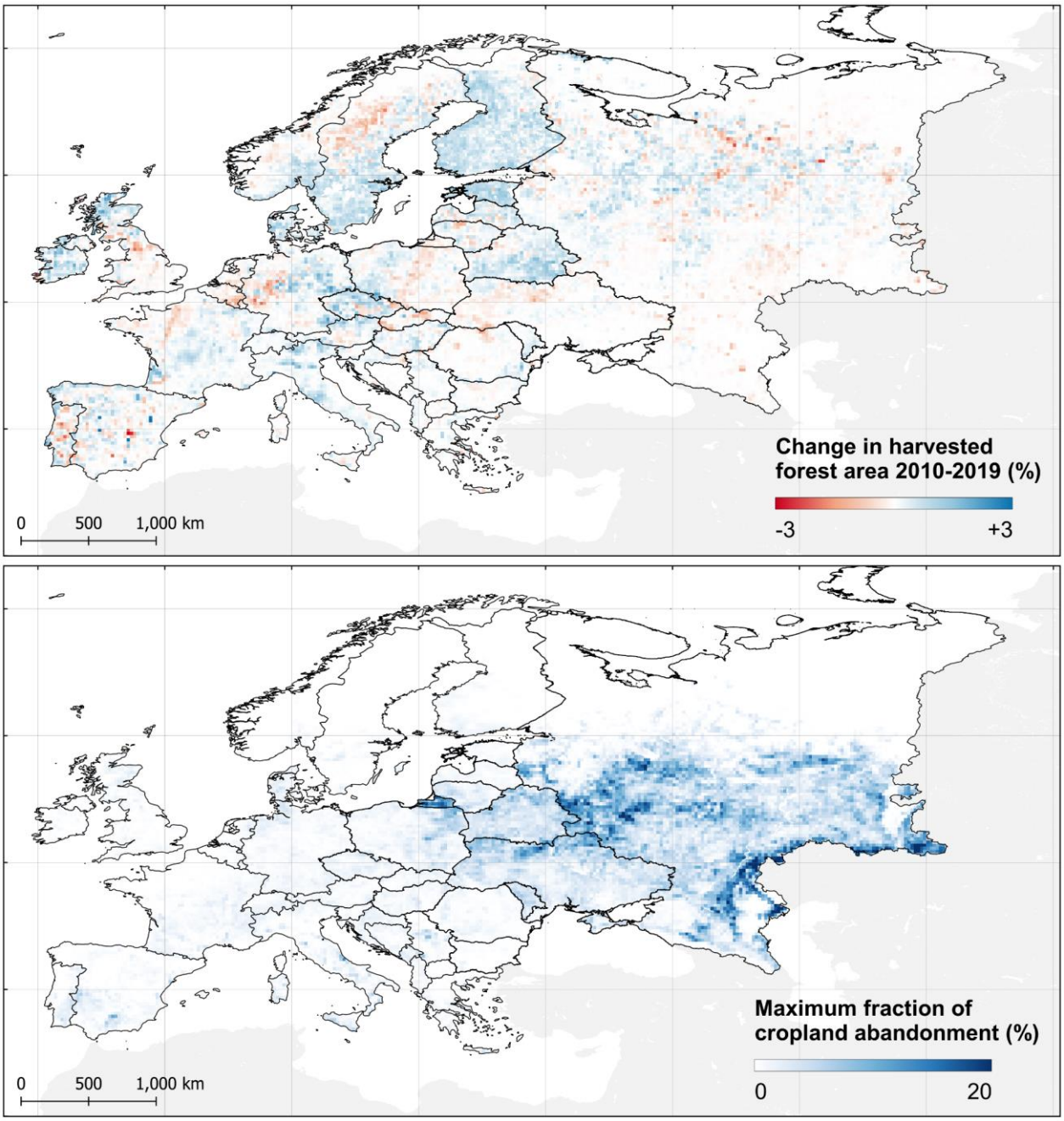

Figure 14 Change in harvested forest area between 2010 and 2019 (top) and maximum fraction of cropland abandonment (bottom) from the Hilda+ land use/land cover dataset. Spatial resolution is 0.25 degrees.

8 Contribution of recent forest disturbances on the European forest carbon balance

8.1 Losses and gains over the last three decades

European forests experience various types of disturbances (mainly harvests, followed by storms, wildfires and insect outbreaks) that damage forests resulting in a loss of productivity and biomass carbon stocks over the short term (Seidl et al., 2014). Several years after a disturbance event, however, a recovery has been observed such as an increase in forest diversity and C stocks (Senf et al., 2019). To evaluate the net impact of forest disturbances on the European carbon budget, we analyzed carbon losses and recovery gains across four regions (Atlantic, Boreal, Mediterranean, and Continental) during three time periods (1990-1999, 2000-2009 and 2010-2018). Note that this analysis is only a partial C budget from disturbances which includes the losses and gains from disturbances that occurred during each decade. Disturbances from previous decades contribute to additional recovery gains which are not accounted for. We utilized two datasets: (i) the European disturbance map from Senf & Seidl (2021) based on Landsat data and (ii) the CCI-ESA Above Ground Biomass data for 2010, 2017, and 2018, corrected for possible biases due to the use of different sensors between 2010 and other epochs based on the assumption that the biomass of undisturbed forest plots was constant (see section 2.6.1). Estimates of carbon budget changes based on the above-mentioned products integrate the effects of both human- and natural-induced disturbances on forests.

The data in Figure 15 shows the location of disturbances and the average fraction of disturbed forests per decade. The dataset from Senf & Seidl (2021) only indicates the year of the most severe disturbance within the last 30 years, implying that a forest that experienced multiple disturbances since 1990 is considered as disturbed only once, which underestimates the disturbed fraction. The data in Figure 15 show that forests in boreal countries experienced more disturbances than in other regions, due to intensive forest management practices (Ceccherini et al., 2020). The fraction of disturbed forests increased over time in Europe, the Atlantic and Mediterranean regions reaching peaks of disturbed areas during the period 2000-2010. This increase may reflect increasing frequency and intensity of natural disturbances, discussed in more detail later on, but could also be related to increasing harvested areas in some regions. However, the partition between harvests and natural disturbance is a sensitive topic, as inconsistencies have emerged between ground-based and remote-sensing attributions of disturbance type (Ceccherini et al., 2020; Wernick et al., 2021; Breidenbach et al., 2022; Palahi et al., 2021; Ceccherini et al. 2021).

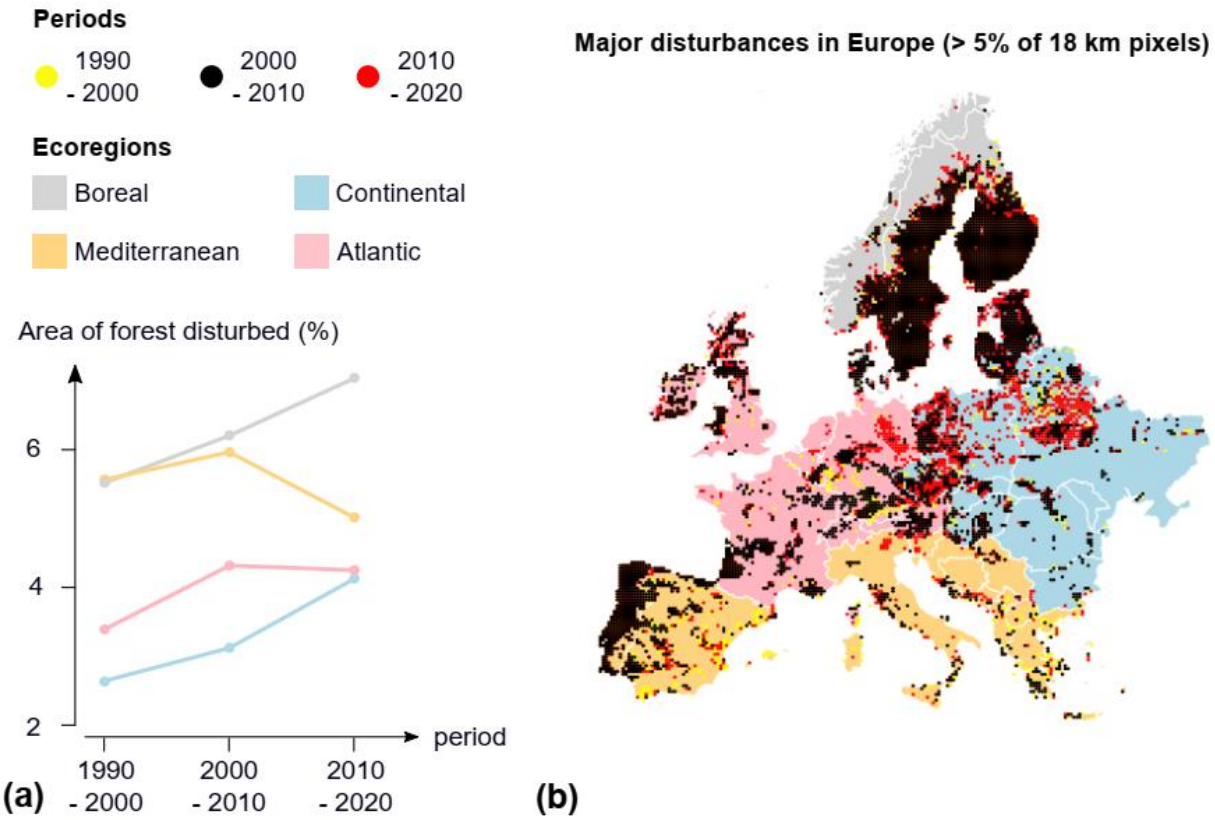

Figure 15. Area disturbed in Europe for four ecoregions (Atlantic, Mediterranean, Boreal & Continental) and three periods (1990-2000, 2000-2010 & 2010-2020) based on the disturbance map of Senf & Seidl (2021). Panel **(a)** shows the spatial mean of the percentage of disturbed forest, and panel **(b)** shows the major disturbances which have occurred in Europe (forested pixels of 18 km disturbed by more than 5%).

Table 5 presents the gains and losses of biomass carbon due to disturbances in the four regions of Figure 15. The largest carbon losses are observed in the Boreal region, followed by the Continental, Atlantic, and Mediterranean regions. On average, disturbances caused a cumulative loss of 690 TgC from 1990 to 2018, which represents 24% of the cumulative forest biomass carbon sink estimated from national inventories (Grassi et al., 2022). Decadal carbon gains associated with recovery from disturbances that occurred during the same decade are smaller than the losses. This implies that regrowing forests cannot fully compensate for the carbon losses due to disturbances during the same decade, which is consistent with a previous study (Nabuurs et al., 2013). This finding is also in line with recovery biomass curves in Europe, which show typical recovery times of 30 years (Senf & Seidl, 2021 GEB). However, gains continue to accrue after the decade when disturbances occur. The regions with the largest net carbon losses (i.e. losses exceeding gains) on a decadal window are ranked as follows: Boreal, Mediterranean, Continental,

1419 and Atlantic. Increasing disturbances observed in the last decade have led to higher losses in all
1420 the regions, so that the balance between losses and gains has become more negative in recent
1421 years.
1422

Table 5. Gains and losses of carbon due to disturbances for three different periods (1990-1999, 2000-2009, 2010-2018) across four different ecoregions (Atlantic, Mediterranean, Boreal & Continental) based on the AGB maps 2017 & 2018 (mean values).*

Period	Gain of C	Loss of C	Net budget
		[Tg C yr^{-1}]	
		Atlantic	
1990-1999	8.70 ± 0.10	-8.26 ± 0.06	+0.44 ± 0.12
2000-2009	8.53 ± 0.11	-13.96 ± 0.12	-5.43 ± 0.18
2010-2018	5.38 ± 0.75	-9.94 ± 0.06	-4.56 ± 0.71
		Mediterranean	
1990-1999	0.02 ± 0.40	-6.71 ± 0.16	-6.69 ± 0.44
2000-2009	-0.93 ± 0.47	-8.15 ± 0.20	-9.08 ± 0.53
2010-2018	-0.59 ± 0.84	-7.12 ± 0.14	-7.71 ± 0.83
		Boreal	
1990-1999	21.58 ± 0.34	-23.78 ± 0.25	-2.20 ± 0.46
2000-2009	15.03 ± 0.29	-25.71 ± 0.25	-10.68 ± 0.41
2010-2018	13.14 ± 1.84	-25.27 ± 0.22	-12.13 ± 1.77
		Continental	
1990-1999	11.49 ± 0.42	-12.41 ± 0.22	-0.92 ± 0.50
2000-2009	10.75 ± 0.42	-16.30 ± 0.26	-5.55 ± 0.53
2010-2018	11.05 ± 0.40	-18.79 ± 0.26	-7.73 ± 0.52

* Uncertainties for the sources and sinks represent the absolute difference between the 2017 & 2018 maps. Uncertainties for the net budget have been obtained with a bootstrapping method ($n=10^5$).

1423

1424 **8.2 Contribution of natural disturbances**

1425 We complemented the aforementioned analyses of the role of disturbances within each decade on
1426 the C budgets with an assessment of the impact of major natural disturbances, including fires,
1427 windthrows and insect outbreaks, based on the DFDE database (Pattaca et al. 2023). Windthrows
1428 provide the largest contribution to the overall damage induced by natural agents in European
1429 forests causing in average 24 Mm^3 (~5.5 Tg C yr^{-1}) annually corresponding to 46% of the total

timber volume disturbed over the 1950-2019 period. Northern and Western European regions are more prominently exposed to strong wind gusts typically associated with areas of deep low atmospheric pressure (Roberts et al., 2014). Windthrows, being an extreme event strongly dependent on exceptional weather conditions, show high interannual variability dominated by individual extreme events such as the storms Vivian and Wiebke in 1990, Lothar and Martin in 1999, Gudrun in 2005, Kyrill in 2007, Klaus in 2009, and Xynthia in 2010. Despite the high stochasticity, wind disturbances experienced a significant positive trend at European scale with 310,000 m^3 timber volume lost more per year. Such an estimate agrees with independent assessments based on satellite retrievals (Senf & Seidl, 2021).

Fire is the second most important natural disturbance in Europe's forests, with an annual average biomass loss of 12.5 Mm^3 (~2.9 Tg C yr^{-1}) corresponding to 24% of the total timber volume damage over the study period. Severe aridity conditions typical of Southern European regions - affecting both triggering and susceptibility mechanisms - make these areas in particular subject to such disturbance (Littell et al., 2009). Fire impact has increased significantly between 1950 and 2019 at the European level with 99,609 m^3 timber volume lost per year and a sharper trend between 1970 and 1990. Large peaks of strong individual disturbance years are evident from the 1990 onward and are plausibly associated to severe droughts which have triggered extreme fire years (Senf et al., 2020).

The timber volume damaged by bark beetles accounts for 8.9 Mm^3 (~2.0 Tg C yr^{-1}) which corresponds to 17% of the total volume disturbed between 1950 and 2019. The magnitude of bark beetle disturbance shows a significant increase over the observational period with a trend of 182,897 of m^3 timber volume lost per year. A substantial higher damage rate manifested from 2000 onwards. This is consistent with the abrupt increase in vulnerability of forests to insect outbreaks observed for warming levels that occurred around year 2000 at European scale and documented in previous studies (Forzieri et al., 2021). Such pronounced increases in temperature have likely reduced plant defense mechanisms by ultimately favoring triggering processes and making forests more vulnerable to insect attacks. This seems confirmed by independent evidence documenting the recent rise in infestations of bark beetles responsible for massive and destructive attacks on coniferous forests of many northern and eastern European regions (Biedermann et al., 2019).

We highlight that estimates of biomass losses based on DFDE should be viewed with caution as subject to multiple sources of potential biases. The DFDE database is based on damage data statistics reported at country scale and collected by literature search and therefore is built on the contribution of data retrieved from different actors and through different acquisition methods. Despite the relevance of these issues, there is still a substantial lack of systematic monitoring systems of forest disturbances at the European level (McDowell et al., 2011). Recent joint efforts across European research institutions and forestry services have contributed to the collection of

harmonized databases of spatially explicit records of windthrows (Forzieri et al., 2020) and pest outbreaks (Forzieri et al., 2023) at Pan-European scale. These products have paved the way for the future development of novel methodologies for forest disturbance detection and attribution which could provide enhanced estimates of the impact of forest disturbances on the land carbon budget.

9 Conclusion

Our BU estimate of the European GHG budget for the decade 2010-2019 gives net emissions of 3.9 Pg CO_2-eq. yr^{-1} (100 year horizon). These net emissions are mainly driven by direct anthropogenic emissions of 4.9 Pg CO_2-eq. yr^{-1}, to which CO_2 emissions from fossil fuel combustion (Energy + IPPU sector) contribute about 85%. The land GHG budget gives a net-sink of 0.9 Pg CO_2-eq. yr^{-1}, mainly driven by the land CO_2 sink of 1.4 Pg CO_2-eq. yr^{-1}, which is only partially offset by net-emissions of CH_4 and N_2O. Our BU CH_4 and N_2O budgets agree well with regional and global inversions. In contrast, our BU estimate of the land CO_2 sink is at the higher end of the range of global inversions, and substantially higher than that estimated by regional inversions.

Over the decades of the 1990s, 2000s, and 2010s, our BU estimates give decreasing average net-GHG emissions (anthropogenic emissions + land budget) of 5.1 Pg CO_2-eq. yr^{-1}, 4.6 Pg CO_2-eq. yr^{-1}, and 3.9 Pg CO_2-eq. yr^{-1}, respectively. This decrease in net-emissions is mainly driven by decreases in direct anthropogenic emissions of CO_2 and CH_4, and in particular by a reduction in fossil fuel emissions. From the 2000s to the 2010s, the reduction in fossil fuel CO_2 emissions was particularly strong (by 0.7 Pg CO_2 yr^{-1}), but partly counterbalanced by a substantial weakening of the land CO_2 sink (by 0.2 Pg CO_2 yr^{-1}). N_2O contributes less to the overall GHG budgets, but also shows a pronounced decrease in total emissions, largely due to reduced emissions from the IPPU sector, for which however large uncertainties persist.

Global inversions, which cover the last two (CH_4, N_2O, but only until 2016) or three (CO_2) decades, confirm the decreasing trend in CH_4 and N_2O emissions. For the land CO_2 budget, the trend is less clear, but a pronounced interannual variability is visible. The drought in 2003 and the hot summers of 2018 and 2020, associated with unprecedented disturbances, are likely responsible for a weakened land CO_2 sink visible for these years. The drought year of 2003 also shows the highest net-GHG emissions in terms of combined global warming potential of the three GHGs.

Regional inversions permit us to identify large scale spatial patterns in GHG emissions over Europe. For CO_2, direct anthropogenic emissions (mainly fossil fuel emissions) show many local hotpots linked to large cities, power plants and industrial complexes. For the land CO_2 budget, regional inversions reveal sinks mainly in the northern half of Europe, whereas southern France and the Iberian Peninsula appear as large CO_2 sources. CH_4 and N_2O emissions stem largely from diffusive sources on agricultural land (fertilizer- and manure-driven N_2O emissions from soils,

and CH_4 emissions from ruminant livestock). Belgium, the Netherlands and southern UK appear as large areas of intense emissions of both GHGs.

Our BU C budget is based on the fluxes from the land budgets of CO_2 and CH_4, and further including estimates of lateral C net-exports through the trade of crop, wood, and peat products and the fluvial export of C to the sea. Alternatively, we constructed a C budget for the 2010s as a sum of individual estimates of changes in different C stocks, most importantly the biospheric C stocks of forest, grassland and cropland systems and the stock of harvested wood products.

For the 2010s, our flux-based estimate gives an average increase in the overall C stocks of 0.3 Pg C yr^{-1}. The stock-based BU estimate is substantially lower with only 0.1 Pg C yr^{-1}. However, we have to acknowledge that both estimates are associated with large uncertainties, larger in fact than the difference between both estimates. Nevertheless, our stock-based estimate is quite close to the UNFCCC estimate and the ensemble-median of the TRENDYv10 simulations. However, the range between individual TRENDYv10 simulations is also much larger than the difference between our flux-based and our stock-based estimates, highlighting that DGVMs are not an adequate tool to constrain the European C budget.

When comparing the flux-based BU estimates of C budgets for the last three decades, we find very much the same trend as for the land CO_2 budgets, which is largely driving C stock changes, while changes in CH_4 emissions and lateral C exports play a minor role. We find a substantial decrease of ~90 Tg C yr^{-1} in the land C sink from the 2000s to the 2010s, which is dominated by increases in ecosystem respiration Re_{terr} and emissions from the use, decay, or burning of biological products. At the same time, GPP also slightly decreased between these two decades. Note that changes in ecosystem respiration and GPP are based here on extrapolated flux tower managements of the FLUXCOM dataset. The TRENDYv10 ensemble does not reproduce the decrease in the land C sink, nor the underlying trends in GPP and Re_{terr}. In contrast, a slight decrease in the C budget is estimated by the UNFCCC national inventories, suggesting that changes in land management also play a role in decreased C sink strength.

We evaluated what is known about spatial patterns in the recent temporal trends in the land C sink strength by comparing different spatialized TD and BU estimates. On the TD side, this included the ensembles of regional and global inversions of the land CO_2 budget. On the BU side, we include inventory and remote sensing based estimates of changes in forest biomass, the FLUXCOM dataset and the VRPM model, both of which represent spatial extrapolations of flux tower measurements, and the TRENDYv10 ensemble. While over large parts of Europe, these datasets disagree whether we have an strengthening or weakening of the land C sink, we found a general agreement for increasing sink strengths over larger areas in and north-west of Romania and in the northern part of Spain, as well as for a weakening of the sink strength over the Czech Republic. To a certain degree, these trends can be explained by changes in land use but extreme events and climate-driven disturbances are also likely to have played an important role. We also

find a certain degree of agreement on a decreasing land C sink over large parts of Scandinavia, which can be explained by an intensification of forest management.

We finally investigated the impact of disturbances on forest biomass stocks in Europe, including disturbances through management (wood harvest in particular) as well as natural disturbances. Naturally, these disturbances play the largest role in Scandinavia and the Baltic, where we find large, managed forest areas. In Europe, net-losses of forest biomass have increased since the 1990s. In the last decade, they amounted to about 32 Tg C yr^{-1}, which equals one third to one tenth of our estimates of the European land C sink. Most of the net-losses are likely due to management practices, though natural disturbances may still play a non-negligible role. The most important form of natural disturbances of forest biomass loss in Europe is windthrow, followed by forest fires and bark beetle outbreaks. However, more research is required to quantitatively disentangle the effects of natural disturbance and management on the forest biomass C stocks.

Overall, our study provides the most up-to-date and comprehensive assessment of the European budget for CO_2, CH_4 and N_2O for the past three decades, including their combined GWP, as well as their trends and interannual variability. We combine a wide range of TD and BU estimates to separate these budgets into their different components and to produce a best estimate of their budget for the 2010s decade. By comparing our estimates with those of UNFCCC reports, our study provides a key contribution to the evaluation of national reporting of GHG and C emission at continental scale. Moreover, our study helps to set the path towards an improved carbon monitoring framework at European scale that can guide policy making.

Acknowledgements

R.L. acknowledges funding from French state aid, managed by ANR under the “Investissements d'avenir” programme (ANR-16-CONV-0003) and from EU's Horizon Europe Research and Innovation Programme under Grant Agreement No. 101060423. A.B. was funded by the European Union (ERC StG, ForExD, grant agreement No. 101039567). Views and opinions expressed are however those of the authors only and do not necessarily reflect those of the European Union or the European Research Council. Neither the European Union nor the granting authority can be held responsible for them. AMRP, MJM, RMA, MJS, GJN, PC were supported by the European Commission, Horizon 2020 Framework Programme (VERIFY, grant no. 776810), AMRP, MJM, RMA by grant agreement no. 958927 (CoCO2), AMRP by grant agreement no. 101081322 (AVENGERS) and RMA, PC and PP by grant agreement no. 10108139 (EYE-CLIMA). P.K.P. is partly supported by the Environmental Research and Technology Development Fund (JPMEERF21S20800) of the MOEJ and ERCA. G.F. was supported by the Horizon Europe Project ECO2ADAPT (grant agreement No. 101059498). MJS and GJN were partly funded by Ministry Agriculture, Nature Management and Food Quality in

Netherlands and its Knowledge Bases programme. GJN acknowledges RESONATE project (H2020 Grant 101000574) and the Horizon Europe Project SUPERB (grant 101036849) and FORWARDS (grant 101084481). For the aggregated national forest inventory data behind the EFISCEN simulations MJS and GJN acknowledge the national forest inventories of 27 EU countries, CW was funded by the Natural Environment Research Council through its grants to the UK National Centre for Earth Observation (NCEO; NERC grant numbers NE/R016518/1 and NE/N018079/1). CTE2021 runs were supported by the HPC cluster Aether at the University of Bremen, financed by DFG within the scope of the Excellence Initiative. PR acknowledges funding from the FRS-FRNS PDR project T.0191.23 CH4-lakes.

Data availability statement

Data used for the RECCAP2 project are available from https://www.bgc-jena.mpg.de/geodb/projects/Home.php. Additional data used for our study was taken from: Jung et al. (2020) for gridded FLUXCOM data; Andrew (2020) for updated fossil fuel emission inventories; https://unfccc.int/ for national inventories collected by UNFCCC; www.fao.org/faostat/ for the FAOSTAT database; Byrne et al. (2023) for gridded estimates of lateral carbon transfers; https://zenodo.org/records/6884342 for TRENDYv10 simulations; McGrath et al. (2023) and Petrescu et al. (2023) for regional atmospheric inversions; Chang et al. (2021) for estimates of livestock grazing; Hirschler & Oldenburg (2022) for estimates of peat harvest, trade and use; Murguia-Flores et al. (2018) for MeMo simulation data; Gerbig & Koch (2021) for gridded VPRM simulation outputs; Ganzenmüller et al. (2022) for gridded BLUE simulation results; Winkler et al. (2021) for gridded HILDA+ land use and land use change data; Mandani and Parazoo (2020), Zhao et al. (2005), and Jiang & Ryu (2016) for gridded estimates of terrestrial primary production; Yao et al. (2021) for gridded estimate of soil heterotrophic respiration; Mendonca et al. (2017) for regionalized estimates of lake carbon burial; Etiope et al. (2019) for spatially resolved estimates of geogenic methane emissions; Nabuurs et al. (2018) and Petrescu et al. (2020) for EFISCEN estimates of forest carbon stock changes; Fan et al. (2023) for the L-VOD based estimates of changes in above ground biomass; https://thredds.met.no/thredds/catalog/data/EMEP/2021_Reporting/catalog.html for EMEP data; https://daac.ornl.gov/VEGETATION/guides/fire_emissions_v4.html for GFEDv4 data; https://www.ecmwf.int/en/forecasts/dataset/global-fire-assimilation-system for GFASv1.2 data.

References

Ahlström, A., Canadell, J. G., & Metcalfe, D. B. (2022). Widespread Unquantified Conversion of Old Boreal Forests to Plantations. *Earth's Future*, 10(11), e2022EF003221. https://doi.org/10.1029/2022EF003221

Anderegg, W. R. L., Trugman, A. T., Badgley, G., Anderson, C. M., Bartuska, A., Ciais, P., et al. (2020). Climate-driven risks to the climate mitigation potential of forests. *Science*, 368(6497), eaaz7005. https://doi.org/10.1126/science.aaz7005

Anderegg, W. R. L., Wu, C., Acil, N., Carvalhais, N., Pugh, T. A. M., Sadler, J. P., & Seidl, R. (2022). A climate risk analysis of Earth's forests in the 21st century. *Science*, 377(6610), 1099–1103. https://doi.org/10.1126/science.abp9723

Andrew, R. M. (2020). A comparison of estimates of global carbon dioxide emissions from fossil carbon sources. *Earth System Science Data*, 12(2), 1437–1465. https://doi.org/10.5194/essd-12-1437-2020

Bastos, A., Gouveia, C. M., Trigo, R. M., & Running, S. W. (2014). Analysing the spatio-temporal impacts of the 2003 and 2010 extreme heatwaves on plant productivity in Europe. *Biogeosciences*, 11(13), 3421–3435. https://doi.org/10.5194/bg-11-3421-2014

Bastos, A., Fu, Z., Ciais, P., Friedlingstein, P., Sitch, S., Pongratz, J., et al. (2020). Impacts of extreme summers on European ecosystems: A comparative analysis of 2003, 2010 and 2018: European extreme summers and the C-cycle. *Philosophical Transactions of the Royal Society B: Biological Sciences*, 375(1810). https://doi.org/10.1098/rstb.2019.0507

Bastos, Ana, Janssens, I. A., Gouveia, C. M., Trigo, R. M., Ciais, P., Chevallier, F., et al. (2016). European land CO2 sink influenced by NAO and East-Atlantic Pattern coupling. *Nature Communications*, 7(1), 10315. https://doi.org/10.1038/ncomms10315

Battin, T. J., Lauerwald, R., Bernhardt, E. S., Bertuzzo, E., Gener, L. G., Hall, R. O., et al. (2023). River ecosystem metabolism and carbon biogeochemistry in a changing world. *Nature*, 613(7944), 449–459. https://doi.org/10.1038/s41586-022-05500-8

Biedermann, P. H. W., Müller, J., Grégoire, J.-C., Gruppe, A., Hagge, J., Hammerbacher, A., et al. (2019). Bark Beetle Population Dynamics in the Anthropocene: Challenges and Solutions. *Trends in Ecology & Evolution*, 34(10), 914–924. https://doi.org/10.1016/j.tree.2019.06.002

Breidenbach, J., Ellison, D., Petersson, H., Korhonen, K. T., Henttonen, H. M., Wallerman, J., et al. (2022). Harvested area did not increase abruptly—how advancements in satellite-based mapping led to erroneous conclusions. *Annals of Forest Science*, 79(1), 2. https://doi.org/10.1186/s13595-022-01120-4

Buermann, W., Forkel, M., O'Sullivan, M., Sitch, S., Friedlingstein, P., Haverd, V., et al. (2018). Widespread seasonal compensation effects of spring warming on northern plant productivity. *Nature*, 562(7725), 110–114. https://doi.org/10.1038/s41586-018-0555-7

1644 Byrne, B., Baker, D. F., Basu, S., Bertolacci, M., Bowman, K. W., Carroll, D., et al. (2023).
1645 National CO_2 budgets (2015–2020) inferred from atmospheric CO_2 observations in support of
1646 the global stocktake. *Earth System Science Data*, 15(2), 963–1004. https://doi.org/10.5194/essd-
1647 15-963-2023

1648 Canadell, J. G., Ciais, P., Gurney, K., Le Quéré, C., Piao, S., Raupach, M. R., & Sabine, C. L.
1649 (2011). An International Effort to Quantify Regional Carbon Fluxes. *Eos, Transactions American*
1650 *Geophysical Union*, 92(10), 81–82. https://doi.org/10.1029/2011EO100001

1651 Carlson, K., Gerber, J., Mueller, N. *et al.* (2017). Greenhouse gas emissions intensity of global
1652 croplands. *Nature Clim Change* 7, 63–68 . https://doi.org/10.1038/nclimate3158

1653 Ceccherini, G., Duveiller, G., Grassi, G., Lemoine, G., Avitabile, V., Pilli, R., & Cescatti, A.
1654 (2020). Abrupt increase in harvested forest area over Europe after 2015. *Nature*, 583(7814), 72–
1655 77. https://doi.org/10.1038/s41586-020-2438-y

1656 Ceccherini, G., Duveiller, G., Grassi, G., Lemoine, G., Avitabile, V., Pilli, R., & Cescatti, A.
1657 (2021). Reply to Wernick, I. K. et al.; Palahí, M. et al. *Nature*, 592(7856), E18–E23.
1658 https://doi.org/10.1038/s41586-021-03294-9

1659 Chang, J., Ciais, P., Gasser, T., Smith, P., Herrero, M., Havlík, P., et al. (2021). Climate warming
1660 from managed grasslands cancels the cooling effect of carbon sinks in sparsely grazed and
1661 natural grasslands. *Nature Communications*, 12(1), 118. https://doi.org/10.1038/s41467-020-
1662 20406-7

1663 Ciais, P., Borges, A. V., Abril, G., Meybeck, M., Folberth, G., Hauglustaine, D., & Janssens, I.
1664 A. (2008). The impact of lateral carbon fluxes on the European carbon balance. *Biogeosciences*,
1665 5(5), 1259–1271. https://doi.org/10.5194/bg-5-1259-2008

1666 Ciais, P., Wattenbach, M., Vuichard, N., Smith, P., Piao, S. L., Don, A., et al. (2010). The
1667 European carbon balance. Part 2: croplands. *Global Change Biology*, 16(5), 1409–1428.
1668 https://doi.org/10.1111/j.1365-2486.2009.02055.x

1669 Ciais, P., Soussana, J. F., Vuichard, N., Luyssaert, S., Don, A., Janssens, I. A., et al. (2010). The
1670 greenhouse gas balance of European grasslands. *Biogeosciences Discuss.*, 2010, 5997–6050.
1671 https://doi.org/10.5194/bgd-7-5997-2010

1672 Ciais, P., Yao, Y., Gasser, T., Baccini, A., Wang, Y., Lauerwald, R., et al. (2021). Empirical
1673 estimates of regional carbon budgets imply reduced global soil heterotrophic respiration.
1674 *National Science Review*, 8(2). https://doi.org/10.1093/nsr/nwaa145

1675 Ciais, P., Bastos, A., Chevallier, F., Lauerwald, R., Poulter, B., Canadell, J. G., et al. (2022).
1676 Definitions and methods to estimate regional land carbon fluxes for the second phase of the
1677 REgional Carbon Cycle Assessment and Processes Project (RECCAP-2). *Geoscientific Model*
1678 *Development*, 15(3), 1289–1316. https://doi.org/10.5194/gmd-15-1289-2022

1679 Ciais, Ph, Reichstein, M., Viovy, N., Granier, A., Ogée, J., Allard, V., et al. (2005). Europe-wide
1680 reduction in primary productivity caused by the heat and drought in 2003. *Nature*, 437(7058),
1681 529–533. https://doi.org/10.1038/nature03972

1682 Deng, Z., Ciais, P., Tzompa-Sosa, Z. A., Saunois, M., Qiu, C., Tan, C., et al. (2022). Comparing
1683 national greenhouse gas budgets reported in UNFCCC inventories against atmospheric
1684 inversions. *Earth System Science Data*, 14(4), 1639–1675. https://doi.org/10.5194/essd-14-1639-
1685 2022

1686 De Rosa, D., Ballabio, C., Lugato, E., Fasiolo, M., Jones, A., & Panagos, P. (2024). Soil organic
1687 carbon stocks in European croplands and grasslands: How much have we lost in the past decade?
1688 *Global Change Biology*, 30, e16992. https://doi.org/10.1111/gcb.16992

1689 Eggers, T. (2002). The Impacts of Manufacturing and Utilisation of Wood Products on the
1690 European Carbon Budget. Internal Report 9.

1691 EMEP. (n.d.). Daily N deposition data (from the co-operative programme for monitoring and
1692 evaluation of the long-range transmission of air pollutants in Europe - EMEP).
1693 https://thredds.met.no/thredds/catalog/data/EMEP/2021_Reporting/catalog.html). Accessed
1694 2022-12-04.

1695 Etiope, G., Ciotoli, G., Schwietzke, S., & Schoell, M. (2019). Gridded maps of geological
1696 methane emissions and their isotopic signature. *Earth System Science Data*, 11(1), 1–22.
1697 https://doi.org/10.5194/essd-11-1-2019

1698 European Communities Council [EEC. (n.d.). Council directive of the 12 December 1991
1699 concerning the protection of water against pollution caused by nitrates from agricultural sources
1700 (91/676/EEC). Official Journal of the European Communities No. L 375/1, 1991. (online:
1701 https://eur-lex.europa.eu/legal-content/EN/TXT/PDF/?uri=CELEX:31991L0676, accessed 2023-
1702 11-01.).

1703 Fan, L., Wigneron, JP., Ciais, P. *et al.* (2023). Siberian carbon sink reduced by forest
1704 disturbances. *Nat. Geosci.* 16, 56–62. https://doi.org/10.1038/s41561-022-01087-x

1705 Forzieri, G., Pecchi, M., Girardello, M., Mauri, A., Klaus, M., Nikolov, C., et al. (2020). A
1706 spatially explicit database of wind disturbances in European forests over the period 2000–2018.
1707 *Earth System Science Data*, 12(1), 257–276. https://doi.org/10.5194/essd-12-257-2020

1708 Forzieri, Giovanni, Girardello, M., Ceccherini, G., Spinoni, J., Feyen, L., Hartmann, H., et al.
1709 (2021). Emergent vulnerability to climate-driven disturbances in European forests. *Nature*
1710 *Communications*, 12(1), 1081. https://doi.org/10.1038/s41467-021-21399-7

1711 Forzieri, Giovanni, Dakos, V., McDowell, N. G., Ramdane, A., & Cescatti, A. (2022). Emerging
1712 signals of declining forest resilience under climate change. *Nature*, 608(7923), 534–539.
1713 https://doi.org/10.1038/s41586-022-04959-9

1714 Forzieri, Giovanni, Dutrieux, L. P., Elia, A., Eckhardt, B., Caudullo, G., Taboada, F. Á., et al.
1715 (2023). The Database of European Forest Insect and Disease Disturbances: DEFID2. *Global*
1716 *Change Biology*, 29(21), 6040–6065. https://doi.org/10.1111/gcb.16912

1717 Friedlingstein, P., O'Sullivan, M., Jones, M. W., Andrew, R. M., Hauck, J., Olsen, A., et al.
1718 (2020). Global Carbon Budget 2020. *Earth System Science Data*, 12(4), 3269–3340.
1719 https://doi.org/10.5194/essd-12-3269-2020

1720 Friedlingstein, P., Jones, M. W., O'Sullivan, M., Andrew, R. M., Bakker, D. C. E., Hauck, J., et
1721 al. (2022). Global Carbon Budget 2021. *Earth System Science Data*, 14(4), 1917–2005.
1722 https://doi.org/10.5194/essd-14-1917-2022

1723 Ganzenmüller, R., Bultan, S., Winkler, K., Fuchs, R., Zabel, F., & Pongratz, J. (2022). Land-use
1724 change emissions based on high-resolution activity data substantially lower than previously
1725 estimated. *Environmental Research Letters*, 17(6), 064050. https://doi.org/10.1088/1748-
1726 9326/ac70d8

1727 Grassi, G., Conchedda, G., Federici, S., Abad Viñas, R., Korosuo, A., Melo, J., et al. (2022).
1728 Carbon fluxes from land 2000–2020: bringing clarity to countries' reporting. *Earth System*
1729 *Science Data*, 14(10), 4643–4666. https://doi.org/10.5194/essd-14-4643-2022

1730 Guimberteau, M., Zhu, D., Maignan, F., Huang, Y., Yue, C., Dantec-Nédélec, S., et al. (2018).
1731 ORCHIDEE-MICT (v8.4.1), a land surface model for the high latitudes: model description and
1732 validation. *Geoscientific Model Development*, 11(1), 121–163. https://doi.org/10.5194/gmd-11-
1733 121-2018

1734 Hansis, E., Davis, S. J., & Pongratz, J. (2015). Relevance of methodological choices for
1735 accounting of land use change carbon fluxes. *Global Biogeochemical Cycles*, 29(8), 1230–1246.
1736 https://doi.org/10.1002/2014GB004997

1737 Hartmann, J., Jansen, N., Dürr, H. H., Kempe, S., & Köhler, P. (2009). Global CO2-consumption
1738 by chemical weathering: What is the contribution of highly active weathering regions? *Global*
1739 *and Planetary Change*, 69(4), 185–194. https://doi.org/10.1016/j.gloplacha.2009.07.007

1740 Hersbach, H., Bell, B., Berrisford, P., Hirahara, S., Horányi, A., Muñoz-Sabater, J., et al. (2020).
1741 The ERA5 global reanalysis. *Quarterly Journal of the Royal Meteorological Society*, 146(730),
1742 1999–2049. https://doi.org/10.1002/qj.3803

1743 Hirschler, O., & Osterburg, B. (2022). Peat extraction, trade and use in Europe: a material flow
1744 analysis. *Mires and Peat*, 28. https://doi.org/10.19189/MaP.2021.SNPG.StA.2315

1745 Houghton, R. A., & Nassikas, A. A. (2017). Global and regional fluxes of carbon from land use
1746 and land cover change 1850–2015. *Global Biogeochemical Cycles*, 31(3), 456–472.
1747 https://doi.org/10.1002/2016GB005546

1748 Hurtt, G. C., Chini, L., Sahajpal, R., Frolking, S., Bodirsky, B. L., Calvin, K., et al. (2020).
1749 Harmonization of global land use change and management for the period 850–2100 (LUH2) for
1750 CMIP6. *Geoscientific Model Development*, 13(11), 5425–5464. https://doi.org/10.5194/gmd-13-
1751 5425-2020

1752 IPCC. (2019). 2019 Refinement to the 2006 IPCC Guidelines for National Greenhouse Gas
1753 Inventories. https://www.ipcc-nggip.iges.or.jp/public/2019rf/index.html.

1754 Jiang, C., & Ryu, Y. (2016). Multi-scale evaluation of global gross primary productivity and
1755 evapotranspiration products derived from Breathing Earth System Simulator (BESS). *Remote*
1756 *Sensing of Environment*, 186, 528–547. https://doi.org/10.1016/j.rse.2016.08.030

1757 Jung, M., Schwalm, C., Migliavacca, M., Walther, S., Camps-Valls, G., Koirala, S., et al. (2020).
1758 Scaling carbon fluxes from eddy covariance sites to globe: synthesis and evaluation of the
1759 FLUXCOM approach. *Biogeosciences*, 17(5), 1343–1365. https://doi.org/10.5194/bg-17-1343-
1760 2020

1761 Kaiser, J. W., Heil, A., Andreae, M. O., Benedetti, A., Chubarova, N., Jones, L., et al. (2012).
1762 Biomass burning emissions estimated with a global fire assimilation system based on observed
1763 fire radiative power. *Biogeosciences*, 9(1), 527–554. https://doi.org/10.5194/bg-9-527-2012

1764 Katalin Petz, Catharina J. E. Schulp, Emma H. van der Zanden, Clara Veerkamp, Mart-Jan
1765 Schelhaas, Gert-Jan Nabuurs, & Geerten Hengeveld. (2016). Indicators and modelling of land
1766 use, land management and ecosystem services. Methodological documentation Nature Outlook.
1767 PBL Netherlands Environmental Assessment Agency. PBL publication number: 2386 .

1768 Korosuo, A., Pilli, R., Abad Viñas, R., Blujdea, V. N. B., Colditz, R. R., Fiorese, G., et al.
1769 (2023). The role of forests in the EU climate policy: are we on the right track? *Carbon Balance*
1770 *and Management*, 18(1), 15. https://doi.org/10.1186/s13021-023-00234-0

1771 Lauerwald, R., Allen, G. H., Deemer, B. R., Liu, S., Maavara, T., Raymond, P., et al. (2023).
1772 Inland Water Greenhouse Gas Budgets for RECCAP2: 2. Regionalization and Homogenization
1773 of Estimates. *Global Biogeochemical Cycles*, 37(5). https://doi.org/10.1029/2022GB007658

1774 Li, N., Sippel, S., Winkler, A. J., Mahecha, M. D., Reichstein, M., & Bastos, A. (2022).
1775 Interannual global carbon cycle variations linked to atmospheric circulation variability. *Earth*
1776 *System Dynamics*, 13(4), 1505–1533. https://doi.org/10.5194/esd-13-1505-2022

1777 Littell, J. S., McKenzie, D., Peterson, D. L., & Westerling, A. L. (2009). Climate and wildfire
1778 area burned in western U.S. ecoprovinces, 1916–2003. *Ecological Applications*, 19(4), 1003–
1779 1021. https://doi.org/10.1890/07-1183.1

1780 Luyssaert, S., Ciais, P., Piao, S. L., Schulze, E.-D., Jung, M., Zaehle, S., et al. (2010). The
1781 European carbon balance. Part 3: forests. *Global Change Biology*, 16(5), 1429–1450.
1782 https://doi.org/10.1111/j.1365-2486.2009.02056.x

1783 Luyssaert, S., Abril, G., Andres, R., Bastviken, D., Bellassen, V., Bergamaschi, P., et al. (2012).
1784 The European land and inland water CO_2, CO, CH_4 and N_2O balance between 2001 and 2005.
1785 *Biogeosciences*, 9(8), 3357–3380. https://doi.org/10.5194/bg-9-3357-2012

1786 Madani, N., Parazoo, N.C. (2020). Global Monthly GPP from an Improved Light Use Efficiency
1787 Model, 1982-2016. ORNL DAAC, Oak Ridge, Tennessee, USA.
1788 https://doi.org/10.3334/ORNLDAAC/1789

1789 Mayorga, E., Seitzinger, S. P., Harrison, J. A., Dumont, E., Beusen, A. H. W., Bouwman, A. F.,
1790 et al. (2010). Global Nutrient Export from WaterSheds 2 (NEWS 2): Model development and
1791 implementation. *Environmental Modelling & Software*, 25(7), 837–853.
1792 https://doi.org/10.1016/j.envsoft.2010.01.007

1793 McDowell, N. G., Beerling, D. J., Breshears, D. D., Fisher, R. A., Raffa, K. F., & Stitt, M.
1794 (2011). The interdependence of mechanisms underlying climate-driven vegetation mortality.
1795 *Trends in Ecology & Evolution*, 26(10), 523–532. https://doi.org/10.1016/j.tree.2011.06.003

1796 McDowell, N. G., Allen, C. D., Anderson-Teixeira, K., Aukema, B. H., Bond-Lamberty, B.,
1797 Chini, L., et al. (2020). Pervasive shifts in forest dynamics in a changing world. *Science*,
1798 368(6494), eaaz9463. https://doi.org/10.1126/science.aaz9463

1799 McGrath, M. J., Petrescu, A. M. R., Peylin, P., Andrew, R. M., Matthews, B., Dentener, F., et al.
1800 (2023). The consolidated European synthesis of CO2 emissions and removals for the European
1801 Union and United Kingdom: 1990-2020. *Earth System Science Data*, 15(10), 4295–4370.
1802 https://doi.org/10.5194/essd-15-4295-2023

1803 Mendonça, R., Müller, R. A., Clow, D., Verpoorter, C., Raymond, P., Tranvik, L. J., & Sobek, S.
1804 (2017). Organic carbon burial in global lakes and reservoirs. *Nature Communications*, 8(1), 1694.
1805 https://doi.org/10.1038/s41467-017-01789-6

1806 Meybeck, M., Dürr, H. H., & Vörösmarty, C. J. (2006). Global coastal segmentation and its river
1807 catchment contributors: A new look at land-ocean linkage. *Global Biogeochemical Cycles*, 20(1).
1808 https://doi.org/10.1029/2005GB002540

1809 Monteil, G., Broquet, G., Scholze, M., Lang, M., Karstens, U., Gerbig, C., et al. (2020). The
1810 regional European atmospheric transport inversion comparison, EUROCOM: first results on
1811 European-wide terrestrial carbon fluxes for the period 2006–2015. *Atmospheric Chemistry and*
1812 *Physics*, 20(20), 12063–12091. https://doi.org/10.5194/acp-20-12063-2020

1813 Moran, D., Pichler, P.-P., Zheng, H., Muri, H., Klenner, J., Kramel, D., et al. (2022). Estimating
1814 CO_2 emissions for 108000 European cities. *Earth System Science Data*, 14(2), 845–864.
1815 https://doi.org/10.5194/essd-14-845-2022

1816 Murguia-Flores, F., Arndt, S., Ganesan, A. L., Murray-Tortarolo, G., & Hornibrook, E. R. C.
1817 (2018). Soil Methanotrophy Model (MeMo v1.0): a process-based model to quantify global
1818 uptake of atmospheric methane by soil. *Geoscientific Model Development*, 11(6), 2009–2032.
1819 https://doi.org/10.5194/gmd-11-2009-2018

1820 Nabuurs, G. J., Pussinen, A., van Brusselen, J., & Schelhaas, M. J. (2007). Future harvesting
1821 pressure on European forests. *European Journal of Forest Research*, 126(3), 391–400.
1822 https://doi.org/10.1007/s10342-006-0158-y

1823 Nabuurs, G.-J., Lindner, M., Verkerk, P. J., Gunia, K., Deda, P., Michalak, R., & Grassi, G.
1824 (2013). First signs of carbon sink saturation in European forest biomass. *Nature Climate Change*,
1825 3(9), 792–796. https://doi.org/10.1038/nclimate1853

1826 Nabuurs, G.-J., Arets, E. J. M. M., & Schelhaas, M.-J. (2018). Understanding the implications of
1827 the EU-LULUCF regulation for the wood supply from EU forests to the EU. *Carbon Balance*
1828 *and Management*, 13(1), 18. https://doi.org/10.1186/s13021-018-0107-3

1829 Palahí, M., Valbuena, R., Senf, C., Acil, N., Pugh, T. A. M., Sadler, J., et al. (2021). Concerns
1830 about reported harvests in European forests. *Nature*, 592(7856), E15–E17.
1831 https://doi.org/10.1038/s41586-021-03292-x

1832 Patacca, M., Lindner, M., Lucas-Borja, M. E., Cordonnier, T., Fidej, G., Gardiner, B., et al.
1833 (2023). Significant increase in natural disturbance impacts on European forests since 1950.
1834 *Global Change Biology*, 29(5), 1359–1376. https://doi.org/10.1111/gcb.16531

Petrescu, A. M. R., Peters, G. P., Janssens-Maenhout, G., Ciais, P., Tubiello, F. N., Grassi, G., et al. (2020). European anthropogenic AFOLU greenhouse gas emissions: a review and benchmark data. *Earth System Science Data*, 12(2), 961–1001. https://doi.org/10.5194/essd-12-961-2020

Petrescu, A. M. R., Qiu, C., Ciais, P., Thompson, R. L., Peylin, P., McGrath, M. J., et al. (2021). The consolidated European synthesis of CH_4 and N_2O emissions for the European Union and United Kingdom: 1990–2017 *Earth System Science Data*, 13(5), 2307–2362. https://doi.org/10.5194/essd-13-2307-2021

Petrescu, A. M. R., McGrath, M. J., Andrew, R. M., Peylin, P., Peters, G. P., Ciais, P., et al. (2021). The consolidated European synthesis of CO_2 emissions and removals for the European Union and United Kingdom: 1990-2018. *Earth System Science Data*, 13(5), 2363–2406. https://doi.org/10.5194/essd-13-2363-2021

Petrescu, A. M. R., Qiu, C., McGrath, M. J., Peylin, P., Peters, G. P., Ciais, P., et al. (2023). The consolidated European synthesis of CH_4 and N_2O emissions for the European Union and United Kingdom: 1990-2019. *Earth System Science Data*, 15(3), 1197–1268. https://doi.org/10.5194/essd-15-1197-2023

Roberts, J. F., Champion, A. J., Dawkins, L. C., Hodges, K. I., Shaffrey, L. C., Stephenson, D. B., et al. (2014). The XWS open access catalogue of extreme European windstorms from 1979 to 2012. *Nat. Hazards Earth Syst. Sci.*, 14(9), 2487–2501. https://doi.org/10.5194/nhess-14-2487-2014

Rosentreter, J. A., Laruelle, G. G., Bange, H. W., Bianchi, T. S., Busecke, J. J. M., Cai, W.-J., et al. (2023). Coastal vegetation and estuaries are collectively a greenhouse gas sink. *Nature Climate Change*, 13(6), 579–587. https://doi.org/10.1038/s41558-023-01682-9

Santoro, M., & Cartus, O. (2021). ESA Biomass Climate Change Initiative (Biomass_cci): Global datasets of forest above-ground biomass for the years 2010, 2017 and 2018, v3.

Saunois, M., Stavert, A. R., Poulter, B., Bousquet, P., Canadell, J. G., Jackson, R. B., et al. (2020). The Global Methane Budget 2000–2017. *Earth System Science Data*, 12(3), 1561–1623. https://doi.org/10.5194/essd-12-1561-2020

Schelhaas, M.-J., Nabuurs, G.-J., & Schuck, A. (2003). Natural disturbances in the European forests in the 19th and 20th centuries. *Global Change Biology*, 9(11), 1620–1633. https://doi.org/10.1046/j.1365-2486.2003.00684.x

Sedano, F., & Randerson, J. T. (2014). Multi-scale influence of vapor pressure deficit on fire ignition and spread in boreal forest ecosystems. *Biogeosciences*, 11(14), 3739–3755. https://doi.org/10.5194/bg-11-3739-2014

1868 Seidl, R., Schelhaas, M.-J., Rammer, W., & Verkerk, P. J. (2014). Increasing forest disturbances
1869 in Europe and their impact on carbon storage. *Nature Climate Change*, 4(9), 806–810.
1870 https://doi.org/10.1038/nclimate2318

1871 Senf, C., & Seidl, R. (2021a). Mapping the forest disturbance regimes of Europe. *Nature*
1872 *Sustainability*, 4(1), 63–70. https://doi.org/10.1038/s41893-020-00609-y

1873 Senf, C., & Seidl, R. (2021b). Post-disturbance canopy recovery and the resilience of Europe's
1874 forests. *Global Ecology and Biogeography*, 31(1), 25–36. https://doi.org/10.1111/geb.13406

1875 Senf, C., & Seidl, R. (2021c). Storm and fire disturbances in Europe: Distribution and trends.
1876 *Global Change Biology*, 27(15), 3605–3619. https://doi.org/10.1111/gcb.15679

1877 Senf, C., Müller, J., & Seidl, R. (2019). Post-disturbance recovery of forest cover and tree height
1878 differ with management in Central Europe. *Landscape Ecology*, 34(12), 2837–2850.
1879 https://doi.org/10.1007/s10980-019-00921-9

1880 Senf, C., Buras, A., Zang, C. S., Rammig, A., & Seidl, R. (2020). Excess forest mortality is
1881 consistently linked to drought across Europe. *Nature Communications*, 11(1), 6200.
1882 https://doi.org/10.1038/s41467-020-19924-1

1883 Smith, T., Traxl, D., & Boers, N. (2022). Empirical evidence for recent global shifts in vegetation
1884 resilience. *Nature Climate Change*, 12(5), 477–484. https://doi.org/10.1038/s41558-022-01352-2

1885 Solazzo, E., Crippa, M., Guizzardi, D., Muntean, M., Choulga, M., & Janssens-Maenhout, G.
1886 (2021). Uncertainties in the Emissions Database for Global Atmospheric Research (EDGAR)
1887 emission inventory of greenhouse gases. *Atmospheric Chemistry and Physics*, 21(7), 5655–5683.
1888 https://doi.org/10.5194/acp-21-5655-2021

1889 Tian, H., Yang, J., Xu, R., Lu, C., Canadell, J. G., Davidson, E. A., et al. (2019). Global soil
1890 nitrous oxide emissions since the preindustrial era estimated by an ensemble of terrestrial
1891 biosphere models: Magnitude, attribution, and uncertainty. *Global Change Biology*, 25(2), 640–
1892 659. https://doi.org/10.1111/gcb.14514

1893 Tian, H., Xu, R., Canadell, J. G., Thompson, R. L., Winiwarter, W., Suntharalingam, P., et al.
1894 (2020). A comprehensive quantification of global nitrous oxide sources and sinks. *Nature*,
1895 586(7828), 248–256. https://doi.org/10.1038/s41586-020-2780-0

1896 Tian, Hanqin, Lu, C., Ciais, P., Michalak, A. M., Canadell, J. G., Saikawa, E., et al. (2016). The
1897 terrestrial biosphere as a net source of greenhouse gases to the atmosphere. *Nature*, 531(7593),
1898 225–228. https://doi.org/10.1038/nature16946

1899 Tubiello, F. N., Salvatore, M., Rossi, S., Ferrara, A., Fitton, N., & Smith, P. (2013). The
1900 FAOSTAT database of greenhouse gas emissions from agriculture. *Environmental Research*
1901 *Letters*, 8(1). https://doi.org/10.1088/1748-9326/8/1/015009

1902 Velthof, G. L., Lesschen, J. P., Webb, J., Pietrzak, S., Miatkowski, Z., Pinto, M., et al. (2014).
1903 The impact of the Nitrates Directive on nitrogen emissions from agriculture in the EU-27 during
1904 2000–2008. *Science of The Total Environment*, 468–469, 1225–1233.
1905 https://doi.org/10.1016/j.scitotenv.2013.04.058

1906 de Vries, W., Schulte-Uebbing, L., Kros, H., Voogd, J. C., & Louwagie, G. (2021). Spatially
1907 explicit boundaries for agricultural nitrogen inputs in the European Union to meet air and water
1908 quality targets. *Science of The Total Environment*, 786, 147283.
1909 https://doi.org/10.1016/j.scitotenv.2021.147283

1910 van der Werf, G. R., Randerson, J. T., Giglio, L., van Leeuwen, T. T., Chen, Y., Rogers, B. M., et
1911 al. (2017). Global fire emissions estimates during 1997–2016. *Earth System Science Data*, 9(2),
1912 697–720. https://doi.org/10.5194/essd-9-697-2017

1913 Wernick, I. K., Ciais, P., Fridman, J., Högberg, P., Korhonen, K. T., Nordin, A., & Kauppi, P. E.
1914 (2021). Quantifying forest change in the European Union. *Nature*, 592(7856), E13–E14.
1915 https://doi.org/10.1038/s41586-021-03293-w

1916 Winkler, K., Fuchs, R., Rounsevell, M., & Herold, M. (2021). Global land use changes are four
1917 times greater than previously estimated. *Nature Communications*, 12(1), 2501.
1918 https://doi.org/10.1038/s41467-021-22702-2

1919 Winkler, K., Yang, H., Ganzenmüller, R., Fuchs, R., Ceccherini, G., Duveiller, G., et al. (2023).
1920 Changes in land use and management led to a decline in Eastern Europe's terrestrial carbon sink.
1921 *Communications Earth & Environment*, 4(1), 237. https://doi.org/10.1038/s43247-023-00893-4

1922 Yao, Yitong, Ciais, P., Viovy, N., Li, W., Cresto-Aleina, F., Yang, H., et al. (2021). A Data-
1923 Driven Global Soil Heterotrophic Respiration Dataset and the Drivers of Its Inter-Annual
1924 Variability. *Global Biogeochemical Cycles*, 35(8), e2020GB006918.
1925 https://doi.org/10.1029/2020GB006918

1926 Yao, Yuanzhi, Tian, H., Shi, H., Pan, S., Xu, R., Pan, N., & Canadell, J. G. (2020). Increased
1927 global nitrous oxide emissions from streams and rivers in the Anthropocene. *Nature Climate*
1928 *Change*, 10(2), 138–142. https://doi.org/10.1038/s41558-019-0665-8

1929 Zaehle, S., & Friend, A. D. (2010). Carbon and nitrogen cycle dynamics in the O-CN land
1930 surface model: 1. Model description, site-scale evaluation, and sensitivity to parameter estimates.
1931 *Global Biogeochemical Cycles*, 24(1). https://doi.org/10.1029/2009GB003521

1932 Zhao, M., Heinsch, F. A., Nemani, R. R., & Running, S. W. (2005). Improvements of the MODIS
1933 terrestrial gross and net primary production global data set. *Remote Sensing of Environment*,
1934 95(2), 164–176. https://doi.org/10.1016/j.rse.2004.12.011

1935 Zscheischler, J., Mahecha, M. D., Avitabile, V., Calle, L., Carvalhais, N., Ciais, P., et al. (2017).
1936 Reviews and syntheses: An empirical spatiotemporal description of the global surface-
1937 atmosphere carbon fluxes: Opportunities and data limitations. *Biogeosciences*, 14(15), 3685–
1938 3703. https://doi.org/10.5194/bg-14-3685-2017

1939